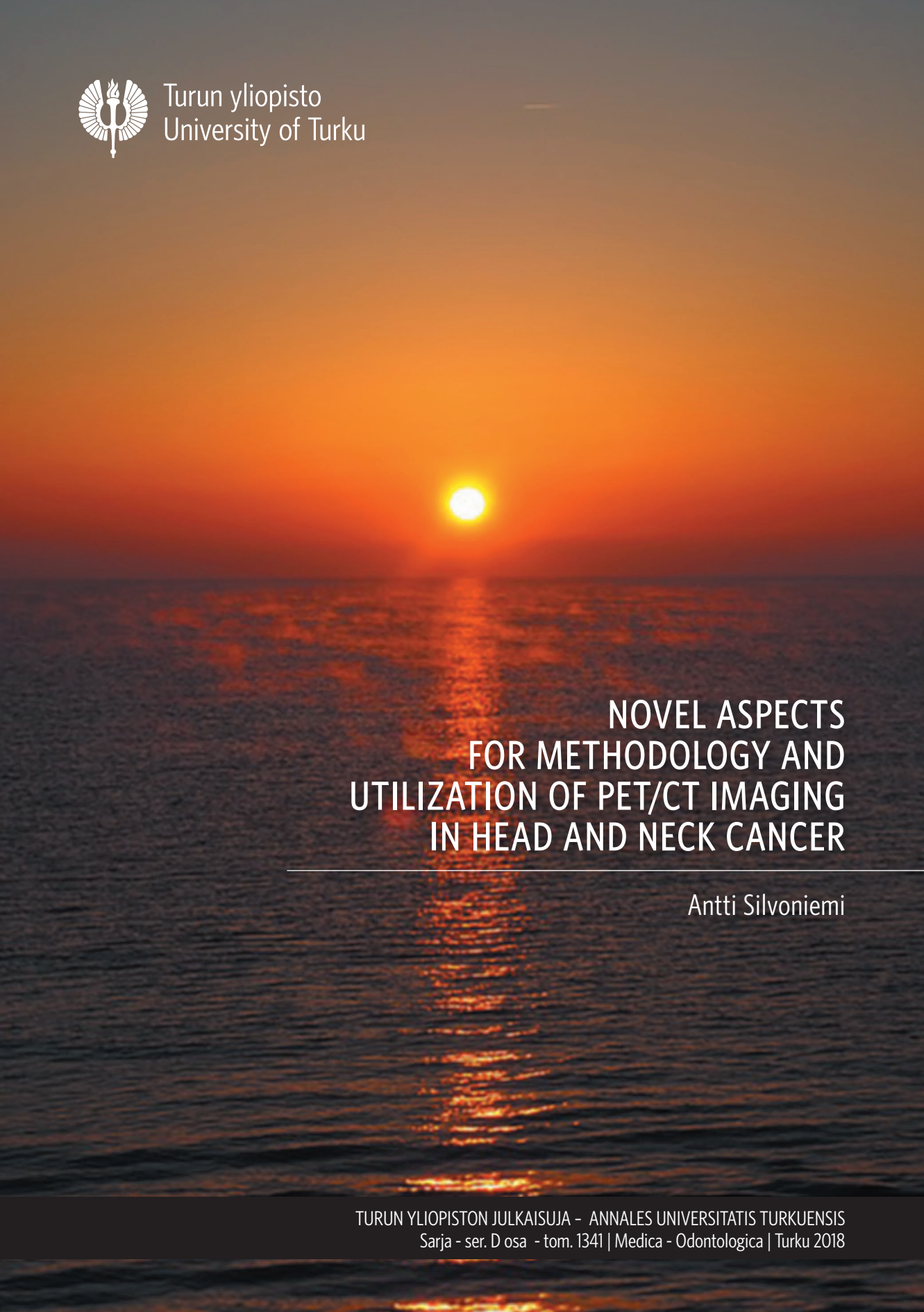




Turun yliopisto
University of Turku



NOVEL ASPECTS
FOR METHODOLOGY AND
UTILIZATION OF PET/CT IMAGING
IN HEAD AND NECK CANCER

Antti Silvonieni



Turun yliopisto
University of Turku

NOVEL ASPECTS FOR METHODOLOGY AND UTILIZATION OF PET/CT IMAGING IN HEAD AND NECK CANCER

Antti Silvoniemi

University of Turku

Faculty of Medicine
Department of Otorhinolaryngology – Head and Neck Surgery
Doctoral Programme in Clinical Research (DPCR)
Turku PET Centre
Turku University Hospital
National Graduate School of Clinical Investigation

Supervised by

Professor Heikki Minn, MD, PhD
Turku PET Centre and
Department of Oncology and Radiotherapy
University of Turku, Finland

Adjunct Professor Tove J. Grönroos, PhD
Turku PET Centre
University of Turku, Finland

Professor (Emeritus) Reidar Grénman, MD, PhD
Department of Otorhinolaryngology – Head
and Neck Surgery
University of Turku, Finland

Reviewed by

Professor Esther G.C. Troost
Department of Radiation Oncology
University Hospital Carl Gustav Carus of
Technische Universität
Dresden, Germany

Professor Eirik Malinen
Department of Medical Physics
Oslo University Hospital
Oslo, Norway

Opponent

Adjunct Professor, Chief Physicist
Mikko Tenhunen
Helsinki University Hospital Cancer Center
University of Helsinki, Finland

Cover photo “Sunrise” is downloaded from www.pixabay.com and reproduced under the Creative Commons License CC0.

The originality of this thesis has been checked in accordance with the University of Turku quality assurance system using the Turnitin OriginalityCheck service.

ISBN 978-951-29-7185-5 (PRINT)

ISBN 978-951-29-7186-2 (PDF)

ISSN 0355-9483 (Print)

ISSN 2343-3213 (Online)

Painosalama Oy – Turku, Finland 2018

*This work is dedicated to all patients
with head and neck cancer*

ABSTRACT

Antti Silvoniemä

Novel aspects for methodology and utilization of PET/CT imaging in head and neck cancer

University of Turku, Faculty of Medicine, Department of Otorhinolaryngology – Head and Neck Surgery, Doctoral Programme in Clinical Research (DPCR), Turku PET Centre – Annales Universitatis Turkuensis, Turku, Finland, 2018

Positron emission tomography (PET), combined with computed tomography (CT), plays a key role in the management of head and neck cancer (HNC). In this thesis, novel aspects for PET/CT imaging of HNC regarding low oxygen levels, or hypoxia, and detection of glucose metabolism were evaluated. Hypoxia is a frequently observed hallmark of cancer contributing to radiotherapy resistance and poor prognosis. Enhanced glucose metabolism is characteristic of a malignant tumor, which is exploited in an everyday clinical application of [^{18}F]FDG PET imaging.

This study aimed to further investigate the feasibility of a novel hypoxia PET tracer [^{18}F]EF5 and the potential of dynamic [^{18}F]FDG PET/CT imaging in HNC. The first study indicated a favorable human biodistribution and radiation dosimetric profile of the hypoxia tracer [^{18}F]EF5. The second preclinical study showed that the growth rate of human HNC xenografts in nude mice during the exponential growth period correlated with [^{18}F]EF5 uptake in PET/CT images. In the third study, paired [^{18}F]EF5 PET/CT scans performed for untreated HNC patients with a median time interval of seven days presented predominantly highly repeatable results. In the fourth study, advanced mathematical methodology for tracer uptake analysis was evaluated using dynamic [^{18}F]FDG PET/CT in patients who were referred to chemoradiotherapy for oropharyngeal cancer. However, the method showed only a modest performance in the distinction of malignant, inflammatory and healthy tissues. In conclusion, further evaluation of [^{18}F]EF5 PET/CT imaging and dynamic [^{18}F]FDG PET/CT imaging seems important in the development of more effective strategies for the management of HNC.

Keywords: PET, PET/CT, head and neck cancer, [^{18}F]EF5, [^{18}F]FDG, hypoxia, molecular imaging, radiotherapy planning

TIIVISTELMÄ

Antti Silvoniemmi

Pään ja kaulan alueen syövän PET/TT-kuvantaminen – menetelmien ja hyödyntämisen uusia näkökulmia

Turun yliopisto, Lääketieteellinen tiedekunta, Korva-, nenä- ja kurkkutautioppi, Turun kliininen tohtoriohjelma (TKT), Valtakunnallinen PET-keskus – Annales Universitatis Turkuensis, Turku, Suomi, 2018

Positroniemissiotomografian (PET) ja tietokonetomografian (TT) yhdistävää PET/TT-kuvausta käytetään yleisesti pään ja kaulan alueen syövän hoidon suunnittelussa ja hoitovasteen seurannassa. Nykyään käytettävässä PET-kuvantamistekniikassa kasvainkudoksen osoittaminen perustuu vilkastuneeseen sokeriaineenvaihduntaan, joka on syöpäkasvaimen yleinen ominaispiirre. PET-kuvantamiseen liittyy myös monia uusia sovellusmahdollisuuksia. Tässä väitöskirjatyössä tutkittiin sokeriaineenvaihduntaan perustuvien menetelmien lisäksi kasvaimessa esiintyvän matalan happiosapaineen eli hypoksian osoittamista. Hypoksia on syöpäkasvaimen aggressiivisuuteen liittyvä ominaisuus, joka huonontaa potilaan paranemistustetta ja erityisesti sädehoidon tehoa kasvaimen.

Ensimmäisessä osatyössä osoitettiin, että uusi hypoksiaa kuvaava PET-merkkiaine [¹⁸F]EF5 on säteilyannoksen ja muidenkin ominaisuuksiensa puolesta turvallinen ja se soveltuu käytettäväksi ihmiselimestön PET-kuvauksessa. Toisessa osatyössä kasvatettiin hiirille kokeellisia kasvaimia ihmisen pään ja kaulan alueen syöpäkasvaimista eristetyistä soluista. Hiirille suoritettiin PET/TT-kuvauksia, joissa todettiin [¹⁸F]EF5-merkkiaineen kerääntyvän eniten niihin kasvaimiin, jotka olivat kasvaneet eksponentiaalisen kasvujakson aikana nopeasti. Kolmannessa osatyössä tutkittiin [¹⁸F]EF5-PET/TT-kuvauksen tulosten toistettavuutta kuvaamalla pään ja kaulan alueen syöpään sairastuneita potilaita kaksi kertaa 5-7 vuorokauden välein. Peräkkäisten kuvausten tulosten todettiin olevan pääosin varsin yhteneviä keskenään. Neljännessä osatyössä tehtiin suunielun syöpään sairastuneille potilaille sokeriaineenvaihdunnan osoittamiseen perustuva dynaaminen [¹⁸F]FDG-PET/TT-kuvauks. Kuvien tulkinnassa arvioitiin uutta matemaattista menetelmää syöpäkasvaimen, tulehduksen ja terveen kudoksen erottamiseen toisistaan. Tutkimushavainnot olivat mielenkiintoisia, mutta menetelmää tulee vielä kehittää käytännön sovellusten aikaansaamiseksi. Tässä väitöskirjatutkimuksessa saatiin täsmentävää tietoa pään ja kaulan alueen syövän PET/TT-kuvauksen menetelmiin liittyvistä mahdollisuuksista ja rajoituksista. Jatkossa on edelleen tärkeää tutkia sekä [¹⁸F]EF5-PET/TT-kuvauksen että dynaamisen [¹⁸F]FDG-PET/TT-kuvauksen hyödyntämistä, kun kehitetään uusia ja tehokkaampia syövän hoitomenetelmiä.

Avainsanat: PET, PET/TT, pään ja kaulan alueen syöpä, [¹⁸F]EF5, [¹⁸F]FDG, hypoksia, molekulaarinen kuvantaminen, sädehoidon suunnittelu

TABLE OF CONTENTS

ABSTRACT.....	4
TIIVISTELMÄ.....	5
ABBREVIATIONS.....	8
LIST OF ORIGINAL PUBLICATIONS.....	10
1 INTRODUCTION.....	11
2 REVIEW OF LITERATURE.....	13
2.1 Principles of PET/CT imaging.....	13
2.1.1 Production of PET tracers.....	13
2.1.2 Physical and technical principles of PET imaging.....	14
2.1.3 Hybrid imaging modalities and coregistration of images.....	15
2.1.4 Biological aspects of radiation exposure of a PET tracer.....	16
2.2 Head and neck cancer.....	17
2.3 Microenvironment of HNC as a target for PET/CT imaging.....	20
2.3.1 Glucose metabolism.....	21
2.3.1.1 [¹⁸ F]FDG as an oncologic PET tracer for detection of glucose metabolism.....	22
2.3.1.2 Static [¹⁸ F]FDG PET/CT imaging.....	23
2.3.1.3 Clinical applications of [¹⁸ F]FDG PET/CT in HNC.....	24
2.3.1.4 Temporal dimension and quantitative analysis of [¹⁸ F]FDG PET/CT imaging.....	27
2.3.2 Tumor hypoxia.....	28
2.3.2.1 Angiogenesis and blood flow in malignant tumors.....	29
2.3.2.2 Hypoxia in malignant tumors.....	29
2.3.2.3 Therapeutic interventions involving hypoxia in HNC	32
2.3.2.4 Non-PET methods for detection and quantification of tumor hypoxia.....	35
2.3.2.5 PET imaging of tumor hypoxia.....	38
2.3.2.6 Dynamic nature of tumor hypoxia.....	46
2.3.3 Additional cellular and molecular processes feasible for PET/CT imaging in HNC.....	48
2.4 Image segmentation and clustering algorithms.....	49
2.5 Advanced applications of PET/CT imaging in RT planning of HNC.....	50
3 AIMS OF THE STUDY.....	54
4 PATIENTS AND EXPERIMENTAL TUMOR MODELS.....	55
4.1 Patients.....	55
4.2 Experimental animals, cell lines and tumor models.....	56
4.3 Ethical considerations.....	57

5	METHODS	59
5.1	Synthesis of PET tracers (Studies I-IV).....	59
5.2	Imaging protocols (Studies I-IV)	59
5.2.1	Study I.....	59
5.2.2	Study II.....	60
5.2.3	Study III.....	61
5.2.4	Study IV.....	61
5.3	Clinical and biological safety monitoring of exposure of [¹⁸ F]EF5 (Study I)	62
5.4	Direct oxygen measurements (Study II)	63
5.5	Image analysis (Study I-IV).....	63
5.5.1	Image reconstruction	63
5.5.2	Analysis of tracer uptakes	64
5.6	Radiation absorbed dose calculations (Study I).....	65
5.7	Evaluation of the performance of dynamic features in the distinction of different tissue types (Study IV).....	66
5.8	Statistical analysis (Study I-IV)	68
6	RESULTS	69
6.1	Biodistribution and radiation dosimetry of [¹⁸ F]EF5 (Study I)	69
6.2	Clinical safety of [¹⁸ F]EF5 (Study I).....	70
6.3	Uptake of PET tracers in experimental tumors and tumor growth rate (Study II)	71
6.4	Direct oxygen measurements of experimental tumors (Study II).....	73
6.5	Repeatability of intratumor uptake in paired [¹⁸ F]EF5 PET/CT scans (Study III).....	76
6.6	Analysis of dynamic [¹⁸ F]FDG images (Study IV)	81
7	DISCUSSION	87
7.1	Biodistribution, dosimetry and clinical safety of [¹⁸ F]EF5 (Study I)	87
7.2	Association between PET tracer uptake and experimental tumor growth (Study II).....	89
7.3	Repeatability of hypoxia imaging using [¹⁸ F]EF5 PET/CT scans (Study III).....	91
7.4	Performance of dynamic features of [¹⁸ F]FDG uptake in the distinction of different tissue types (Study IV).....	94
7.5	Future perspectives	98
8	CONCLUSIONS.....	101
	ACKNOWLEDGEMENTS	102
	REFERENCES.....	105
	ORIGINAL PUBLICATIONS.....	125

ABBREVIATIONS

[¹⁸ F]JEF5	2-(2-nitro-1H-imidazol-1-yl)-N-(2,2,3,3,3-pentafluoropropyl)-acetamide labeled with [¹⁸ F]
[¹⁸ F]FAZA	¹⁸ F-fluoroazomycinarabioside
[¹⁸ F]FDG	¹⁸ F-fluorodeoxyglucose
[¹⁸ F]FETNIM	¹⁸ F-fluoroerythronitroimidazole
[¹⁸ F]FMISO	¹⁸ F-fluoromisonidazole
[¹⁸ F]HX4	¹⁸ F-flortanidazole
BTV	Biological target volume
CAIX	Carbonic anhydrase 9
CoR	Coefficient of repeatability
COV	Coefficient of variation
CRT	Chemoradiotherapy
CT	Computed tomography
DPBC	Dose painting by contours
DPBN	Dose painting by numbers
DTPI	Dual-time-point imaging
ECG	Electrocardiogram
ED	Effective dose
EDE	Effective dose equivalent
EGFR	Epidermal growth factor receptor
FHV	Fractional hypoxic volume
FOV	Field of view
GLUT	Glucose transporter protein
GMM	Gaussian mixture model
GTV	Gross tumor volume
HC	Hottest cluster of tumor voxels
HIF	Hypoxia inducible factor
HNC	Head and neck cancer
HPLC	High-performance liquid chromatography

Abbreviations

HPV	Human papilloma virus
HV	Hypoxic volume
ICC	Intraclass correlation coefficient
IHC	Immunohistochemistry
LoA	Limit of agreement
MATV	Metabolically active tumor volume
MRI	Magnetic resonance imaging
NPV	Negative predictive value
NSCLC	Non-small-cell lung cancer
PENN	University of Pennsylvania
PET	Positron emission tomography
PPV	Positive predictive value
$p_{ti}O_2$	Oxygen partial pressure in tissue
PTV	Planning target volume
PVE	Partial volume effect
RT	Radiotherapy
SCC	Squamous cell carcinoma
SD	Standard deviation
SPECT	Single-photon emission computed tomography
SUV	Standardized uptake value
TAC	Time-activity curve
TMR	Tumor-to-muscle uptake ratio
TNM	Cancer staging system
TURKU	University of Turku
VEGF	Vascular endothelial growth factor
VOI	Volume of interest

LIST OF ORIGINAL PUBLICATIONS

This thesis is based on the following original publications, which are referred to in the text by the Roman numerals I-IV.

- I Lin LL*, Silvonieminen A*, Stubbs JB, Rengan R, Suilamo S, Solin O, Divgi C, Eskola O, Sorger J, Kachur A, Hahn SM, Grönroos TJ, Forsback S, Evans SM, Koch CJ, Minn H. Radiation dosimetry and biodistribution of the hypoxia tracer [¹⁸F]EF5 in oncologic patients. *Cancer Biother Radiopharm*. 2012 Sep;27(7):412-419
- II Silvonieminen A, Silén J, Forsback S, Löyttyniemi E, Schrey AR, Solin O, Grénman R, Minn H, Grönroos TJ. Evaluation of repeated [¹⁸F]EF5 PET/CT scans and tumor growth rate in experimental head and neck carcinomas. *EJNMMI Res*. 2014 Dec 16;4:65
- III Silvonieminen A, Suilamo S, Laitinen T, Forsback S, Löyttyniemi E, Vaitinen S, Saunavaara V, Solin O, Grönroos TJ, Minn H. Repeatability of tumour hypoxia imaging using [¹⁸F]EF5 PET/CT in head and neck cancer. *Eur J Nucl Med Mol Imaging*. 2018 Feb;45(2):161-169
- IV Silvonieminen A, Din MU, Suilamo S, Shepherd T, Minn H. Radiotherapy volume delineation using dynamic [¹⁸F]FDG PET/CT imaging in patients with oropharyngeal cancer: a pilot study. *Int J Comput Assist Radiol Surg*. 2016 Nov;11(11):2059-2069

* These two authors have contributed equally to the manuscript.

The original publications have been reprinted with permission of the copyright holders.

1 INTRODUCTION

Hybrid positron emission tomography and computed tomography (PET/CT) is a fundamental imaging tool in clinical oncology and translational cancer research. Head and neck cancer (HNC) belongs to tumor types for which PET/CT imaging has proven to be a powerful diagnostic tool (Branstetter et al. 2005). In general, the main advantage of hybrid PET imaging is that it allows for combining functional and molecular information about living tissues obtained with PET imaging into anatomical information derived from a CT or magnetic resonance (MR) image.

In clinical practice, the use of ^{18}F -fluorodeoxyglucose ($[^{18}\text{F}]\text{FDG}$) PET/CT is well established in staging, treatment planning and monitoring therapy response of squamous cell carcinoma of the head and neck. Moreover, there are many additional applications of PET imaging under evaluation, since numerous other tracers are available for mirroring the different phenomena in the microenvironment of the tumor. In recent years, several new PET tracers for imaging of HNC have been investigated, and innovative imaging protocols and applications have been examined (Differding et al. 2015).

There are some special characteristics of tumor biology that are particularly interesting in the study of HNC. One of these is the low oxygen level, or hypoxia, in tumors, which has been shown to contribute to treatment resistance and poor prognosis (Brizel et al. 1997, Vaupel et al. 2004, Janssen et al. 2005). For years, researchers have patiently attempted to acquire more knowledge and experience on hypoxia imaging with PET. The results of hypoxia PET images have also been evaluated in the light of treatment outcomes and overall survival (Fleming et al. 2015). Being a complex phenomenon, tumor hypoxia has proven to be challenging to understand. There is still a great need for further research to better recognize the potential of hypoxia imaging with PET and overcome hypoxia-related challenges in the treatment of HNC.

Recently, the concept of personalized medicine has gained a central position in modern cancer management, with a special interest in the advent of genome-based tailored medical therapies (Renfro et al. 2017). In HNC, there are also some innovative strategies for individualized radiotherapy (e.g., personalized dose-escalation and de-escalation protocols and adaptive radiotherapy) (Grégoire et al. 2015, Schinagl et al. 2009). All of these upcoming advancements in cancer treatment will require multidisciplinary expertise. PET imaging promises to be an essential part of these new procedures, serving as a modality for imaging of metabolism and tumor receptors on a whole-body level (Mena et al. 2017).

In this thesis, selected fields of PET/CT imaging in HNC were investigated in separate study protocols. First, the characteristics of a novel hypoxia PET tracer [^{18}F]EF5 were evaluated in two clinical studies, which addressed radiation dosimetry and safety of the tracer and the repeatability of intratumoral uptake in repeated PET/CT scans, respectively. Second, tumor growth rate and uptake of [^{18}F]EF5 in human HNC xenografts were evaluated in an experimental study. Finally, advanced mathematical methodology for interpretation of dynamic [^{18}F]FDG PET/CT images was introduced in a pilot clinical study, the aim of which was to differentiate malignant, inflammatory and healthy tissues.

2 REVIEW OF LITERATURE

2.1 Principles of PET/CT imaging

Positron emission tomography (PET) is a method that utilizes short-lived isotopes in functional imaging of living tissues. PET imaging is based on the use of a radiolabeled compound that binds to specific sites in a living organism to depict physiological or pathological processes in the target tissue. Hybrid imaging, where PET is combined with computed tomography (CT) or magnetic resonance imaging (MRI), provides both functional (PET) and anatomical information (CT or MRI).

2.1.1 Production of PET tracers

The first step in PET imaging is the production of a radioactive tracer. Several short-lived radioactive nuclides that are so-called beta⁺ emitters (e.g., ¹⁸F, ¹⁵O, ¹³N and ¹¹C, with half-lives of 109.8 min, 2.0 min, 10.0 min and 20.4 min, respectively) may be used. The nuclides are usually produced with a particle accelerator called cyclotron. In the cyclotron, charged particles are accelerated by a rapidly varying electric field and static magnetic field. Target nuclides are then bombarded with charged particles in order to achieve a daughter nuclide. As an example, ¹⁸F is produced in a reaction in which enriched water [¹⁸O]H₂O is bombarded with protons.

The radiochemical synthesis of a PET tracer includes several steps from the handling of the precursors to the finalization of the product (Basu et al. 2011). The process is performed and controlled by qualified personnel. During all periods of the synthesis, there are significant time constraints because of the short half-lives of the isotopes. An important final step of the production of the PET tracer is the quality control step, in which the chemical, radiochemical and microbiological purity of the product is confirmed.

There is an uncountable number of compounds that can be labeled with a radioactive isotope in radiochemical reactions. Nevertheless, development of a new PET tracer is an extensive process, which includes the chemical characterization of the molecule and a thorough evaluation of the pharmacokinetics and pharmacodynamics of the compound, first in preclinical and then in clinical studies. All of the processes in the production of a tracer have to be qualified and validated by certified personnel according to the principals of Good Manufacturing Practices (GMP).

2.1.2 Physical and technical principles of PET imaging

Beta⁺ emitters are unstable nuclides that undergo radioactive beta⁺ decay. In this reaction, a proton is transformed into a neutron, and the nucleus emits a positron (p⁺) and an electron neutrino (ν_e). A positron is an antiparticle with a positive charge and ‘mass’ corresponding to that of electron. The emitted positron may traverse only a few millimeters before it interacts with an electron. This interaction leads to annihilation, in which both particles are transformed into energy in the form of two photons of gamma radiation. The photons are then emitted in opposite directions at an angle of approximately 180 degrees (Figure 1).

In PET imaging, the gamma photons derived from annihilation are registered in a detector ring, which can determine a coincidence event (Figure 1). This refers to a simultaneous detection of photons on a horizontal axis at opposite sites of the detector ring. The line between these two detector units is called the line of response (LOR). The number of coincidence events is directly correlated to the radioactivity located on the LOR. Using the LORs from all different angles makes it possible to produce a sinogram, which is an initial projection image from the raw data (Turkington 2001).

The attenuation of gamma radiation varies depending on the depth of the site of beta emission as well as the electron concentration of tissues between the imaged target site and PET scanner detector. Therefore, performing the attenuation correction for raw data before the image reconstruction is crucial, because the loss of true coincidence event detection can range between 50% and 90% due to the attenuation. There are also other important factors affecting the acquisition of raw data that have to be corrected, such as scattering of radiation, detector dead time and random events (Basu et al. 2011).

A PET scanner consists of a detector ring composed of scintillation crystals and photomultiplier tubes arranged in several rings. These detector units register gamma radiation and convert it into visible light. Thereafter, the light signal is converted into digital form to be further processed. During the reconstruction of the PET image, the raw data of gamma counts is first processed to sinograms; then, specific reconstruction algorithms are needed to produce the final PET images (Turkington 2001).

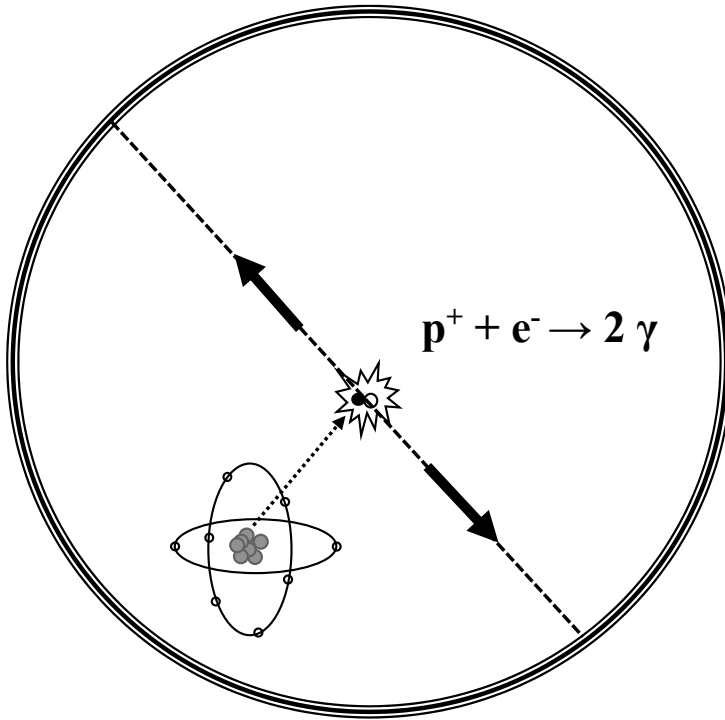


Figure 1 The principles of beta⁺ decay, annihilation and detection of gamma photons with PET scanner detector ring. The beta⁺ decay of 18-fluorine, which is converted into 18-oxygen, is presented as an example. In this reaction, a positron (p^+) and an electron neutrino (ν_e) are emitted. When the positron interacts with an electron (e^-), this particle-antiparticle unit is annihilated and transformed to energy. Two photons of gamma radiation (γ) are emitted to opposite directions. The PET scanner detector ring registers the simultaneous detection of gamma photons.

2.1.3 Hybrid imaging modalities and coregistration of images

Over the last decade, combination of functional PET with anatomical reference method such as CT or MRI has been a standard. Both of these combination modalities have advantages and disadvantages in practical use.

Briefly, CT imaging is based on a system in which an x-ray source rotates around the object to be imaged while at the same time an x-ray sensor on the opposite side

of the circle is detecting. In modern CT scanners, there are multiple rows of detectors, which acquire multiple cross-sections simultaneously. As in a PET scanner, the raw data is processed with numerous algorithms to perform image reconstruction. Distinction between different types of soft tissues with CT is generally challenging, but it offers a favorable contrast in the imaging of bone lesions. Furthermore, CT is also appropriate for imaging of the thoracic region. In hybrid imaging, attenuation correction for PET images is easily performed with the use of CT-based information of tissue electron densities.

MRI is an advantageous imaging method, as it does not utilize radioactivity or ionizing radiation. MRI is based on a phenomenon called nuclear magnetic resonance. For example, nuclei of hydrogen atoms (protons) are able to absorb and emit radio frequency energy under the influence of a strong external magnetic field. Different contrasts between tissues can be generated using different protocols of pulse sequences. MRI shows outstanding performance in the differentiation of soft tissues such as brain tissues or muscles. In the head and neck region, MRI is able to offer remarkably better soft tissue differentiation compared to CT. On the other hand, larger air-filled cavities (e.g., lungs) are challenging to image with MRI and therefore are not a favorable target for MRI. A specific problem in the use of PET/MRI is the performance of attenuation correction (Becker and Zaidi 2014).

In hybrid imaging, an anatomical reference image (CT or MRI) is co-registered with the PET image to obtain fused images. Registration can be performed based solely on anatomical landmarks (rigid registration) or while also paying attention to various other aspect, such as rotation and movements (non-rigid registration). Recent developments in computational resources have enabled remarkable advancements in the processes utilized in registration algorithms (Oliveira and Tavares 2014).

2.1.4 Biological aspects of radiation exposure of a PET tracer

Medical imaging is intended to directly benefit the patient. On the other hand, ionizing radiation, such as gamma radiation or X-ray, is harmful because it increases the risk of cancerous mutations in the genome and may cause teratogenic harms. Thus, radiation exposure is a critical issue in the field of clinical imaging and should be assessed to consider the justification of an individual imaging procedure.

Absorbed dose is a physical quantity that represents the energy of ionizing radiation imparted to matter per unit mass. In the SI system, the unit of absorbed dose is gray (Gy), which is determined as joules per kilogram. Equivalent dose is a

quantity that takes into account the radiation type as a factor of health risk. The unit of equivalent dose is sievert (Sv), and the coefficient between absorbed dose and equivalent dose is 1 in the case of gamma radiation.

Effective dose (ED) is a quantity that is generally used in radiation protection. It is the tissue-weighted sum of the equivalent doses of all organs and tissues of the human body. The principle of calculation of ED is determined by the International Commission on Radiological Protection (ICRP 1991). ED represents the whole body risk of stochastic effects, such as solid cancers. There is a list of weighting factors for different organs and tissues that are used in the calculation of ED. A specific weighting factor is based on the radiation sensitivity of the organ and the proportion of the body mass that the organ represents. For example, red bone marrow and gonads are highly sensitive to radiation, whereas muscles and cortical bones have remarkably lower sensitivity. Previously, the term effective dose equivalent (EDE) was used (ICRP 1976). It is calculated in a similar way to ED, but the list of organ-specific weighting factors includes fewer organs, and more organs are referred as 'remainder of body' compared to the calculation protocol of ED.

Every PET tracer must be evaluated in a biodistribution and dosimetry study before larger clinical use in order to consider the radiation exposure and safety of the tracer. In a dosimetry study, the absorbed doses of individual organs as well as the ED are determined. For these calculations, the uptake data of the tracer in specific organs is needed, as well as a phantom system that also takes into account the absorbed doses for specific organs from the surrounding adjacent organs.

2.2 Head and neck cancer

Head and neck cancer (HNC) comprises a group of malignant neoplasms occurring in the lips, oral cavity, pharynx, larynx, salivary glands and nasal and paranasal cavities. In the ICD-10 system, these diseases are classified with the following code numbers: C00-14, C30-31 and C32. Of all HNC cases, at least 90% are squamous cell carcinomas (SCC). The proportion of SCCs of all malignancies is even higher in cancers of the lips, oral cavity, pharynx and larynx, whereas the histopathologic spectrum is more diverse among the tumors involving the salivary glands and the nasal and paranasal cavities. HNC constitutes a 6% proportion of all new malignancies and more than 650,000 cases, with more than 350,000 deaths worldwide annually (Chaturvedi et al. 2013, Ferlay et al. 2015). There were, on average, 784 registered cases of HNC and 262 deaths due to the disease annually in Finland during the years 2010–2014 (www.cancer.fi/syoparekisteri/en).

There are two major groups of HNC patients with different etiologic profiles. The first one refers to the most important risk factors, smoking and heavy alcohol use, which may also act as synergistic risk factors (Blot et al. 1988). Another important etiologic profile for HNC refers to human papilloma virus (HPV) infection, which is strongly associated with oropharyngeal cancer, especially tonsillar cancer and cancer of the base of tongue. HPV-positive tumors have a different molecular pathogenesis and a better prognosis compared to their HPV-negative counterparts (Ang et al. 2010). In addition to these two profiles, there are also some other well-characterized etiological factors for HNC. Chronic Epstein-Barr virus (EBV) infection is associated with nasopharyngeal cancer, and especially with its non-keratinizing subtypes, which are observed in higher incidence rate in some endemic regions (e.g., in East and South-East Asia) compared to the rest of the world (Chua et al. 2016). Solar ultraviolet radiation is considered to be a causal factor for lip cancer (Kenborg et al. 2010). Chronic mucosal inflammation, such as oral lichen planus, has been proposed to have a role in the carcinogenesis of oral cancers (Rödström et al. 2004, van der Meij et al. 2007). Moreover, some other factors have been suggested to be associated with the risk of HNC, such as a diet low in fresh fruits and vegetables (McLaughlin et al. 1988).

The typical symptoms of HNC depend on the site and size of the tumor. The most common symptoms are hoarseness, odynophagia, dysphagia, sore throat, stridor and the sensation of a mass in the oral cavity or throat. Furthermore, patients very often present with a painless neck mass. The diagnostic and staging procedures consist of a thorough physical examination (Figure 2), endoscopic procedures, histopathological biopsy from primary tumor and possibly also from a metastatic lymph node and imaging with CT, MRI and/or PET.

The treatment protocol is diverse depending on the tumor site, histopathology, size and stage. In general, first-line treatment is either surgery or (chemo)radiotherapy (CRT) or a combination of these. The surgical treatment of the primary tumor consists of a resection of the tumor with margins and reconstruction of the tissue defects when necessary. Modern surgical treatment modalities allow for favorable functional results even in many cases of a large primary tumor. In the cases of locally advanced disease and also in many cases of a larger (T3-T4) primary tumor with no signs of metastasis in the neck, the regional lymph nodes are also removed in an operation called neck dissection (Green et al. 2016, Robbins et al. 2013, Coskun et al. 2015).

CRT may be a definitive treatment or part of a combination treatment in cases of irradical resection of primary tumor and/or lymph nodes and extracapsular tumor spread in lymph nodes. In CRT, a platinum-based cytotoxic drug, mostly cisplatin,

is administered during radiotherapy (RT) for an additive effect in the therapy (Bernier et al. 2004, Adelstein et al. 2003). Cetuximab, a monoclonal antibody that binds to epidermal growth factor receptors (EGFR), may be an alternative agent for use in CRT in cases of renal injury or sensorineural hearing loss (Bonner et al. 2006). Already for several years, CRT has been the standard recommended definitive treatment in, for example, stage III and IV tumors in oropharynx, hypopharynx and nasopharynx. In these cases, the neck is also treated with RT.



Figure 2 Cancer of the mobile tongue is usually detected in a clinical examination. A squamous cell carcinoma of the tongue in a young woman is presented in this picture. (Reproduced from Credé et al. 2012 under the terms of the Creative Commons Attribution License. <http://www.oapublishinglondon.com/images/article/pdf/1354880418.pdf>)

The prophylactic treatment of neck lymph nodes (N0) when necessary varies largely depending on the primary tumor site and size and several other factors. Surgical treatment, RT, CRT or clinical follow-up are alternative or combinable procedures in distinct situations. Sentinel lymph node biopsy may also be utilized in some particular types of mucosal SCC of the head and neck (de Bree et al. 2015, Leusink et al. 2012, Green et al. 2016).

In residual cases after CRT and in cases of local recurrence after primary surgery, second-line surgical treatment is considered. In recurrent and metastatic disease, platinum-based treatment, with either cisplatin or carboplatin combined with 5-fluorouracil, has traditionally been recommended. Additionally, cetuximab has been confirmed to be effective when using combination therapy (Vermorken et al. 2008). Recently, evidence supporting the use of two immunotherapeutic drugs,

pembrolizumab and nivolumab, has been obtained, and these drugs have been approved by Food and Drug Administration (FDA) for recurrent and metastatic HNSCC in a 3-month period (Moreira et al. 2017).

The treatment of HNC may have a significant impact on the performance and quality of life of the patient. Radical resection of a large tumor, even with optimal reconstructive surgery, may lead to disturbance of speech and/or swallowing. The development of intensity-modulated and image-guided RT has improved local and regional control of the disease, and side effects have been reduced. Nevertheless, RT and CRT may also cause long-standing or even lifelong side effects, such as dysfunction of the thyroid gland and salivary glands, dysphagia or osteoradionecrosis of the mandible (Boomsma et al. 2011, Hawkins et al. 2018, Lambade et al. 2013).

The prognosis of HNC varies largely depending on the site, size, stage, histopathological grade and HPV-status of the tumor. High survival rates have typically been reported in, for example, lip cancer and glottic cancer, whereas hypopharyngeal cancer has a markedly lower survival rate. The large size of the primary tumor as well as nodal involvement contribute significantly to the lower survival rate (Argiris et al. 2008, Baatenburg de Jong et al. 2001, Gourin and Podolsky 2006). In the whole group of HNC combining all stages of disease, five-year disease-specific survival rates of some 50–66 % have been reported (Argiris et al. 2008, Ringash 2015).

In the clinical setting of HNC, one of the major challenges is that, in many cases, the disease is found at an advanced stage. Developing better screening strategies and tools for early diagnosis of HNC would definitely be a desirable goal. Nevertheless, extensive research efforts should be directed to the development of improved treatment strategies of advanced HNC. Detailed knowledge on the biological as well as the clinical features of HNC is expected to play a key role in the improvement of the overall survival and quality of life of these patients.

2.3 Microenvironment of HNC as a target for PET/CT imaging

Functional imaging, and particularly PET/CT imaging, provides countless possibilities to illustrate specific processes in the cells and microenvironment of living tissues. In malignant solid tumors, various characteristics of cellular and microenvironmental processes differ greatly from those of normal healthy tissues. Based on this fact, it is possible to detect and even identify malignant tissue with PET/CT imaging. Furthermore, some PET tracers allow for the categorization of different

tumor phenotypes, such as dominantly hypoxic tumors. Another important approach is tumor receptor imaging, which refers to studying of molecular pathways and gene expression in malignant tissue. This chapter focuses on two major processes, glucose and oxygen metabolism, which are especially important in the field of HNC. Also, a few additional processes in HNC that are already exploited as targets for PET/CT imaging are mentioned briefly.

2.3.1 Glucose metabolism

Glucose is the main energy source for mammalian cells. As a polar molecule, glucose is transported into the cell by glucose transporter proteins (GLUT) (Figure 3). Energy production is initiated with glycolysis, the process of breaking down a glucose molecule, which is possible in both aerobic and anaerobic conditions. The first reaction of glycolysis is the transformation of glucose to glucose-6-phosphate, and this reaction is catalyzed by hexokinase enzymes. Glucose-6-phosphate is no longer able to exit the cell. The end product of glycolysis is pyruvate, which can proceed in aerobic conditions to mitochondria, where oxidative phosphorylation takes place. In anaerobic conditions, glycolysis continues in the cytoplasm (anaerobic glycolysis) with a reaction in which pyruvate is transformed to lactate. This is an inefficient way to produce energy compared to oxidative phosphorylation (Figure 3).

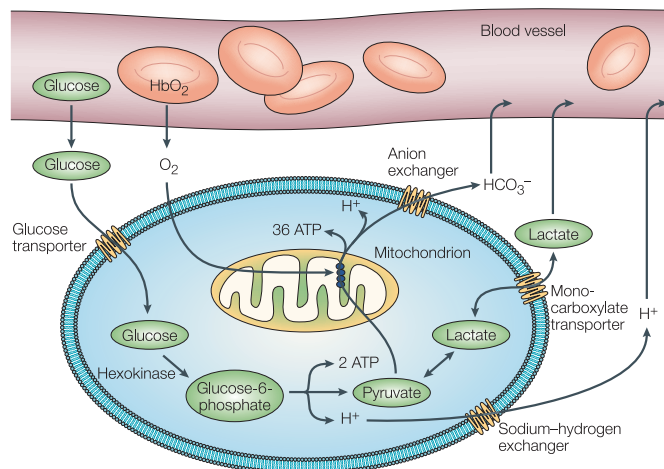


Figure 3 Glucose metabolism in mammalian cells (Gatenby and Gillies 2004). (Reprinted by permission from Macmillan Publishers Ltd/ Springer Nature: *Nature Reviews Cancer* 4:891-899: Why do cancers have high aerobic glycolysis? Gatenby RA, Gillies RJ, 2004. The journal's homepage: www.nature.com/nrc/)

The presence of oxygen causes inhibition of glycolysis, a phenomenon called the Pasteur effect (Racker 1974). This is a normal way to limit the rate of glycolysis in a healthy mammalian cell. In cancer cells, glycolysis is highly enhanced, even in the presence of oxygen. This special characteristic of cancer cells is called the Warburg effect, having been discovered by Otto Warburg in the 1920s (Warburg 1930). Warburg proposed that this was the cause of cancer (Warburg hypothesis). The Warburg hypothesis has since been disproven, but the Warburg effect has been confirmed in numerous studies (Potter et al. 2016).

Glycolysis is mainly regulated with GLUT proteins and hexokinases. There is probably a very complex regulation system behind these processes, and at least 13 glucose transporter proteins have been discovered. In cancer cells, there is upregulation of the expression of GLUT-1 and GLUT-3 proteins compared to healthy cells (Mellanen et al. 1994). GLUT-3 has been reported to have both a clearly higher affinity for glucose and at least a fivefold greater transport capacity compared to GLUT-1 (Simpson et al. 2008). In inflammatory tissues, the glucose transportation is more similar to that of normal tissues, but GLUT-3 is also present in inflammatory tissue, since it is expressed in platelets and all types of white cells, including neutrophils, lymphocytes, monocytes and macrophages (Calvo et al. 2010, Mochizuki et al. 2001).

2.3.1.1 [¹⁸F]FDG as an oncologic PET tracer for detection of glucose metabolism

2-deoxy-2-[¹⁸F]fluoro-D-glucose, generally called ¹⁸F-fluorodeoxyglucose ([¹⁸F]FDG), is the most commonly used and also the most well-known PET tracer. The history of human use of [¹⁸F]FDG derives from the 1970s, and the first oncological human PET studies with [¹⁸F]FDG were performed in the 1980s (Alavi and Reivich 2002). [¹⁸F]FDG imaging of cancer is based on enhanced glycolysis in cancer cells (the Warburg effect). Because of the different chemical structure of [¹⁸F]FDG compared to glucose, it does not proceed from the first reaction step of glycolysis, namely transformation to glucose-6-phosphate. Thus, [¹⁸F]FDG is trapped in the cells in a phosphorylated form. The irreversible binding of [¹⁸F]FDG inside the cells is a favorable feature for achieving a proper target-to-background tissue contrast in PET images. [¹⁸F]FDG also has additional advantageous characteristics for being a clinical PET tracer. For instance, there are few metabolites of [¹⁸F]FDG in the blood in the first few hours after administration of [¹⁸F]FDG. Another important characteristic is that [¹⁸F]FDG is, unlike glucose, actively excreted in urine. This feature leads to more rapid blood clearance and allows for even more improved target-to-background contrast (Bar-Shalom et al. 2000).

[¹⁸F]FDG PET imaging is used in detection, staging, treatment planning and monitoring of therapy response in various types of cancers. HNCs, lymphomas and melanoma are generally very well detectable in PET images. The group of other cancers favorably imaged with [¹⁸F]FDG PET includes, for example, breast, cervical, colorectal, esophageal, lung, pancreatic and thyroid cancers. [¹⁸F]FDG PET has a high sensitivity, but a modest specificity in cancer imaging. Several conditions (e.g., infections, inflammation and increase in muscular activity) can cause false positive uptakes and therefore also false suspicions of malignancies. Moreover, metabolic activity in the background tissue (e.g., in the heart muscle and brain), is a limiting factor in tumor imaging (Kellof et al. 2005).

2.3.1.2 *Static [¹⁸F]FDG PET/CT imaging*

A conventional [¹⁸F]FDG PET/CT scan for oncological purposes is performed as static imaging. The patient must fast for at least 4–6 hours before the imaging session. A tracer bolus is administered intravenously, and the patient must be at rest before the imaging session begins. The PET image acquisition usually occurs 50–60 minutes after the injection. With modern PET scanners, the time needed for image acquisition is very short (only 2–3 minutes per bed position). The activity data is summed over the acquisition period. In cases of HNC, the imaging area typically includes the head and neck region, thoracic and upper abdominal regions. Conventional image analysis is based on the determination of tracer uptake in the volume of interest (VOI) as standardized uptake value (SUV). SUV is corrected for the injected activity and most often for the body weight (Equation 1.).

$$SUV = \frac{\text{Activity concentration (kBq/ml)}}{\text{Injected activity (MBq)/Body mass (kg)}}$$

Equation 1. Standardized uptake value.

Alternatively, the factor of body weight may be replaced by the lean body weight or the body surface area. SUV is a semiquantitative unit and has several limitations based on many confounding factors, such as timing of data acquisition, image reconstruction and alternations in body metabolism (Thie 2004). Nevertheless, being a robust and simple value to achieve and calculate, SUV is largely used in clinical cancer imaging. In addition to mean SUV of the whole VOI, SUV_{max} from the voxel of the highest uptake is also typically determined in the targets of interest (e.g., in the suspicion of a malignant lesion).

Uptake data presented as SUV units is not directly comparable between institutions and between patients because of several previously described confounding factors

(Boellaard 2009). Some efforts have been made to standardize and harmonize [^{18}F]FDG PET/CT imaging procedures and reduce the variability of PET image quantification between institutions and scanners. One of these is the EANM/EARL FDG-PET/CT Accreditation Program, which is guided by the European Association of Nuclear Medicine (EANM) Research Ltd. (EARL). This program has led to promising results in harmonizing quantitative PET/CT performance (Kaalep et al. 2018). Nonetheless, it has not proven to be possible to define any specific reference values for SUV to be used in differential diagnosis between benign and malignant lesions. On the other hand, studies on the repeatability of [^{18}F]FDG uptake in malignant tumors have been performed. Based on these, the test-re-test variability of [^{18}F]FDG uptake in tumors using SUV_{mean} or SUV_{max} as a measure of uptake has been observed to be approximately 20–30% (de Langen et al. 2012, Lodge 2017). With regard to these limitations, it is possible to set criteria for clinically significant inpatient changes between tumor SUVs measured before and after treatment for monitoring of therapy response (see below).

Alternative static [^{18}F]FDG uptake parameters have also been evaluated, one of which is tumor-to-blood standard uptake ratio (SUR), which was introduced a few years ago. Initial validation studies have shown promising results reporting improved correlation with the metabolic rate of [^{18}F]FDG and higher repeatability when traditional SUV is replaced with SUR (van den Hoff et al. 2013, Hofheinz et al. 2017).

2.3.1.3 Clinical applications of [^{18}F]FDG PET/CT in HNC

HNC is generally a favorable target for [^{18}F]FDG PET/CT imaging. In fact, there is only one important exception, namely salivary gland tumors, which express variable FDG uptakes not correlated with the rate of malignancy (Johnson and Branstetter 2014). As an example, a benign Warthin's tumor may be very FDG-avid (Horiuchi et al. 1998). However, in SCCs of the head and neck, the feasibility of this method is reasonably consistent and determined by two major characteristics; high sensitivity and limited spatial resolution.

In the head and neck region, [^{18}F]FDG PET/CT is the most sensitive imaging modality of malignant tissue, excluding microscopic metastases less than 5 millimeters in diameter (Manca et al. 2016). On the other hand, the low spatial resolution of the PET image is the major reason for the fact that other modalities, especially MRI, are needed in the anatomical demarcation of the primary tumor. Despite limitations in resolution, [^{18}F]FDG PET/CT is highly useful in the detection of the primary tumor in patients with a SCC metastasis in the neck that is from an un-

known origin. In such cases, the tumor detection rate has been reported to be approximately 40% (Kwee and Kwee 2009, Wong et al. 2012, Zhu and Wang 2013). When the diagnosis of HNC has been made, there are three major indications for [¹⁸F]FDG PET/CT: staging, treatment planning and monitoring therapy response.

STAGING

Staging the primary tumor (T-staging) consists of determining the tumor size and its invasion to adjacent structures. Although [¹⁸F]FDG PET may provide additional information for the delineation of tumor boundaries, the most important methods are anatomical imaging (principally MRI) and clinical examination (Differding et al. 2015).

The nodal involvement of HNC has a significant effect on the prognosis of the patient. Based on higher sensitivity, [¹⁸F]FDG PET/CT is more accurate than other imaging modalities, such as CT and MRI, particularly in the nodal staging of HNC (Evangelista et al. 2014). Along with qualitative visual interpretation of images, several protocols and algorithms have been used to improve the specificity of [¹⁸F]FDG PET in nodal staging, such as utilizing quantitative SUV_{max} cutoff values (Krabbe et al. 2011, Murakami et al. 2007, Ng et al. 2006). Nevertheless, the highest accuracy has been achieved with the interpretation of anatomical findings in the CT image together with [¹⁸F]FDG uptake in the PET image. Using [¹⁸F]FDG PET/CT, the negative predictive value (NPV) of a lymph node involvement in clinically N0 (cN0) patients is ~80% when a histopathological specimen from elective neck dissection is used as a gold standard for nodal involvement. Therefore, the role of [¹⁸F]FDG PET/CT in the detection of lymph nodes in cN0 patients is still limited and it is generally not recommended to withhold a prophylactic neck dissection based on a negative finding from [¹⁸F]FDG PET/CT imaging (Differding et al. 2015, Kyzas et al. 2008). However, a recent randomized controlled study involving a special group of HNC patients treated with CRT indicated a similar survival rate of those who underwent a routine neck dissection after CRT compared to those who underwent [¹⁸F]FDG PET/CT guided surveillance and a neck dissection only in the case of a positive PET finding (Mehanna et al. 2016).

The detection of distant metastases in HNC is successfully performed with [¹⁸F]FDG PET/CT and seems to outperform both CT and MRI (Gao et al. 2014, Rohde et al. 2017). Especially patients with recurrent disease have a higher risk of distant metastases, but also, at the time of diagnosis, up to 10 % of patients with locally advanced disease will harbor distant metastases, the most common sites of which are the lung and liver (Haerle et al. 2011b). Less frequently, [¹⁸F]FDG PET/CT may also detect a simultaneous second primary tumor, which usually has a remarkable influence on the treatment and prognosis of the patient. For these reasons, [¹⁸F]FDG PET/CT has been recommended for all patients with stage III

or IV diseases at the time of diagnosis according to the National Comprehensive Cancer Network guidelines (Pfister et al. 2013).

TREATMENT PLANNING

Another important indication to use [^{18}F]FDG PET/CT in the management of HNC is RT planning. In several studies, it has been shown that [^{18}F]FDG PET/CT offers additional value in the contouring of RT target volumes compared to the use of traditional imaging modalities CT and MRI (Wang et al. 2006, Bird et al. 2015, Leclerc et al. 2015). However, there is no consensus of criteria in the detection of boundaries of malignant tissue in [^{18}F]FDG PET imaging. Several procedures mainly based on quantitative analysis of [^{18}F]FDG uptake have been proposed, but the results are controversial (Zaidi et al. 2012, Schinagl et al. 2007). An important factor to account for is partial volume effect (PVE), which refers to the blurring of uptake data of voxels of interest by adjacent background voxels because of low spatial resolution. In the clinical setting, this is an essential issue, such as in the oropharynx, where prominent mucosal growth of the tumor has to be included in the target volume (Daisne et al. 2004, Troost et al. 2010b). In such cases, even the physical examination of the patients plays a key role in avoiding marginal failures. The role of [^{18}F]FDG PET/CT in RT planning is discussed further in chapter 2.5.

The prognostic significance of pretreatment [^{18}F]FDG PET/CT has been a subject of particular interest, and numerous studies and meta-analyses have been performed in this field (Cacicedo et al. 2016). SUV_{mean} , SUV_{max} and volumetric parameters such as metabolically active tumor volume (MATV) have been negatively correlated with patient survival (Xie et al. 2011, Querellou et al. 2012). However, the clinical significance of the prognostic data acquired with pretreatment [^{18}F]FDG PET/CT is so far negligible in the treatment planning of HNC patients.

MONITORING OF THERAPY RESPONSE AND FOLLOW-UP

The third generally used clinical indication of [^{18}F]FDG PET/CT imaging in HNC is the monitoring of therapy response after CRT. [^{18}F]FDG PET/CT is accurate in the detection of viable tumor cells if processes causing false positive findings such as inflammation can be ruled out (Isles et al. 2008). Positron Emission Tomography Response Criteria in Solid Tumors (PERCIST) have been defined to establish optimal protocols for the monitoring of response to CRT (Gupta et al. 2011). The response PET/CT imaging is generally recommended 12 weeks after the completion of CRT in order to achieve higher diagnostic accuracy compared to earlier time points as well as an opportunity to recognize failure of the treatment, indicating a need for salvage surgery in time (Gupta et al. 2011).

Additionally, [^{18}F]FDG PET/CT has been suggested for surveillance of asymptomatic patients. Studies involving the follow-up period after treatment have shown favorable accuracy of [^{18}F]FDG PET/CT in the assessment of recurrence (Wong 2008). Analogically, the sensitivity and NPV of [^{18}F]FDG PET/CT in surveillance have proven to be especially outstanding (Abgral et al. 2009, Wang et al. 2009). Nevertheless, the current evidence does not support a routine follow-up with [^{18}F]FDG PET/CT imaging (Beswick et al. 2012).

2.3.1.4 Temporal dimension and quantitative analysis of [^{18}F]FDG PET/CT imaging

The conventional static imaging procedure has been optimized based on the substantial knowledge and experience of [^{18}F]FDG PET/CT imaging and its clinical applications. Nevertheless, it is well known that a considerable amount of potentially useful information may be lost when performing a single-time-point static imaging. The most important clinical goal of protocols using longer PET acquisition and temporal evaluation of tracer uptake is improving specificity of [^{18}F]FDG PET for identification of malignant tissue.

The most commonly investigated [^{18}F]FDG PET/CT imaging protocol that utilizes the temporal changes of the tracer uptake is dual-time-point imaging (DTPI). The idea of this protocol is to perform two static acquisitions at distinct time points (e.g., 60 and 100 min post injection), in order to obtain more data for differentiation of inflammatory and malignant tissues. DTPI has been evaluated in detail in lung cancer patients, but the results are controversial (Barger and Nandalur 2012, Schilacci 2012). On the other hand, a recent meta-analysis including studies on metastatic lymph nodes of various types of cancers found the DTPI protocol to be more sensitive but less specific in detecting metastatic lymph nodes compared to conventional single-time-point imaging (Shen et al. 2014). A prospective study with 74 HNC patients who underwent DTPI presented modest specificity, sensitivity, PPV (positive predictive value) and NPV in the comparison of the imaging data with the histopathological findings of a later performed neck dissection (Carlson et al. 2013).

As an alternative to a steady-state procedure, a dynamic acquisition may be used. In dynamic imaging protocols, tracer uptake is measured as a function of time. Data acquisition is typically performed with list-mode application, which makes it possible to divide the data into serial time frames. A time-activity curve (TAC) is usually constructed to evaluate the tracer uptake in specific VOIs. Information from dynamic images can be processed using advanced kinetic models if the blood activity during the time frames is also known. Traditionally, the blood activity data

is obtained by extracting arterial blood from the patient during the scan. Today, with modern PET scanners, it may be possible to determine accurately the blood activity from the images in the region of a great vessel (e.g. ascending aorta).

The true quantitative analysis of [^{18}F]FDG uptake is based on a two-tissue compartment model, in which there are three parameters of [^{18}F]FDG concentrations: free FDG in plasma, extravascular non-metabolized FDG and intracellular metabolized FDG. The most accurate quantification is obtained in multiparametric (or full kinetic) analysis (Minn et al. 1995b). Also, the Patlak method, which is a slight simplification of the full kinetic model, can be used in a case of an irreversibly binding tracer such as [^{18}F]FDG (Patlak et al. 1983).

In HNC, little is known about longitudinal changes in [^{18}F]FDG kinetics, since very few studies achieving real parametric images have been performed (Manca et al. 2016). The main reason for this is undoubtedly the challenge associated with obtaining dynamic data simultaneously from the blood pool and from the tumor area. One interesting technique, which was presented recently and which would probably be applicable for the head and neck region, is dynamic imaging with continuous bed movement (Karakatsanis et al. 2013, Osborne and Acuff 2016). The idea of this technique is to split the imaging session into shorter periods in which the input function (e.g., from the aorta and the region of interest elsewhere) are imaged in turn and the periods of lacking data are extrapolated using advanced mathematical methods.

In general, dynamic PET imaging provides true quantitative tracer uptake data with overwhelming accuracy. However, the design of clinical imaging protocols should be guided by the right balance of simplicity and accuracy, as stated in a review article by Adriaan A. Lammertsma (Lammertsma 2017). Interestingly, it has also been proposed that quantitative [^{18}F]FDG data might be useful with regard to future personalized medicine (Manca et al. 2016). Nevertheless, so far there is a remarkable lack of knowledge and experience on the potential utilization of quantitative [^{18}F]FDG PET/CT imaging in patients with HNC.

2.3.2 Tumor hypoxia

Living cells need a sufficient oxygen supply to have normal functional properties and energy production. In the human body, arterial blood is well oxygenated, and the normal partial pressure of oxygen (pO_2) (normoxia) is approximately 75–105 mmHg (10–14 kPa). Most healthy tissues tend to have sufficient oxygenation, if there is no disturbance of the perfusion or oxygen diffusion. However, the normal level of oxygen partial pressure in tissue ($\text{p}_{\text{ti}}\text{O}_2$) varies from 20 mmHg in the liver

to 70 mmHg in the kidneys (Vaupel et al. 1989, Carreau et al. 2011). Hypoxia is generally defined as a condition of lower tissue oxygen tension, commonly below 8–10 mmHg, whereas the total absence of oxygen is called anoxia. In many pathological conditions, such as coronary artery disease, ischemic brain disorders and chronic wounds, hypoxia is a characteristic feature in the pathogenesis. In a malignant tumor, hypoxia contributes to several pathophysiological processes that alter tumor behavior.

2.3.2.1 Angiogenesis and blood flow in malignant tumors

The process of forming new blood vessels, called angiogenesis, is a crucial phenomenon in the growth of malignant tumors. As the cancer cells proliferate, they need an appropriate supply of oxygen and nutrients (glucose), as well as some cytokines (e.g., growth factors). Nevertheless, angiogenesis is not systematically regulated in the malignant tissue during the growth, which is different than in normal tissues, where the formation of new vessels is strictly regulated. In a malignant tumor, the vessels appear to grow in a disorganized network, and the structure of the vessels also tends to be abnormal. Several morphological abnormalities of the tumor blood vessels have been described, including dysfunction and leakiness of the endothelial cell layer, inappropriate connectivity and multiple protrusions. All of these features of the development of the vascular network may lead to an inappropriate oxygen supply in the tumor, causing oxygen gradients and hypoxia. In the hypoxic regions, the acid concentration is also higher than in normally oxygenated tissues (Carmeliet and Jain 2000).

The rate of the blood flow varies greatly in a malignant tumor and often is not sufficiently high. Based on a variety of abnormalities in the vessels, the erythrocytes may not reach all the parenchymal cells in the tumor. Many abnormal phenomena have also been observed in malignant tumors, including markedly increased interstitial pressure causing compression of microvessels in the tumor and even reversing blood flow (Vaupel et al. 1989).

2.3.2.2 Hypoxia in malignant tumors

Two main types of tumor hypoxia can be distinguished: chronic and acute. Chronic, or diffusion-limited, hypoxia is a consequence of impaired diffusion of oxygen from blood vessels. The critical limit of distance from a blood vessel to a cell is around 150 μm ; in a case of higher distance, oxygen is not able to diffuse into the cell (Horsman 1998). Because of the unorganized blood vessel network,

subvolumes of chronic hypoxia occur frequently. Acute, or perfusion-limited, hypoxia is believed to be caused due to a transient block of a vessel. Acute hypoxia may be transient or even cyclic (Dewhirst 2009). Temporal changes in tumor hypoxia have been demonstrated using several methods, e.g., performing immunohistochemical staining of tumor sections after consecutive injections of two different exogenous hypoxia markers (Ljungkvist et al. 2007).

Tumor hypoxia has been the subject of research for a reasonably long time. The very first report of the lower radiosensitivity of hypoxic mammalian cells dates back to the year 1909, when Schwarz and colleagues published their observations (Bertout et al. 2008). In 1920's, the fundamental findings of altered metabolism in hypoxic cancer cells (described in chapter 2.3.1) were reported by Otto Warburg. The first groundbreaking observations of abnormal vasculature in malignant lung tumors were reported in 1955 by Thomlinson and Gray, who also proposed that hypoxic cancer cells might be more resistant to RT than normoxic cancer cells (Thomlinson and Gray 1955). Since then, a large amount of knowledge on tumor hypoxia has been discovered, and hypoxic subvolumes have been observed frequently in almost all solid tumors (Brown and Wilson 2004).

The presence of hypoxia has remarkable consequences on the behavior of a malignant tumor. In parallel to normal cells, hypoxia is also a challenge for cancer cells, because it causes substantial changes in energy production and normal cell function. Nevertheless, the cancer cells that endure hypoxia gain a growth advantage and succeed in the competition for survival. Consequently, hypoxia promotes the progression to a more malignant tumor phenotype.

Several cellular and molecular processes occur under hypoxic conditions to maintain cell function and enhance cell survival. Hypoxia inducible factors (HIFs) are transcription factors responsible for changes of cell function under hypoxic conditions. Three HIFs (HIF1-3) have been discovered, all of which consist of a stable beta unit and an alpha unit that is unstable in normoxic conditions (Duan 2016). The role of HIF-1 α has been described extensively. Recently, more knowledge of the important role of HIF-2 α in cancer cells, especially during chronic hypoxic exposure, has been achieved (Zhao et al. 2015). For the present, very little is known about the expression, action and significance of HIF-3 α (Duan 2016).

HIF-1 α is transcribed and synthesized independently of the intracellular O₂-concentration (Masoud and Li 2015). However, in normoxic conditions, HIF-1 α is hydroxylated by prolylhydroxylase proteins (PHDs) and degraded by proteosomal degradation in interaction with the von Hippel Lindau protein (pVHL). In contrast, under hypoxia there are several mechanisms maintaining the stability of HIF-1 α , allowing its transcriptional actions after it has been combined with the beta unit and bound to hypoxia-responsive elements (HREs) of DNA.

HIF-1 α is responsible for several transcriptionally related changes occurring in hypoxia which promote cancer progression. Angiogenesis is induced, for example, with the induction of vascular endothelial growth factor (VEGF) and transforming growth factor β 3 (TGF- β 3), and glucose metabolism is enhanced via the expression of GLUT-1 and GLUT-3 proteins and hexokinases 1 and 3 (HK1 and HK3). Myelocytomatosis virus oncogene cellular homologue (C-MYC) and insulin-like growth factor 2 (IGF-2) are representative examples of mediators involved in the cell proliferation induced by HIF-1 α (Harris 2002). It has also been proposed that hypoxia promotes tumor invasion and metastasis, and these processes seem to be regulated, at least in part, by HIF-1 α . An example of these mediators is lysyl oxidase (LOX), an enzyme that catalyzes the crosslinking of collagens and elastins and is associated with invasion and metastasis formation (Erler et al. 2006, Sidikuzzaman et al. 2011). In general, several HIF-1 α -related processes occur in the hypoxic microenvironment, altering the extracellular matrix and modulating the tumor immune response (LaGory and Giaccia 2016). Additionally, there are numerous other HIF-1 α -induced genes expressed in hypoxia, promoting, for example, cell survival, apoptosis, and the immortalization and migration of the cell.

In healthy cells, hypoxia and glucose metabolism are linked to each other, as stated in chapter 2.3.1. When there is a low oxygen concentration in a cell, anaerobic glycolysis is induced to compensate for the lack of energy production of the cell. Nevertheless, there is growing evidence that the linkage between hypoxia and glucose metabolism is more complex. In hypoxia, a cell is able to utilize intracellular glycogen to maintain its proliferative activity (Pescador et al. 2010). Moreover, there are several other processes in a hypoxic cell that are thought to help the cell to adapt its metabolism and energy production in hypoxic conditions (Eales et al. 2016). However, in cancer cells, these links are even more complex considering, e.g., the presence of the Warburg effect (chapter 2.3.1).

The tumor suppressor p53 is an important restrictor of malignant tumor growth. Generally, it prevents mutations in the genome and induces the apoptosis of tumor cells. Hypoxia may initiate or prevent the stabilization of p53 in an unknown manner. On the other hand, it has also been shown that hypoxia promotes apoptosis of the p53-positive cancer cells and therefore selects those cells that have lost their p53 activity (Graeber et al. 1996). Nevertheless, the interplay between HIF-1 α and p53 is still an unclear issue, although these two transcription factors have been studied extensively (Eales et al. 2016).

Hypoxia in a tumor contributes to resistance against RT (Janssen et al. 2005). The biological effect of RT is based on the damage of DNA caused by ionizing radiation. In the majority of cases, the damage is caused indirectly by the action of free

radicals. Photon radiation causes the ionization of water molecules and other compounds in the cells, which leads to the formation of free radicals. In the presence of oxygen, these free radicals form peroxides, which are toxic to DNA and possibly to cell membrane structures as well. These peroxide compounds cause irreparable damage to DNA structures, leading to the death of the cell in the next mitosis. Less frequently, the damage of a DNA structure produced by photon radiation may also be direct, causing a break in the DNA strand. These breaks are commonly sublethal if only one strand is affected, since the DNA repair mechanism may be able to repair the break. In more rare cases, however, a fatal double-strand break may occur. Nonetheless, the majority of the therapeutic effect of RT is oxygen-dependent, and it has been estimated that hypoxic cells are three times more resistant to radiation damage compared to well-oxygenated cancer cells (Brown and Wilson 2004).

Hypoxia might also have an effect on the outcome of chemotherapy. Several cytotoxic drugs are effective only in cells in the mitotic phase. Hypoxia causes deceleration of the cell cycle in spite of some compensatory processes it induces (Harris 2002); consequently, hypoxia is considered to contribute to a poorer effect of the cycle-selective chemotherapeutic drugs. Moreover, several other mechanisms occur in hypoxic conditions which can have an effect on the chemotherapy of hypoxic tumors, including but not limited to extracellular acidification, resistance of apoptosis and suppression of DNA repair. It has also been suggested that a poorer vascular supply in hypoxic tumors causes difficulties in drug penetration. This might be an explanation for a worse treatment outcome of hypoxic tumors compared to that of their non-hypoxic counterparts when treated with chemotherapy (Wilson and Hay 2011).

Finally, the survival of surgically treated patients with hypoxic tumors has been observed to be worse compared to patients with non-hypoxic tumors (Höckel et al. 1996). This might be associated with the higher tendency of distant spread of hypoxic tumors (Brizel et al. 1996); however, the explanation for this observation has been poorly understood (Janssen et al. 2005).

2.3.2.3 Therapeutic interventions involving hypoxia in HNC

Tumor hypoxia has been an interesting target for developing new therapeutic modalities and modifying the present ones because of its negative prognostic nature. In this section, some of the important interventions to overcome tumor hypoxia are presented briefly.

Knowledge of the impact of hypoxia on the outcome of RT has encouraged several efforts to improve the radiosensitivity of hypoxic tumors and reduce the impact of hypoxia. One important goal has been to modify the level of hemoglobin before the start of RT. In several observational studies, anemia has been indicated as a negative prognostic factor of HNC patients undergoing RT (Lee et al. 1998, Hoff 2012). However, the correction of anemia with a transfusion has not been observed to correct tumor hypoxia evaluated with dynamic-contrast-enhanced MR imaging (DCE-MRI) (Welsh et al. 2017), and the use of erythropoietin (EPO) to manipulate the level of hemoglobin has not been associated with a better outcome rate (Hoff 2012). In fact, EPO has even proven to be harmful for HNC patients undergoing RT (Lambin et al. 2009), which might be due to changes in the microcirculation of the tumor and a possible thromboembolism caused by a too-high hemoglobin concentration (Hoff 2012).

Other approaches to improve tumor oxygenation during RT have included the use of hyperbaric oxygen to increase soluble oxygen in plasma (Haffty et al. 1999) and breathing of carbogen (mixture of 95% oxygen and 5% carbon dioxide) to increase the tumor blood flow (Mendenhall et al. 2005). Carbogen inhalation therapy with combination of administration of nicotinamide has also been studied, but improved regional tumor control was observed only in patients with hypoxic tumors and not in patients with well-oxygenated tumors (Janssens et al. 2012). Moreover, attempts have been made to reduce cellular oxygen consumption with metformin (Koritzinsky 2015). However, none of these interventions has yet proven to be so beneficial and useful as to deserve a place in clinical practice. Nevertheless, cessation of smoking seems to be an effective intervention if performed prior to the initiation of RT. In a few observational studies, inferior rates of loco-regional control and disease-free survival have been observed among those HNC patients who continued smoking during the course of RT (Browman et al. 1993, Chen et al. 2011).

Nitroimidazoles are compounds that have special characteristics to accumulate inside cells with a low oxygen tension. Some nitroimidazole compounds were already being used as radiosensitizers of head and neck tumors in the 1980s, when several studies were conducted using misonidazole during a curatively intended RT (van den Bogaert et al. 1986, Overgaard et al. 1989). Some significant side effects of misonidazole were observed, especially peripheral neuropathy, and since then other nitroimidazoles such as etanidazole and nimorazole have been evaluated. A phase III study reported a significantly improved locoregional control and disease-specific survival of patients with pharyngeal and supraglottic laryngeal cancer who received nimorazole together with conventional primary RT (Overgaard et al. 1998). Nevertheless, a retrospective evaluation of the genetic profile of these tumors indicated that the treatment with nitroimidazole was effective only in more hypoxic tumors. HPV-positive tumors had a significantly better outcome,

irrespective of the hypoxic modification, compared to HPV-negative tumors (Toustrup et al. 2012). Currently, there is an interesting ongoing randomized study regarding the effect of nimorazole compared to placebo during modern RT among patients with HPV-negative HNC (NCT01880359, www.clinicaltrials.gov).

A meta-analysis published in 2011 reported level 1a evidence (Oxford Centre 2009) for the benefit of hypoxic modification during RT of HNC. The loco-regional control and disease-free survival were significantly better among patients who underwent any hypoxic treatment modifications (HBO, carbogen alone or combined with nicotinamide, radiosensitizer) compared to control groups, although patients were not selected with regard to tumor oxygenation status for the randomized controlled trials included in the meta-analysis (Overgaard 2011). However, the number needed to treat (NNT) for these modification protocols was reasonably high; therefore, identification of patients with hypoxic tumors prior to therapy would be beneficial in order to prove the clinical impact. Nimorazole has been used in clinical practice in Denmark (Toustrup et al. 2016), but the rest of the previously described interventions are currently not included in routine clinical treatment protocols of HNC patients.

An important approach of hypoxia-related treatment interventions is the modification of RT dose delivery. This procedure is called dose painting, in which a higher radiation dose is targeted to hypoxic subvolume(s) of tumor. This technique may be utilized in two different ways: Dose painting by contours (DPBC) refers to targeting a uniform dose to a hypoxic subvolume of the tumor, whereas dose painting by numbers (DPBN) involves modifications of dose delivery at voxel scale, calculating an individual dose prescription for principally every single voxel (Bentzen and Grégoire 2011). RT dose delivery modifications are further discussed in chapter 2.5.

Hypoxia-targeted medical therapy is another major approach for therapeutic intervention among hypoxic cancers. Hypoxia-activated prodrugs have been of special interest; the first compound of this group was mitomycin C, which is now in clinical use (e.g., for anal cancer, bladder cancer and HNC). However, mitomycin C shows only minor hypoxia-specific potential (Kennedy et al. 1980). Tirapazamine is the most thoroughly evaluated drug that has been developed especially for the purpose of hypoxia-targeted therapy. Nevertheless, discouraging results were found in a phase III study, which showed no improvement in the overall survival rate attributed to the addition of tirapazamine for HNC patients receiving CRT (Rischin et al. 2010). Moreover, significant toxicity of tirapazamine has been observed in clinical use (von Pawel et al. 2000, Rischin et al. 2005). The next generation of hypoxia-activated prodrugs includes, among others, evofosfamide (formerly known as TH-302), CEN-209, PR-104 and EO-9 (Phillips 2016).

Evofosfamide has recently been evaluated in advanced soft tissue sarcoma and pancreatic cancer, but two large phase III studies did not observe any significant improvement in overall survival (Mistry et al. 2017). Furthermore, there are also other molecular targets for hypoxia-specific drugs, such as inhibition of HIF-1 α (Semenza 2007). Several compounds of this group are currently also under evaluation (Masoud and Li 2015). Nevertheless, one of the major drawbacks in the development and evaluation of these hypoxia-targeted drugs has been the lack of a practical and clinically applicable method to determine and quantify the oxygenation status of the malignant tumors.

2.3.2.4 Non-PET methods for detection and quantification of tumor hypoxia

Substantial efforts have been made over the past decades to develop and evaluate appropriate methods for the detection and measurement of tumor hypoxia. In this section, the most important techniques (excluding PET) are reviewed briefly.

DIRECT NEEDLE ELECTRODE MEASUREMENTS

Direct invasive hypoxia measurement using polarographic needle electrodes has been an important tool in the study of tumor hypoxia. This method was one of the first tissue hypoxia measuring modalities in use (Severinghaus and Astrup 1986). Especially in the 1990s and 2000s, a commercially available device (Eppendorf pO₂-Histogram) was used in several clinical and preclinical studies. This needle electrode system consists of a probe with a gold cathode covered by an oxygen-permeable Teflon membrane that is inserted into the target tissue. A silver/silver chloride anode is attached to the skin or underlying muscle near the site where the probe (cathode) is inserted. The measuring process is based on electrochemical reduction of oxygen at the cathode surface, which occurs when the system has a polarization potential of a low voltage. The computerized system allows for a step-wise measuring with dozens of individual measurements from several tracks while the probe is moving in the investigated tissue. The device produces a histogram of partial oxygen pressure distribution (Vaupel et al. 1991).

A polarographic needle electrode system has been suggested to be the gold standard for measuring hypoxia in cancer, since it is a truly direct measuring method. Furthermore, several studies have indicated a clear connection between the measured high partial oxygen pressure and a poor patient outcome (Olive et al. 2001, Vaupel et al. 2007). Studies with HNC patients have shown strong evidence of a significant correlation between low p_iO₂ and a worse outcome of RT (Nordsmark and Overgaard 2000, Nordsmark et al. 2005). Analogous results have also been achieved in studies of patients with cervical cancer (Höckel et al. 1996) and soft

tissue sarcoma (Brizel et al. 1996, Nordmark et al. 2001). Nevertheless, there are also several limitations and disadvantages associated with the use of this method. Measuring with a needle electrode system is technically demanding, and the results are not completely reproducible. The invasive nature of the procedure limits the use in less-accessible tumors. It has also been established that a needle electrode system is not able to distinguish severely hypoxic viable cells from necrotic cells (Vaupel et al. 2007). The Eppendorf pO₂-Histogram is no longer commercially available.

ENDOGENOUS MARKERS

Endogenous molecular markers are applicable in the detection of hypoxia relatively easily, since no intervention is needed and they are available from archival biopsy samples. Traditionally, the best-characterized endogenous hypoxia marker has been HIF1- α . The expression of HIF1- α has been associated with a poor outcome of HNC patients (Hong et al. 2013, Zheng et al. 2013), although conflicting results have also been published (Beasley et al. 2002, Fillies et al. 2005). Nevertheless, in a meta-analysis of 28 studies involving HNC patients, overexpression of HIF1- α was significantly associated with an increased mortality risk, although the prognostic value of HIF1- α varied in different HNC subtypes (Gong et al. 2013). In addition, corresponding results indicating an association between HIF1- α overexpression and a poor outcome have been achieved in meta-analyses involving studies of gastric cancer (Lin et al. 2014), breast cancer (Wang et al. 2014) and lung cancer (Ren et al. 2013) patients. Nevertheless, the expression of HIF1- α is not an ideal marker of tumor hypoxia, since intratumor heterogeneity as well as diffuse non-hypoxia-specific changes in the expression of HIF1- α have been observed (Swartz et al. 2015, Ljungkvist et al. 2007).

There are also a few HIF1- α related markers that have been evaluated as surrogates of hypoxia. Two of these are carbonic dehydratase 9 (CAIX) and GLUT-1. CAIX is a transmembrane protein that helps a cell to survive in acidic conditions by catalyzing the hydration reaction of carbon dioxide to carbonic acid. Expression of CAIX has been strongly associated with the hypoxic condition, and it is negatively correlated with the microvessel density in a tumor (Beasley et al. 2001). Moreover, in several HNC studies, higher CAIX levels have been observed to be associated with an inferior treatment outcome within various treatment modalities (Swartz et al. 2015). However, the observations of cell line dependence of CAIX expression under hypoxic conditions have been discussed recently (Li et al. 2015). GLUT-1 (see chapter 2.3.1), the expression of which is also induced by HIF1- α , has been associated with an inferior outcome in various types of cancer, including HNC (Vaupel and Mayer 2007b). Nevertheless, there are a number of factors other than hypoxia promoting the expression of GLUT-1 (Janssen et al. 2005).

A modern approach to the detection of tumor hypoxia using endogenous markers is the transcriptomic analysis of hypoxia gene signatures. In this method the entire mRNA of the cell population is analyzed. In HNC, a few hypoxia gene signatures have been designed, and a recent study using three different panels indicated a significant association between these gene signatures and the overall survival of the patients (Tawk et al. 2016).

TISSUE ANALYSIS USING EXOGENOUS MARKERS

Hypoxia-avid compounds have been used as exogenous markers to detect hypoxic cells in tissue sections. The most common strategy is to administer the compound intravenously. Thereafter, a tissue sample is obtained, and an immunohistochemical staining is performed. In this method, specific fluorescent antibodies are used to detect the bounded marker, and the tissue section is investigated microscopically. Another approach is autoradiography, which utilizes a radioactive marker in the detection of hypoxic cells. Traditionally, an x-ray film or a nuclear emulsion plate was used in autoradiography, but modern techniques involve digital systems.

Nitroimidazoles form the main group of exogenous hypoxia markers. In immunohistochemistry (IHC) studies, the most commonly used compound is pimonidazole, the binding of which has been well characterized as a surrogate marker of oxygen concentration (Arteel et al. 1998) and as a marker of the clinical outcome of HNC patients (Kaanders et al. 2002). Another important compound belonging to 2-nitroimidazoles is EF5 (2-(2-nitro-1H-imidazol-1-yl)-N-(2,2,3,3,3-pentafluoropropyl)-acetamide), which has also been extensively studied (Koch and Evans 2015). An inverse correlation between EF5 binding and tissue oxygen tension has been demonstrated (Koch 2002). Moreover, an association between high EF5 binding and a poor clinical outcome has been observed in studies of patients with soft tissue sarcoma (Evans et al. 2006) and HNC (Evans et al. 2007). In addition to these two compounds, other molecules belonging to the nitroimidazole group have also been studied as exogenous markers of hypoxia, such as misonidazole and CCI-103F (Ljungkvist et al. 2007).

The major advantage of tissue analysis using exogenous markers is the outstanding spatial resolution. However, a need for tissue sampling limits the clinical use of these methods.

FUNCTIONAL IMAGING

Compared to all of the previously described hypoxia measurement methods demanding either a tissue sample or other invasive procedures, functional imaging applications are different because of their noninvasive nature. MRI has been an interesting method in recent years, and several novel applications in this field have

been evaluated. Blood-oxygen-level-dependent MRI (BOLD-MRI) is a method of functional MRI (fMRI) that is able to distinguish deoxyhemoglobin from hemoglobin because of its paramagnetic nature. A major drawback in the use of BOLD-MRI as a hypoxia imaging method is the fact that the data reflect the oxygenation of blood instead of tissue (Sun et al. 2011). Perfusion-weighted MRI utilizes gadolinium as a contrast agent. Two different methods have been introduced, namely dynamic-contrast-enhanced MRI (DCE-MRI) and dynamic-susceptibility-contrast (DSC) MRI. The first is based on the evaluation of perfusion and tissue permeability, whereas the latter only evaluates perfusion. Thus, both of these methods acquire indirect evidence of tissue hypoxia. A recent systematic review presented a reasonable potential of these methods but concluded that more research is needed before these imaging techniques can be used in clinical practice (Noij et al. 2015).

Nuclear medicine applications have been extensively studied and used in hypoxia imaging because of their non-invasive nature. Single-photon emission computed tomography (SPECT) utilizes compounds that are labeled with radioactive single-photon gamma emitters such as [¹²³I]-iodoazomycin arabinoside (¹²³IAZA) (Urtasun et al. 1996). There are also some advantages available when using the SPECT method compared to PET, including the generally longer half-lives of used isotopes, allowing for easier and less expensive protocols for imaging. Nevertheless, PET is overwhelmingly the most commonly investigated and used hypoxia imaging modality.

2.3.2.5 PET imaging of tumor hypoxia

PET imaging is the preferred modality to study tumor hypoxia in the clinical setting (Fleming et al. 2015, Carlin and Humm 2012, Kelada and Carlson 2014). Although the spatial resolution of PET imaging is somewhat limited, there are several benefits that compensate for this shortcoming. As a non-invasive procedure, PET imaging is feasible for targets throughout the whole body, and different, heterogeneous regions of hypoxia inside a tumor are assumed to be easily assessed. Furthermore, PET imaging may be performed repeatedly and at distinct time points of the treatment protocol. As there are virtually innumerable potential compounds that could be used as PET tracers, massive efforts have been made to find an ideal compound for imaging of tumor hypoxia. There are some desirable characteristics for a useful PET tracer, such as a highly specific binding to target tissues and a rapid clearance of the unbound tracer from the blood pool and background tissues in order to get a good target-to-background contrast in PET images. However, an optimal hypoxia tracer has not yet been developed or identified. This has been

the most significant challenge for several years in the progression of clinical applications in the field of hypoxia PET imaging (Fleming et al. 2015).

Nitroimidazoles are currently the most interesting and important hypoxia-avid compounds, as already mentioned in chapter 2.3.2.4. The chemical structures of nitroimidazoles are presented in Figure 4. Nitroimidazole molecules are able to diffuse through the cell membrane and are then reduced into reactive metabolites by intracellular reductases. This action is dependent on the level of hypoxia. The reactive metabolites then form covalent bonds with thiol groups of intracellular macromolecules.

One of the first utilized compounds in the group of nitroimidazoles was metronidazole, an antibiotic, which is still in everyday use in the treatment of anaerobic bacterial and protozoal infections. There have been different indications for the use of nitroimidazoles over the past few decades. After the introduction of metronidazole, some derivatives of it (e.g., misonidazole and etanidazole) were developed for use as a radiosensitizer of hypoxic tumors. However, misonidazole was found to be toxic at the therapeutic dose level (Overgaard et al. 1989). At the end of the 1970s, the use of nitroimidazoles as radiolabeled markers for hypoxia imaging was proposed for the first time (Chapman 1979).

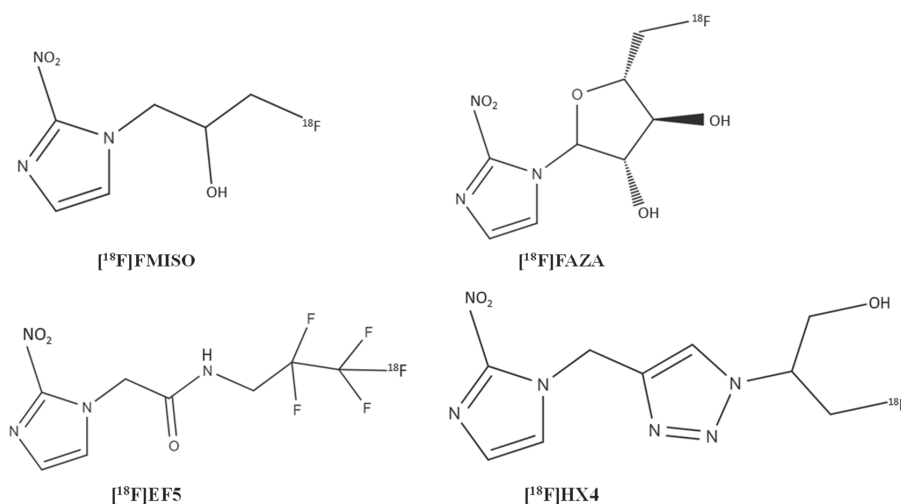


Figure 4 The molecular structure of four nitroimidazole compounds used as hypoxia PET tracers when labeled with 18-fluorine. HX4, FAZA and FMISO are hydrophilic molecules with partition coefficient (P) of 0.20, 0.27 and 0.44, respectively. EF5 is clearly the most lipophilic of these molecules with $P=5.7$ (Rajendran and Krohn 2015).

Lipophilicity and hydrophilicity are some of the central features affecting the usability of a compound as a hypoxia PET tracer. A lipophilic compound is able to

enter the cells easily, since it crosses the cell membranes passively, allowing for a uniform distribution of the tracer in the whole body. Moreover, a lipophilic compound is able to penetrate through the blood-brain barrier. On the other hand, a fast elimination of the unbounded tracer is also an important property. Therefore, an ideal hypoxia PET tracer should also be sufficiently hydrophilic, although the uptake of the tracer should not reflect blood flow instead of intracellular oxygenation. In addition, the rate of early metabolism of the tracer is crucial, since radioactive metabolites may have non-specific and unknown binding, causing disturbance in the images. There are several differences between the currently known nitroimidazole-based compounds in terms of these chemical features. However, none of the currently known hypoxia PET tracers have yet proven to be superior or optimal for clinical use (Fleming et al. 2015). In the following pages, some of the most important hypoxia PET tracers, of those that have already been investigated or are currently under evaluation, are reviewed briefly.

NITROIMIDAZOLE TRACERS

[¹⁸F]FMISO

Misonidazole was the first nitroimidazole compound to be labeled with ¹⁸F-fluorine to develop a hypoxia PET tracer. (Rasey et al. 1987). For the present, [¹⁸F]FMISO is still overwhelmingly the most thoroughly investigated hypoxia PET tracer (Rajendran and Krohn 2015). Since the time of the first clinical studies (Koh et al. 1992), numerous preclinical and clinical trials have been conducted using diverse protocols for imaging of various solid tumors with [¹⁸F]FMISO PET.

The pharmacological features of [¹⁸F]FMISO have certain pros and cons. The lipophilicity of the compound is reasonably low, with a distribution coefficient between octanol and water (partition coefficient, P) of 0.44 (Rajendran and Krohn 2015). However, together with a moderately slow target tissue penetration, the slow background clearance of [¹⁸F]FMISO is a real disadvantage, leading to challenges in obtaining an appropriate image contrast (Fleming et al. 2015). The hypoxia cutoff levels in many studies have commonly been set at a reasonably low level — for example, a tumor-to-muscle uptake ratio (TMR) of 1.25 and tumor-to-blood uptake ratio of 1.2 or 1.4 (Okamoto et al. 2013, Rajendran et al. 2003, Rasey et al. 1996). Furthermore, a rather fast metabolic rate has been reported for [¹⁸F]FMISO (Rasey et al. 1999), which may allow for unknown and non-specific binding of metabolites during the time frame of image acquisition. On the other hand, it has been stated that [¹⁸F]FMISO uptake is less dependent on the blood flow compared to several other hypoxia tracers (Rajendran and Krohn 2015). The radiation exposure in human imaging with [¹⁸F]FMISO is comparable to other common PET tracers, such as [¹⁸F]FDG (Graham et al. 1997).

The correlation between [^{18}F]FMISO uptake and pO_2 histography has been studied several times. The initial studies (Bentzen et al. 2002, Bentzen et al. 2003) did not indicate a clear correlation, but in some later studies a relevant correlation was observed (Gagel et al. 2004, Gagel et al. 2007). Also, [^{18}F]FMISO uptake has been shown to correlate with CAIX and HIF-1 α expression and pimonidazole binding (Dubois et al. 2004, Sato et al. 2013, Troost et al. 2006). The clinical significance of [^{18}F]FMISO PET in various cancers has been evaluated in a number of studies. Among HNC patients, the pretreatment [^{18}F]FMISO uptake of the tumor has been reported to be an independent prognostic factor (Rischin et al. 2006) and to correlate with the RT outcome (Eschmann et al. 2005, Thorwarth et al. 2006) and overall survival (Rajendran et al. 2006). Clinical [^{18}F]FMISO PET/CT studies have also demonstrated radiation-induced reoxygenation (Eschmann et al. 2007) and the prognostic value of [^{18}F]FMISO PET during RT (Zips et al. 2012, Löck et al. 2017). Initial results of the [^{18}F]FMISO PET/CT-based RT dose escalation study have recently been published (Welz et al. 2017).

Although [^{18}F]FMISO has been evaluated extensively and a real potential of the tracer has been indicated, it has not been fully accepted in clinical use. The relatively modest imaging quality and relatively low tumor-to-background contrast have probably been the most important drawbacks. Therefore, new potential tracers are being developed and evaluated. A common view is that every potential new hypoxia PET tracer should be better than [^{18}F]FMISO, if further evaluation is considered.

[^{18}F]FETNIM

Some chemical and pharmacological properties, especially a very low lipophilicity ($P=0.17$), were the key advantages achieved when [^{18}F]fluoroerythronitroimidazole or [^{18}F]FETNIM was developed (Yang et al. 1995). The studies regarding the pharmacokinetics and dosimetry of the tracer (Grönroos et al. 2001, Tolvanen et al. 2002) showed promising results. The tumor uptake of [^{18}F]FETNIM was compared to that of [^{18}F]FMISO in a preclinical study, but no significant differences were found, although some lower background activity was observed with [^{18}F]FETNIM (Grönroos et al. 2004). However, in a clinical study with HNC patients, it was observed that the tumor uptake of [^{18}F]FETNIM was highly variable and associated with blood flow in the early phase of tissue accumulation (Lehtiö et al. 2001), although an inverse correlation between [^{18}F]FETNIM uptake in a tumor and patient survival was also detected (Lehtiö et al. 2004). In more recent studies, analogous preliminary results of prognostic significance of [^{18}F]FETNIM PET/CT have been achieved among patients with cervical cancer (Vercellino et al. 2012) and non-small-cell lung cancer (NSCLC) (Li et al. 2010). Nonetheless, a recent comparative study where paired PET/CT hypoxia images were performed

for 42 lung cancer patients reported significantly lower tumor-to-blood uptake ratios in [^{18}F]FETNIM images compared to [^{18}F]FMISO images (Wei et al. 2016).

[^{18}F]FETA

[^{18}F]fluoroetanidazole is a radiolabeled derivate of etanidazole, which has previously been thoroughly evaluated as a radiosensitizer of hypoxic tumors (Lee et al. 1995). After the presentation of the radiochemical synthesis (Tewson 1997), it was assumed that [^{18}F]FETA with very low lipophilicity (comparable to that of [^{18}F]FETNIM) might be a better tracer than [^{18}F]FMISO. Initial preclinical studies have shown suitable properties of this tracer, including a $p\text{O}_2$ -dependent retention of the tracer in experimental murine tumors (Barthel et al. 2004).

[^{18}F]EF3

The successful synthesis of [^{18}F]EF3 was reported in 2001 (Josse et al. 2001). Pre-clinical studies with tumor-bearing mice showed a favorable biodistribution of [^{18}F]EF3. Furthermore, a significant correlation between [^{18}F]EF3 uptake and binding of the hypoxia IHC marker EF5 in the tumor tissue was observed (Mahy et al. 2004). A phase I clinical study with HNC cancer patients showed the administration of [^{18}F]EF3 to be feasible and safe (Mahy et al. 2008). However, a major drawback in the development of this tracer was the observation of lower levels of tumor uptake and tumor-to-blood ratio compared to those of [^{18}F]FMISO in a pre-clinical study with a comparison protocol (Dubois et al. 2009).

[^{18}F]EF5

The history of EF5 began in the 1990s, when the compound was developed for the purpose of detection of hypoxia (Lord et al. 1993). For several years, EF5 has been used in IHC studies, and those studies have indicated the hypoxia selectivity of EF5 binding (Koch and Evans 2015). EF5 is a very lipophilic compound ($P=5.7$), and its pharmacological half-life in plasma has been reported to be 11.7 ± 2.6 hours ($\pm\text{SD}$). In the initial studies with high-performance liquid chromatography (HPLC), EF5 was observed to be very stable. No nitro-containing metabolites were found in the plasma or urine of either humans or rodents after the administration of EF5 (Laughlin et al. 1996, Koch et al. 2001).

The radiochemical synthesis of [^{18}F]EF5 using electrophilic fluorination was described in 2001 (Dolbier et al. 2001). The first preclinical study with tumor-bearing rats showed even biodistribution of the tracer and TMR from 0.82 to 1.73 at 120 minutes post injection and from 1.47 to 2.95 at 180 minutes post injection (Ziemer et al. 2003). Further studies have shown that the metabolism of [^{18}F]EF5 in the human body is virtually negligible during the first four hours after injection, but in

mice extensive formation of metabolites has been observed (Eskola et al. 2012). The first human study using [^{18}F]EF5 was published in 2008 (Komar et al. 2008). In this study, 15 HNC patients were imaged three times with PET/CT using [^{18}F]EF5, [^{18}F]FDG and [^{15}O]H $_2$ O. The TMR of [^{18}F]EF5 ranged from 1.1 to 3.2 (median 1.38). Based on the voxel-by-voxel analysis of the coregistered blood flow images and dynamic [^{18}F]EF5 images, the cutoff value for clinically significant hypoxia was set at a TMR of 1.5 at 3 hours post-injection. In a later clinical publication, it was reported that a shorter overall survival of HNC patients was associated with maximum TMR and the tumor hypoxic subvolume defined in [^{18}F]EF5 PET image (Komar et al. 2014).

An important strength of [^{18}F]EF5 is the extensive evaluation of the pharmacologically similar, non-labeled “cold-EF5” as a marker for hypoxia. On the other hand, a complicated radiochemical synthesis of [^{18}F]EF5 using high molar activity is a remarkable drawback, limiting a larger utilization of this tracer, although some simplifications in other steps of the tracer production have been reported (Chitneni et al. 2012). The high lipophilicity has raised some doubts regarding [^{18}F]EF5 as a hypoxia PET tracer, since it has been assumed that the background clearance of the tracer would not be rapid enough to achieve a favorable image contrast. Nevertheless, a clear advantage is the negligible metabolism of [^{18}F]EF5 in the human body allowing for a higher specificity of the hypoxia-related binding of the tracer and the improved quality of PET images (Eskola et al. 2012).

[^{18}F]FAZA

Azomycin arabinoside (AZA) has been labeled with various isotopes, such as [^{125}I] and [^{123}I], when used as a tracer for hypoxia imaging with SPECT. The labelling of AZA with 18-fluorine has proven to be the most promising choice when the compound is used as a PET tracer. [^{18}F]FAZA has been observed to have a faster background clearance and a higher tumor-to-background ratio of uptake compared to [^{18}F]FMISO in animal and human studies (Sorger et al. 2003, Piert et al. 2005, Reischl et al. 2007, Souvatzoglou et al. 2007). Several preclinical studies have shown favorable characteristics of this tracer, for example a high correlation of tumor uptake of the tracer with pimonidazole binding (Busk et al. 2013) and electron paramagnetic resonance spectroscopy (Tran et al. 2012).

Additionally, [^{18}F]FAZA PET has been evaluated in clinical trials. A significant correlation between higher [^{18}F]FAZA uptake and a lower patient survival rate has been observed in studies with HNC patients (Mortensen et al. 2012, Saga et al. 2016), whereas a study with a small number of cervical cancer patients did not show such a correlation (Schuetz et al. 2010). A study with eleven NSCLC patients suggested that [^{18}F]FAZA PET imaging is able to detect hypoxic subvolumes in

homogenous regions of [^{18}F]FDG uptake, providing additional information on hypoxic tumors (Bollineni et al. 2013). On the other hand, a study with patients undergoing total laryngectomy due to laryngeal cancer (Bruine de Bruin et al. 2015) did not indicate a significant association between [^{18}F]FAZA tumor uptake and either pimonidazole binding or the expression of endogenous hypoxia markers (HIF-1 α , GLUT-1 and CAIX) in a tumor sample. A few studies regarding the feasibility of [^{18}F]FAZA PET in RT planning have also been performed (Grosu et al. 2007, Servagi-Vernat 2015).

[^{18}F]HX4

An important novel example of a nitroimidazole hypoxia tracer is 3-[^{18}F]fluoro-2-(4-((2-nitro-1H-imidazol-1-yl)methyl)-1H-1,2,3-triazol-1-yl)-propan-1-ol, called [^{18}F]flortanidazole or [^{18}F]HX4, which has recently been a target of intense research. [^{18}F]HX4 has been developed using click chemistry, which utilizes structure-activity relationships in the design of desirable pharmacological properties for the molecule (Kolb et al. 2001). A few preclinical studies comparing [^{18}F]HX4 to other hypoxia PET tracers have been performed (Peeters et al. 2015, Carlin et al. 2014). [^{18}F]HX4 uptake was observed to be associated with pimonidazole binding and CAIX expression in murine HNC xenograft tumors. In the same study (Carlin et al. 2014), the tumor uptake of [^{18}F]HX4 was reported to be at an intermediate level, higher than [^{18}F]FAZA but lower than [^{64}Cu]ATSM (see below).

In initial human studies, radiation exposure caused by [^{18}F]HX4 PET was shown to be comparable to that of other 18-fluorine-based imaging agents (Doss et al. 2010), and no toxicity attributable to [^{18}F]HX4 was observed (van Loon et al. 2010). The optimal acquisition time point for clinical imaging with [^{18}F]HX4 has been determined to be 4 hours post-injection in a study with lung cancer patients (Zegers et al. 2013). A few clinical trials involving HNC have also been conducted. The TMRs of [^{18}F]HX4 and [^{18}F]FMISO have been observed to be at the same level, and [^{18}F]HX4 uptake has also been observed to correlate with CAIX expression (Chen et al. 2012). In another multitracer study, also conducted with HNC patients, it was observed that the uptake parameters of [^{18}F]HX4 correlated with those of [^{18}F]FDG, but a partial mismatch was also observed in a majority of cases (Zegers et al. 2015).

In conclusion, [^{18}F]HX4 has shown some favorable imaging properties as a hypoxia PET tracer. Nevertheless, more studies regarding the association between [^{18}F]HX4 uptake and results of non-PET hypoxia detection modalities are needed. Moreover, an important approach in the future will be the clinical evaluation of the association between [^{18}F]HX4 tumor uptake and treatment outcome.

NON-NITROIMIDAZOLE TRACERS

Copper-based compounds form an important group of evaluated hypoxia PET tracers other than nitroimidazoles. Various radioactive copper nuclides [$^{60,61,62,64}\text{Cu}$] have been used as a label of ATSM (diacetyl-bis(N4-methylthiosemicarbazone)), a compound that has been extensively investigated as a hypoxia PET tracer. The half-life of copper nuclides varies from 9.67 minutes of [^{62}Cu] to 12.7 hours of [^{64}Cu].

The hypoxia avidity and binding of CuATSM resemble those of nitroimidazoles in the sense that CuATSM is also a reasonably lipophilic and highly membrane-permeable molecule that undergoes intracellular reduction under hypoxic conditions and becomes trapped in the cell (Fujibayashi et al. 1997). A typical feature of CuATSM PET images is a high tumor-to-background ratio of uptake, which has been observed to be typically over 2.0 and frequently even markedly higher. Another favorable feature in the clinical use of CuATSM is the rapid uptake and hypoxia-avid binding in tumors, which has been observed to occur as soon as in 10-15 minutes after injection (Lewis et al. 1999, Dehdashti 2003).

In clinical studies, the oxygen-dependent uptake and prognostic significance of CuATSM have been evaluated with promising results in HNC (Minagawa et al. 2011, Tsujikawa et al. 2016), lung cancer (Dehdashti 2003b) and cervical cancer (Dehdashti et al. 2003, Dehdashti et al. 2008). However, drawbacks have also been met in the evaluation of CuATSM. Lack of correlation with IHC hypoxia markers has been observed (Carlin et al. 2014), as well as variation of hypoxia selectivity between different tumor models (Yuan et al. 2006) in preclinical studies. Moreover, cell-dependent distribution and retention kinetics have been reported (Valtorta et al. 2013). An essential issue needing attention is the relatively high amount of radioactivity needed with [^{64}Cu]ATSM compared to nitroimidazoles when used for purpose of clinical PET imaging (Laforest et al. 2005).

In recent years, some compounds totally different from nitroimidazoles or copper-based tracers have also been investigated as hypoxia PET tracers. One of these is cG250, a monoclonal antibody against CAIX. This compound has been labeled with either [^{89}Zr] or [^{124}I] and evaluated in preclinical studies using animal models for renal cell carcinoma (Lawrentschuk et al. 2011) and head and neck carcinoma (Hoeben et al. 2010). A recent study performing pairwise comparison suggested favorable properties of [^{89}Zr]cG250 for providing higher-quality PET images compared to [^{124}I]cG250 (Cheal et al. 2014).

2.3.2.6 Dynamic nature of tumor hypoxia

Despite the growing theoretical and clinical knowledge, there are still some major unanswered questions regarding the variability of hypoxia in a malignant tumor. Temporal changes in tumor oxygenation may cause remarkable challenges both for the evaluation of hypoxia detection methods and for the development of treatment modifications.

One of the poorly understood issues is the connection between the tumor growth rate and hypoxia. Hypoxic tumors are thought to grow more rapidly than their non-hypoxic counterparts, since several processes occurring in hypoxic conditions promote tumor growth (Harris 2002). Nonetheless, little is known about the potential influence of dynamic variation in tumor hypoxia on the tumor growth rate. In contrast, the connection between tumor volume and hypoxia has been investigated in various studies. Both direct measurements with polarographic needles (Vaupel et al. 2007) and PET studies with [¹⁸F]FMISO (Tochon-Danguy et al. 2002, Bentzen et al. 2002, Koh et al. 1995) have indicated that these two parameters are generally not directly related to each other. However, it is unclear how tumor oxygenation varies over a larger time scale and during the tumor growth.

Traditionally, tumor hypoxia has been divided into two forms, acute and chronic hypoxia. However, parallel with growing knowledge on tumor hypoxia, this simplification has been questioned (Bayer et al. 2011) because of the complex nature of the dynamics of tumor oxygenation and the several causative mechanisms behind the phenomenon. These pathophysiological processes have been observed only empirically, and therefore the direct consequences of many of these processes remain unclear. In any case, temporal changes in tumor oxygenation occur frequently; while this is not an overwhelming obstacle, it remains one of the most important challenges in the field of tumor hypoxia research (Kelada and Carlson 2014).

An ideal method for hypoxia detection and quantification should provide highly repeatable results for therapeutic interventions to be designed based on this method. On the other hand, it is challenging to estimate how the methodological issues associated with measuring hypoxia affect temporarily variable results. The majority of hypoxia detection or measuring modalities suffer from a lack of feasibility for repeated procedures. All modalities based on a tissue sample naturally provide only a snapshot of tissue hypoxia. Polarographic needle electrodes may cause damage to tissues, raising doubts about the validity of results of repeated measurements (Rudat et al. 2000). Also, the spatial accuracy of repeated needle electrode measurements is questionable. By contrast, functional imaging methods

such as fMRI and PET are repeatable in principle, and both of these methods have been evaluated in this context (Panek et al. 2016, Kelada and Carlson 2014).

PET studies involving repeatability of baseline tumor hypoxia imaging before initiation of the treatment have been performed in both preclinical and clinical trials. In a preclinical study performed with mice bearing human Siha cervical carcinoma xenografts, two [^{18}F]FAZA PET scans were acquired on consecutive days (Busk et al. 2013). In the voxel-by-voxel analysis, a high linear correlation between the repeated scans ($R=0.82$, range 0.72–0.90) was reported. Additionally, high reproducibility was observed in a preclinical [^{18}F]FMISO PET study where mice bearing HER2+ breast cancer xenografts were imaged twice six hours apart (Whisenant et al. 2013). However, the reproducibility of results was assessed only at the whole tumor level in this study.

Only a few clinical PET studies regarding repeatability of baseline tumor hypoxia imaging have been conducted. These studies are of special interest because of the crucial information provided for the development of clinical applications. A pilot clinical reproducibility study was published in 2008, when 13 patients with HNC underwent two [^{18}F]FMISO PET/CT scans three days apart before the initiation of definitive RT (Nehmeh et al. 2008). The voxel-by-voxel analysis of absolute [^{18}F]FMISO uptake values showed reasonable variation between the repeated scans since a strong correlation ($r > 0.5$) was observed in only 71% of the patients. The proportion of patients exhibiting a strong correlation was even lower (46%), when only fractional hypoxic volumes (FHVs) were compared. In another study with 11 HNC patients (Okamoto et al. 2013), [^{18}F]FMISO PET/CT scans were found to be highly repeatable when the interval between the scans was 48 hours. The voxelwise comparison between the paired images showed a corresponding strong correlation ($r > 0.5$) in all patients, and 9 out of 11 had a correlation of $r > 0.85$. A more recent clinical study involving the repeatability of tumor hypoxia PET/CT imaging with both HNC patients and lung cancer patients was performed with a novel hypoxia tracer [^{18}F]HX4 (Zegers et al. 2015b). High repeatability was observed between the paired scans acquired over an average interval of two days. The tumor-level parameters (SUV_{mean} , SUV_{max} and TMR_{max}) showed a relative coefficient of repeatability between 15–17% and voxelwise analysis reported an average correlation of 0.65 ± 0.14 . Nevertheless, comparisons between quantitative results of these three clinical studies are challenging due to substantial differences between study protocols and different kinds of statistical methods used in these studies.

The repeatability of tumor hypoxia PET imaging has also been investigated in study protocols involving patients with cancers other than HNC. Paired [^{18}F]FET-

NIM PET/CT scans with esophageal cancer patients were observed to obtain variable results (Yue et al. 2012), whereas corresponding [^{18}F]HX4 PET/CT scans with esophageal or pancreatic cancer patients were reported to provide repeatable results (Klaassen et al. 2015). Nevertheless, these two studies were not based on voxel-by-voxel analysis, and the latter one also reported challenges in the registration of repeated images because of the lack of anatomical landmarks available near tumor regions. On the other hand, a recent study reported a high repeatability of [^{18}F]FMISO PET/CT scans performed 1–2 days apart in NSCLC patients (Grkovski et al. 2016). Tumor-level parameters (SUV_{mean} , SUV_{max} , and mean and maximum tumor-to-blood ratios) were highly correlated ($r \geq 0.87$) between the repeated scans, and the voxelwise agreement analysis reported an average relative difference of $0.9 \pm 10.8\%$, as calculated from the pooled dataset, including all analyzed lesions.

2.3.3 Additional cellular and molecular processes feasible for PET/CT imaging in HNC

In addition to glucose metabolism and hypoxia, several other processes in the microenvironment of HNC have been investigated as targets for PET/CT imaging. Many of these have been studied only in an experimental setting, but a few methods have gained more significance, although their clinical use has not yet been established.

Cell proliferation is an interesting target for PET imaging in cancer tissues, since the proliferation rate is markedly elevated in malignant tumors. Furthermore, a high rate of cell repopulation during RT is also considered to be an important factor for radioresistance. The most commonly investigated and used tracer for this purpose is ^{18}F -labelled fluorothymidine ([^{18}F]FLT). The advantage of [^{18}F]FLT compared to [^{18}F]FDG in the detection of malignant cells is the fact that the tracer is taken up actively only by the cells that are dividing, and therefore it does not concentrate on inflammatory tissues as much as [^{18}F]FDG. Therefore, [^{18}F]FLT PET/CT has been evaluated as a method for monitoring RT response of HNC and early remarks of response even before a visible decrease in tumor volume has been observed (Troost et al. 2010, Hoeben et al. 2013). Nevertheless, remarkable challenges in the specificity of [^{18}F]FLT PET in the discrimination of metastatic and inflammatory cervical lymph nodes have been reported (Troost et al. 2007). A recent review article regarding the usability of [^{18}F]FLT PET in various types of cancers stated that the uptake of the tracer shows a good clinical correlation with

progression-free and disease-free survival. Nonetheless, more interventional studies should be performed to determine the clinical impact of [^{18}F]FLT PET in imaging of HNC (Bollineni et al. 2016).

Another interesting molecular target for PET imaging of malignant tissue is amino acid transport and tumor-growth-related protein synthesis. ^{18}F -labelled fluoroethyltyrosine ([^{18}F]FET) has been investigated as a diagnostic tool in cases of suspected HNC. Despite an appropriate specificity in these studies, sensitivity has been quite modest compared to that of [^{18}F]FDG (Pauleit et al. 2006, Balogova et al. 2008, Haerle et al. 2011). [^{18}F]FET is currently used in the imaging of brain tumors (Dunet et al. 2012). Another PET tracer illustrating amino acid transport is ^{11}C -labelled methionine, which has been investigated as a tracer for tumor detection both for the purpose of RT planning and for evaluation of therapy response (Lindholm et al. 1993, Lindholm et al. 1995). Despite fairly encouraging results in the early studies of this tracer, there is currently not a clear role of [^{11}C]methionine PET in the imaging of HNC.

There are also some other targets in the microenvironment of HNC which have been utilized in PET imaging. An interesting one of them is EGFR expression, which has been considered as a target for imaging of treatment response (van Dijk et al. 2015). Some encouraging results of imaging with tracers reflecting e.g. apoptosis and cell membrane synthesis have also been achieved (Höglund et al. 2011, Khan et al. 2004) but further research is needed to develop clinically useful applications.

2.4 Image segmentation and clustering algorithms

In general terms, image segmentation is a process in which a digital image is divided into multiple segments according to some definite characteristics. In digital imaging, the information of every single pixel or voxel can be utilized in this process. During the recent years, several computational methods have been developed for the task of segmentation of structures in medical images (Ma et al. 2009). There are many applications for segmentation of medical images, such as delineation of certain anatomical structures or tumor volumes for RT planning (Pham et al. 2000).

One of the important strategies to perform segmentation on PET images is the use of the threshold function, which detects the voxels above a selected level of radioactivity. Several applications using threshold functions have been established and evaluated in phantom and clinical trials (Daisne et al. 2003, Geets et al. 2007, Moule et al. 2011). Another well-known strategy for medical image segmentation

is the use of pattern recognition algorithms, which are commonly classification algorithms or some derivatives of them (Ma et al. 2009, Pham et al. 2000).

Classification is a method that is generally used in machine learning and statistics to identify to which of a set of categories a new observation belongs. The identification process is based on training data containing observations whose correct category membership is known (Pham et al. 2000). The corresponding unsupervised method, called clustering, utilizes measures of similarity or distance between the observations that are classified (Ma et al. 2009). One of the major tasks in the application of classification algorithms is the selection and extraction of features used in the classification. Clustering is an optimal tool to be used in the feature selection. There are a number of algorithms to be used in cluster analysis, and these can be divided into parametric or non-parametric algorithms depending on whether or not they assume the data points to be normally distributed.

Two clustering algorithms are presented in this thesis. The Gaussian mixture model (GMM) is a parametric unsupervised clustering algorithm, which assumes the data points to be normally distributed. GMM uses a weighted sum of multiple Gaussian densities with several parameters, such as mean vector, covariance matrix and mixture weight. GMM has been utilized in several imaging segmentation applications (Aristophanous et al. 2007, Bui et al. 2015). K-means algorithm is an unsupervised non-parametric clustering algorithm. The predefined number of classes (k value) is needed for the classification process, and the algorithm divides all the data points into the predefined number of clusters based on the distance of the nearest centroid of a cluster (Ma et al. 2009). The K-means algorithm has also been used in the field of medical image segmentation (Janssen et al. 2009, Paldino et al. 2011).

2.5 Advanced applications of PET/CT imaging in RT planning of HNC

The clinical utilization of [^{18}F]FDG PET/CT in staging, monitoring therapy response and detecting recurrences of HNC has proven to be feasible with reasonable effort, although further investigation involving these indications is ongoing and will likely strengthen the clinical impact. In contrast, the applications of PET/CT imaging in RT planning are far more complex and are still far from ideal, indicating a need for intensive research.

In general, the major principle in the advancement of HNC RT is the escalation of the target dose in tumor tissue, together with the reduction of radiation-induced toxicity in nearby organs at risk (OAR) (Grégoire et al. 2015). An important part

of this process is the delineation of gross tumor volume (GTV) in dose planning images. In addition, special attention must be paid to microscopic disease around GTV, the volume of which, together with GTV, is called clinical target volume (CTV). Additional safety margins are needed for systematic and random errors, such as those derived from patient positioning and random shifts in internal anatomy. These safety margins are included in the planning target volume (PTV). In general, an effort is made to safely reduce this volume and sharpen the dose gradient between PTV and surrounding tissues, since PTV is typically remarkably larger than the GTV and CTV. Several approaches to achieve this goal have been developed utilizing a close integration between imaging and RT systems, such as image-guided RT (IGRT), which allows for accurate positioning of patients with image guidance (Simpson et al. 2010).

The traditional ‘gold standard’ for GTV delineation in HNC has been anatomical imaging with CT or MRI combined with physical examination (Delouya et al. 2011). MRI provides a good resolution in the differentiation of soft tissues, which is important in the contouring of tumor boundaries. On the other hand, CT imaging is needed for dose distribution calculations, which are performed with special attention to variable electron densities in tissues. An [^{18}F]FDG PET/CT-based GTV is typically smaller than a corresponding GTV based on pure CT or MRI, but [^{18}F]FDG PET may provide additional information of tumor location and extension that would not be visible in anatomical images (Leclerc et al. 2015, Bird et al. 2015). However, a major challenge is a lack of consensus regarding optimal criteria for GTV delineation in [^{18}F]FDG PET images. Several threshold-based segmentation methods have been evaluated, as well as some adaptive and gradient based algorithms. Furthermore, some applications utilizing advanced mathematical methods such as fuzzy logic have been assessed. Nevertheless, an optimal method for the task of GTV delineation in [^{18}F]FDG PET image has not yet been identified (Differding et al. 2015).

On the other hand, a non-uniform dose delivery to the target tissue is one of the novel approaches of modern RT (Ling et al. 2000). This concept derives from the fact that tumor tissue is heterogenous in radiosensitivity. Therefore, several approaches have been considered and, to some extent, already evaluated in an attempt to successfully escalate the delivered radiation dose in tumor. Typically, dose escalation is targeted to certain parts of the target volume, through a process called dose painting (Bentzen and Grégoire 2011). There are two alternative ways to perform dose painting, either calculating the dose for certain subvolumes of the tumor (i.e. DPBC) or using more accurate voxel-based calculations called dose painting by numbers (DPBN). [^{18}F]FDG PET/CT has been utilized in a few clinical trials where PET-image voxel intensities were used as a template for DPBN (Grégoire et al. 2015). In a phase I clinical trial (Madani et al. 2011), median doses of 80.9

Gy in high-dose CTV and 85.9 Gy in GTV were reached in patients with HNC, but late non-healing mucosal ulcers at the site of dose escalation were considered dose-limiting toxicity. In that study, a median physical dose of 80.9 Gy was determined as the maximum tolerated dose (Madani et al. 2011).

As stated previously, PET imaging of tumor hypoxia for the task of modification of RT dose delivery has been a subject of intense research. The traditional concept has been dose escalation in hypoxic subvolumes based on a pretreatment hypoxia PET image. Several theoretical considerations and modelling studies have been conducted in this field, where PET/CT imaging is considered to be the most promising imaging modality (Grosu et al. 2007, Servagi-Vernat et al. 2015, Chang et al. 2013). One important drawback is the limited spatial resolution of PET imaging, which limits the disclosure of very short distances between distinct hypoxic subvolumes in the tumor microenvironment. Also, the dynamic nature of tumor hypoxia, as well as the questionable repeatability of pretreatment hypoxia imaging (see chapter 2.3.2.6), have raised a shadow over this concept.

Recently, it has become more evident that the presence of residual tumor hypoxia after the first few weeks of RT has a higher impact on the outcome of RT and disease-free survival compared to pretreatment tumor hypoxia (Löck et al. 2017, Zips et al. 2012, Bollineni et al. 2014). Moreover, several studies have reported a general reduction of hypoxic subvolumes observed with [¹⁸F]FMISO, [¹⁸F]FAZA or [¹⁸F]HX4 PET/CT imaging during the first few weeks of RT compared to the baseline hypoxic subvolumes (Wiedenmann et al. 2015, Mortensen et al. 2012, Zegers et al. 2016, Okamoto et al. 2016). This phenomenon has been speculated to be caused by reoxygenation of the tumor as well as changes in perfusion and tracer kinetics (Eschmann et al. 2007, Zips et al. 2012). On the other hand, spatial changes in the location of hypoxia, as well as newborn hypoxic voxels, have been observed in the PET images obtained during RT (Servagi-Vernat et al. 2014). In addition, an important approach to be investigated is the spatial variability of hypoxia tracer distribution during RT and the co-localization of hypoxic subvolumes with later tumor recurrences. A study using [¹⁸F]FMISO PET/CT reported remarkable variability in these parameters and concluded by suggesting an adaptation of treatment plans and an inclusion of sufficient margins for selective dose painting protocols in hypoxic HNC tumors. According to that study, an alternative strategy for the treatment modification might be a compromised dose-escalation targeted at the GTV (Zschaek et al. 2015).

Adaptive RT is a process through which the treatment plan may be modified based on anatomical and biological changes of the target tissue during the treatment (Brouwer et al. 2015). These modifications are performed using feedback provided with repeated imaging, such as CT, MRI and PET imaging. However, thus far,

adaptive approaches have been experimental, and there remain major issues to be evaluated, such as the safety of dose reduction performed with subsequent images as well as the frequency and timing of repeated imaging (Castadot et al. 2011). PET/CT imaging will probably have an important role in the performance of adaptive RT protocols. Frequently, an updated definition of MATV in [¹⁸F]FDG PET/CT imaging might be beneficial for revision plans by reducing the dose in OARs and thus toxicity. In fact, clinical trials combining adaptive RT and DPBN based on [¹⁸F]FDG PET/CT imaging have already been conducted (Duprez et al. 2011, Berwouts et al. 2013). Analogically, hypoxia PET/CT is considered to be a potential imaging tool for adaptive treatment modifications (Servagi-Vernat et al. 2015). Nonetheless, substantial efforts will still be needed in order to establish the role of hypoxia PET/CT imaging in adaptive dose-escalation strategies (Horsman et al. 2012). However, an interim analysis of the very first interventional hypoxia PET-guided dose painting study in HNC has been published recently, and the initial results suggest that [¹⁸F]FMISO PET/CT-based dose-escalation to hypoxic tumor volume is feasible without excess toxicity (Welz et al. 2017).

PET/CT imaging might also have a role in the implementation of de-intensified (C)RT protocols. Recently, a major trend has been the feasibility evaluation of de-intensification of the treatment for patients presenting with HPV-positive oropharyngeal cancer with a very good prognosis (Ang et al. 2010, Swiecicki et al. 2016). Initial clinical trials involving this issue have already been conducted, and several more are ongoing (Bhatia and Burtneß 2015). While providing additional information for GTV delineation, [¹⁸F]FDG PET/CT may be an important tool in the implementation of these treatment protocols. On the other hand, hypoxia PET/CT imaging with [¹⁸F]FMISO has been evaluated as a method for ruling out clinically important hypoxia when conducting de-intensified CRT in HPV-positive oropharyngeal carcinoma patients (Lee et al. 2016).

In addition, [¹⁸F]FDG PET/CT has been considered for RT dose de-escalation protocols in which a reduced elective dose for cervical lymph nodes in HNC is used. This strategy was initially presented in a study evaluating different methods for a FDG PET-based target volume definition of metastatic lymph nodes (Schinagl et al. 2009). Currently, an ongoing prospective study (NCT 02442375) investigates whether a FDG PET-guided de-escalated radiation dose prescription in elective neck irradiation is feasible for the treatment of laryngopharyngeal cancer and whether this leads to improved quality of life after treatment without a higher recurrence rate.

3 AIMS OF THE STUDY

Today, PET/CT imaging is widely used in the clinical management of HNC as well as in translational cancer research. However, a remarkably high and diverse potential has been recognized in the utilization of this imaging modality in the management of HNC. This study focused on the feasibility and utilization of a novel hypoxia tracer [^{18}F]EF5 and further evaluation of dynamic [^{18}F]FDG PET/CT imaging in HNC.

The specific aims of this study were:

1. To investigate biodistribution and dosimetry of the hypoxia tracer [^{18}F]EF5 in oncologic patients to obtain reliable data on the safety and radiation exposure of the tracer in clinical imaging (Study I).
2. To evaluate the uptake of [^{18}F]EF5 in head and neck SCC xenograft tumors and study the variability of the tracer uptake in a larger time scale as well as the association between [^{18}F]EF5 uptake and the tumor growth rate (Study II).
3. To investigate the repeatability of intratumor uptake and spatial distribution of [^{18}F]EF5 in head and neck SCC tumors of newly diagnosed patients subjected to chemoradiotherapy (Study III).
4. To evaluate advanced mathematical methods in the analysis of dynamic [^{18}F]FDG PET/CT imaging to be used in discriminating different tissue types in patients with oropharyngeal cancer (Study IV).

4 PATIENTS AND EXPERIMENTAL TUMOR MODELS

4.1 Patients

Clinical studies I, III and IV were conducted at Turku University Hospital (TURKU) in Finland. In study I, another center, University of Pennsylvania (PENN), collaborated with TURKU. Both sites were responsible for their own patient enrollment. In TURKU, the patients were enrolled for all of the clinical studies through the Department of Otorhinolaryngology – head and neck surgery and the Department of Oncology and Radiotherapy. In PENN, the patients were enrolled through the Department of Radiation Oncology.

Table 1 Patient characteristics in study I. Patients numbered 1–10 were imaged at University of Pennsylvania (with PET scanner), and patients numbered 11–16 at Turku University Hospital (with PET/CT scanner). (Table modified from Publication I).

Patient no.	Gender	Age (years)	Weight (kg)	Tumor Histology
1	female	50	70	Non-small-cell lung carcinoma
2	female	50	58	Non-small-cell lung carcinoma
3	female	49	72	Non-small-cell lung carcinoma
4	male	46	104	Non-small-cell lung carcinoma
5	male	48	88	Non-small-cell lung carcinoma
6	male	21	87	Anaplastic astrocytoma
7	female	28	51	Cervical adenocarcinoma
8	female	39	88	Breast; Invasive ductal carcinoma
9	male	51	128	Brain; Glioblastoma multiforme
10	female	34	84	Breast; Invasive ductal carcinoma
11	male	62	108	Diffuse large B cell lymphoma
12	male	43	107	Diffuse large B cell lymphoma
13	female	56	91	Follicular lymphoma
14	male	32	63	Testicular cancer (seminoma)
15	male	37	64	Hodgkin's lymphoma
16	female	39	73	Hodgkin's lymphoma

In study I, the enrolled patients had previously been treated for a solid malignant tumor (Table 1), whereas in studies III and IV the participants were newly diagnosed patients with SCC of the head and neck subjected to definitive CRT (Table 2). In all three studies, the patients with serious cardiovascular, renal, liver or hematological disease were excluded, as were those who were pregnant or nursing. Eleven subjects participated in study III, but one subject with tonsillar cancer was excluded from analyses due to an extremely low uptake in the [^{18}F]FDG PET/CT image, which was performed after a diagnostic tonsillectomy.

The patients in studies III and IV underwent diagnostic procedures of HNC prior to the study enrollment. The HPV status from the primary tumor histopathological sample was determined using the IHC of p16 antigen (Table 2). These patients underwent standard dental examination, which included extraction of decayed teeth and management of oral chronic infections when necessary. All dental procedures performed prior to the PET scan were depicted in detail in the medical reports available for investigators defining volumes of interest for RT as well as for the protocol of study IV (please see chapter 5).

4.2 Experimental animals, cell lines and tumor models

In study II, four different human head and neck SCC cell lines were utilized (Table 3). The cells were routinely cultured using Dulbecco's modified Eagle's medium (Gibco®, Thermo Scientific, Waltham, MA, USA) containing L-glutamine (Gibco), non-essential amino acids (Gibco), streptomycin, penicillin (Gibco), and 10% FBS (Gibco) at 37 degrees Celsius in a humidified air atmosphere containing 5% CO₂. For detaching and plating, cells were washed with PBS, trypsinized (Trypsin-EDTA in HBSS, Gibco), and centrifuged at 1,300 rpm for 5 minutes.

Male nude mice (Athymic nu/nu; Harlan laboratories, Horst, The Netherlands) were used for the experiments. The animals first received total-body irradiation with 4 Gy one day before the tumor induction in order to suppress the immune system and facilitate tumor growth. Tumor cells ($1-10 \times 10^6$) were subcutaneously injected into the flank or neck of each mouse. The mice were observed on a daily basis, and tumor sizes were closely monitored over the study period ($V = \pi/6 \times a \times b \times c$) using Vernier Caliper measurements. The starting and end points of exponential tumor growth periods were determined from the growth curves. The percentage of tumor growth rate per day from the exponential growth period was calculated. The mice were maintained in individually ventilated cages under controlled pathogen-free environmental conditions with free access to water and standard food.

Table 2 Patient characteristics in studies III and IV. All patients in these studies were men (Table modified from publications III and IV).

Study	Patient no.	Age (years)	Weight (kg)	Tumor site	TNM ¹	Grade	HPV status
III	1	73	77	Base of tongue	T2N1M0	II	+
III	2	68	49	Base of tongue	T3N0M0	III	-
III	3	56	86	Base of tongue	T3N1M0	II	+
III	4	69	66	Oropharyngeal wall	T4aN1M0	II	-
III	5	58	125	Base of tongue	T2N2cM0	II	-
III	6	60	84	Nasopharynx	T4N3bM0	II	+
III	7	69	94	Hypopharynx	T4bN2cM0	II	-
III	8	76	78	Nasopharynx	T4N2bM0	NA	-
III	9	66	77	Tonsil	T4aN2cM0	III	+
III	10	66	85	Hypopharynx	T4aN2bM0	II	-
IV	1	63	79	Tonsil	T2N2bM0	III	+
IV	2	65	74	Tonsil	T3N2bM0	II	+
IV	3	59	80	Tonsil	T2N2bM0	II	+
IV	4	59	88	Base of tongue	T3N2bM0	II	+
IV	5	58	63	Oropharyngeal wall	T3N0M0	I	-

¹ According to the Union for International Cancer Control (UICC) TNM Classification of malignant tumours (7th edition, 2010)

4.3 Ethical considerations

All clinical studies (I, III, IV) were performed in accordance with the Declaration of Helsinki. The clinical studies at TURKU were approved by the Ethics Committee of Hospital District of Southwest Finland; at PENN, the Institutional Review Board at the University of Pennsylvania approved the protocol of the study I. The study drug EF5 in unlabeled form had previously been documented to be safe for humans even in gram doses (Koch et al. 2001). In Finland, the National Agency for Medicines (the previous name for the Finnish Medicines Agency) had supplied

permission for human use of [^{18}F]EF5 prior to these studies (KL nro 165/2005). The human subjects who participated in these trials (studies I, III and IV) were thoroughly informed about the study and had more than a few days' time to consider their participation before giving their final consent.

The animal procedures were reviewed by the local Ethics Committee on Animal Experimentation of the University of Turku and approved by the Provincial State Office of Western Finland. The welfare of the animals was monitored carefully, and the size of the tumors was strictly limited in order to ensure the wellbeing of the animals.

Table 3 Characteristics of the cell lines. (Table modified from publication II).

Cell line	Primary tumor site	TNM-classification	Grade
UT-SCC 8	Supraglottic larynx	T2N0M0	G1
UT-SCC 34	Supraglottic larynx	T4N0M0	G1
UT-SCC 70	Hypopharynx	T4N1M0	G3
UT-SCC 74A	Mobile tongue	T3N1M0	G1 to G2

5 METHODS

5.1 Synthesis of PET tracers (Studies I-IV)

Two different PET tracers were used in these studies. [^{18}F]FDG was synthesized from mannosyl triflate using a nucleophilic method. Radiochemical purity exceeded 95% in every production batch.

The synthesis of [^{18}F]EF5 is described in detail elsewhere (Dolbier et al. 2001, Eskola et al. 2012). Briefly, [^{18}F]EF5 was prepared from an allyl precursor using radioactive fluorine in a one-step reaction in the presence of trifluoroacetic acid at low temperatures. In study I, two individual institutions performed the synthesis. At TURKU, high molar activity ^{18}F -fluorine was used (Bergman and Solin 1997), leading to the final molar activity of about 4 GBq/ μmol , whereas at PENN, ^{18}F -fluorine with a ~ 100 -fold lower molar activity was used (Dolbier et al. 2001). At TURKU, the synthesis of [^{18}F]EF5 in study II was similar to that in study I. In study III, the final molar activity was about 8 GBq/ μmol due to some advancements in tracer production. The radiochemical purity was higher than 98.5% in every production batch of [^{18}F]EF5.

5.2 Imaging protocols (Studies I-IV)

Four different PET or PET/CT scanners were used in the studies of this work (Table 4).

5.2.1 Study I

In study I, the patients underwent whole-body imaging from the vertex to the midline of the thigh. An intravenous dose of 107–364 MBq (mean 217 MBq) of [^{18}F]EF5 was administered to each subject. The image acquisition was performed at 15 minutes and at 1, 2 and 4 hours post-injection. One subject at TURKU (Nr 15) was imaged five times, and the latest image was acquired at 6 hours post-injection.

At TURKU, the image session was divided into 7–8 bed positions depending on the length of the patient. The acquisition time for the 1st and 2nd scan was 3 minutes per bed position, and for the 3rd–5th scan the acquisition time was 4 minutes per bed position. At PENN, the imaging time was between 60 and 100 seconds per bed

position followed by a standard transmission scan. Otherwise, the protocol was similar between the two sites.

Table 4 Information on PET and PET/CT scanners.

Study	Type of scanner	Manufacturer	PET scanner ring	Transverse FOV (cm)	Axial FOV (cm)	CT
I	Philips Allegro PET ¹	Philips	Gadolinium oxyorthosilicate crystals	57.6	18	NA
I, III	Discovery VCT PET/CT	GE Healthcare	Bismuth germinate oxide crystals	70	15.7	64-slice
II	Inveon Multimodality	Siemens Medical Solutions	Lutetium oxyorthosilicate crystals	10	12.7	maximum resolution 40 microns
III, IV	GE D690 PET/CT	GE Healthcare	Lutetium yttrium orthosilicate crystals	70	15.7	64-slice

¹ Philips Allegro PET was used at the University of Pennsylvania.

At both sites, blood samples were collected from the arm contralateral to that used for tracer injection to determine [¹⁸F]EF5 blood activity. The time points for sample collection were 15 minutes before injection; 15 minutes and 1, 2, and 4 hours after the injection; and at the end of the final imaging session. Patients were asked to avoid voiding 45 minutes before tracer injection. After injection of [¹⁸F]EF5, patients were requested to void before each scan, and the time and volume of excretion were recorded. The activity concentration (kBq/ml) of blood and urine samples were measured using a liquid-scintillation counter. The metabolites of the tracer in representative samples were also assessed by HPLC.

5.2.2 Study II

The mice were subjected to PET/CT imaging under general anesthesia induced with 2.5% isoflurane. The body temperature of the mice was maintained using a heating pad. The tumors were clearly visible when the first scan with [¹⁸F]EF5 was performed. Following a transmission scan for attenuation correction using the CT modality, a dynamic 80-minute emission scan was acquired. A second [¹⁸F]EF5 scan and an [¹⁸F]FDG scan were performed on consecutive days after the clear

exponential growth period of tumors. The injected doses (mean \pm SD) of [^{18}F]EF5 and [^{18}F]FDG were 11.1 ± 1.9 MBq and 10.9 ± 2.8 MBq, respectively. The mice were sacrificed after the last PET/CT scan and the direct tissue oxygen measurements (see chapter 5.4) had been performed.

5.2.3 Study III

The patients underwent static [^{18}F]EF5 PET/CT scans twice, with a median interval of 7 days (range 5–7 days). The first (EF5_{1st}) and second (EF5_{2nd}) scans were performed with the same scanner and similar protocol. An intravenous bolus of [^{18}F]EF5 was administered to the patients with a mean (\pm SD) dose of 303 ± 23 MBq (range 246–345 MBq). A CT scan was performed for anatomical reference and attenuation correction purposes prior to PET imaging. Immediately after the CT scan, the PET data acquisition was begun at 178 ± 9 minutes postinjection (mean \pm SD, range 160–190 minutes). The mean (\pm SD) inpatient difference between PET acquisition start times of repeated scans was 7 ± 6 min (range 0–19 min). The PET acquisition time was 6 minutes for one bed position covering the axial field of view (FOV) of 15 cm. The patients were immobilized on the scanner table using a thermoplastic RT mask, and the positioning was performed utilizing the predefined fiducial markers in the mask and the scanner lasers. Venous blood samples for blood activity measurements were taken before and after the imaging session. The blood activity at the mid-time point of image acquisition was defined using linear interpolation with decay-corrected blood activity values.

On a separate day, the patients in study III underwent a whole-body [^{18}F]FDG PET/CT imaging for the purpose of RT planning. The immobilization was performed using the same mask and positioning parameters as in the [^{18}F]EF5 PET/CT scans. The [^{18}F]FDG PET/CT scan was acquired either between the [^{18}F]EF5 PET/CT scans or within one week after these scans using the same scanner, except in the cases of patients 1, 2, 5 and 7, whose [^{18}F]FDG PET/CT was obtained with Discovery VCT PET/CT (Table 4).

5.2.4 Study IV

The PET/CT imaging protocol was designed for both the planning of RT and the purposes of the study. The patients were required to fast for at least 4 hours before the PET scan. The immobilizing and positioning of the patients were performed similarly as in Study III (see Chapter 5.2.3).

The scanning protocol is presented in Figure 5. First, a CT scan from the neck region was acquired. Next, the injection of [^{18}F]FDG was administered, and, simultaneously, the dynamic PET scan was started. During the first 30 minutes, dynamic PET data from the neck region were acquired (0–30 minutes divided into 20 frames). The patients were then allowed to rest outside the scanner room before the second imaging session.

The second imaging session started with a whole-body CT scan followed at 70 minutes post-injection by the standard diagnostic whole-body PET scan for the staging and RT planning purposes. The PET acquisition started with the imaging of two bed positions from the neck region (4 minutes per bed position); next, two bed positions were imaged from the lower part of the body (2 minutes per bed position). Finally, the very last frame of the PET data from the neck region (one bed position, four minutes frame) was acquired. In total, the PET data contained 22 time frames. The imaging data of the 21st frame was used to calculate the uptake value in the form of static parameter SUV.

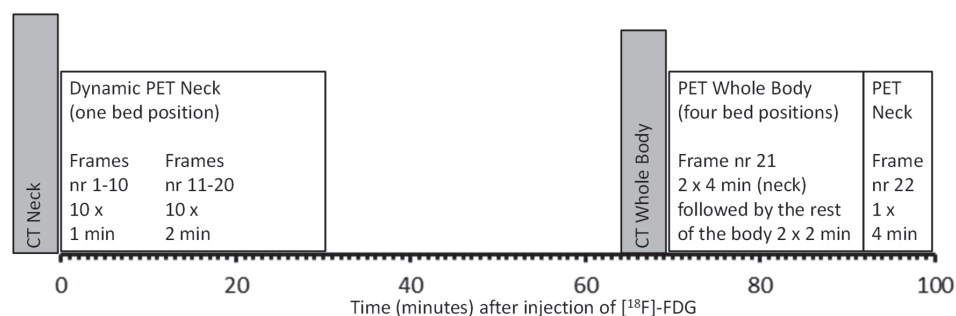


Figure 5 Time sequence of acquisition of CT images and [^{18}F]FDG PET images in study IV (Figure adopted from Publication IV).

5.3 Clinical and biological safety monitoring of exposure of [^{18}F]EF5 (Study I)

In addition to dosimetry calculations, the biological and clinical safety of [^{18}F]EF5 was monitored in Study I. Each subject underwent a complete physical examination prior to the study, including assessment of medical history. A complete blood-count, complete serum biochemical analysis and urine analysis were performed at baseline and repeated after the scans. An electrocardiogram (ECG) registration was obtained 15 minutes before and 15 minutes after the [^{18}F]EF5 injection. Vital signs (heart rate, systolic and diastolic blood pressure, respiratory rate and body

temperature) were monitored at the following time-points: 1–2 hours preinjection; 15 minutes preinjection; and 15 minutes and 1, 2 and 4 hours post-injection.

Patients were questioned about any discomfort or adverse experiences during the study and during a follow-up phone call 24 hours after the imaging study. Common Terminology Criteria for Adverse Events version 3.0 (CTCAE) was used for the scoring of adverse events.

5.4 Direct oxygen measurements (Study II)

In study II, two of the tumors were measured with the Licox (GMS, Kiel-Mielken-dorf, Germany) system in order to determine directly the oxygen partial pressure inside the tumor. The Licox CC1.P1 probe with temperature sensor was used in this study. It was 0.65 mm in diameter and had an 18-mm² oxygen sensitive area, which produced an estimate of nearby oxygen tension (Integra Neuroscience). The mice were first anesthetized in a similar manner to when they were subjected to imaging. Then the probe was inserted inside the tumor, and the recording was continued until the p_{iO_2} level remained stable for at least 20 min.

5.5 Image analysis (Study I-IV)

5.5.1 Image reconstruction

In study I, the reconstruction of static PET images was performed using a filtered back projection or iterative ordered-subset expectation maximization (OSEM) method with 2 iterations and 28 subsets. In study II, a 3D list mode data acquisition was used for the dynamic images, and the sinograms were framed into 25 frames. For the reconstruction, an OSEM 2D iterative algorithm with ramp filter, 4 iterations and 16 subsets was used. In study III, the images obtained with GE D690 PET/CT were reconstructed using a 192x192 matrix with transverse FOV of 70 cm. In order to achieve a uniform voxel size for all PET images in study III, a corresponding 128x128 reconstruction matrix with transaxial FOV of 46.7 cm was selected for the GE Discovery VCT PET/CT. In study IV, the image reconstruction was performed using an iterative VUE Point FX method (GE Healthcare, 2011) with 2 iterations and 24 subsets. A reconstruction matrix of 192 x 192 and transverse FOV 70 cm was used.

In all PET studies, at least attenuation, random, decay and detector deadtime corrections were performed for the raw data. Additionally, in all clinical PET studies, scatter correction was performed.

5.5.2 Analysis of tracer uptakes

In Study I, activity data in the following source-organs were determined: urinary bladder, kidney, liver, gall bladder, heart, brain, lungs, muscle and red marrow (from femur). For PENN patients, the activity values were recorded from attenuation-corrected PET images by delineating the VOIs of the target organs and multiplying the achieved pixel values by an acquisition-specific calibration factor. For TURKU patients, the organ VOIs were delineated on the CT images using iPlan RT Image version 4.1 (BrainLab AG, Munich, Germany), and the average activity concentration of the VOI was measured. It was also possible to determine the activity concentration for the spleen, pancreas and blood (aorta) for TURKU patients due to the advanced capability of the CT to define organ positions.

In Study II, the Inveon Research Workplace Image Analysis software (Siemens Medical Solutions, Knoxville, TN, USA) was used to analyze the PET/CT images. The images were summed from 60 to 80 minutes post injection. The VOIs were drawn over the whole tumors on CT images and then transformed to the corresponding PET images. Radioactivity uptake was calculated as the percentage of injected dose per gram tissue (%ID/g) in the whole tumor. In addition, the hottest cluster of the tumor (HC) containing voxels with the highest 10% of the VOI was determined using the same uptake unit (%ID/g).

In Study III, the tracer uptake in primary tumors and reference tissues was determined using Varian Eclipse software version 13.6 (Varian Medical Systems, Palo Alto, CA, USA). The MATV in the [^{18}F]FDG image was used for delineation of primary tumor VOI. In the definition of MATV, either the threshold of 40% of SUV_{max} or a fixed SUV 5.0 threshold was used, depending on which more closely matched with the anatomical GTV in the CT image. Posterior neck muscles were used as a reference tissue for tracer uptake (Komar et al. 2008). The [^{18}F]EF5 and [^{18}F]FDG images were rigidly registered using anatomical information of CT images.

Voxel-by-voxel analysis between repeated [^{18}F]EF5 images was performed using Carimas 2.9 software (www.turkupetcentre.fi/carimas). The transformation matrices were applied to the [^{18}F]EF5 images in order to define the MATV-based primary tumor VOIs in [^{18}F]EF5 images. The VOI structure transformations were controlled by visual inspection of PET images and cross tabulation of uptake values within tumor VOI. The tracer uptake was measured as kBq/ml and then decay

corrected and converted to SUV under the assumption of water density. The mean and maximum intratumor uptake and the mean uptake in posterior neck muscle reference (SUV_{muscle}) were determined. The tumor-to-muscle uptake ratio (TMR) of 1.5 was used as a threshold for hypoxic tissue. Both absolute hypoxic volume (HV) and fractional hypoxic volume (FHV) were calculated, with the latter based on the ratio of hypoxic voxels and all voxels in tumor VOI.

In Study IV, volumes of interest were determined on the co-registered PET/CT images by a qualified radiation oncologist. The primary tumors and all metastatic lymph nodes were drawn manually on the images from the 21st frame. The identification of the primary tumor was based on the detection of an FDG positive lesion in an area with a history of positive biopsy and, in the case of metastases, detection of an FDG positive lesion in the neck where the overlying lymph node could be seen on the anatomical CT. The largest metastatic lymph node when available (in four out of five cases) was chosen for the analysis.

Healthy tissue surrounding a primary tumor VOI was determined using a voxel threshold function. First, a 3D box-shaped VOI was defined around the irregularly shaped tumor VOI, and the tumor voxels (according to the manually contoured tumor VOI) were subtracted from this box-shaped VOI, leaving behind the healthy tissue voxels. VOIs representing inflammatory lesions in the mandible or other parts of the oral cavity were also drawn, with attention paid to the written information of all dental procedures. All the patients had at least one inflammatory lesion due to extraction of decayed teeth, which was feasible for further analysis of PET data. Finally, all the VOIs that were contoured on the PET/CT images from the 21st frame were rigidly registered with the corresponding PET/CT images from the first part of the imaging session (frames 1–20).

5.6 Radiation absorbed dose calculations (Study I)

The total activity in each organ was determined by multiplying the previously described VOI concentration (kBq/ml) by that organ's volume according to the OLINDA/EXM software (Vanderbilt University, Nashville, TN, USA) adult male phantom (Stabin et al. 2005). The percentage of activity in each source organ was defined. For this dataset, a monoexponential function was iteratively fit to each source organ TAC using a nonlinear least-squares regression algorithm (SAAM II v1.2 software; The SAAM Institute, Inc.). The cumulative activity of each source organ was determined by analytically integrating the curve-fit function from time equals zero to infinity after correcting the terms of activity by the isotope decay. The area under the curve (AUC) represented the residence time of the organ.

When defining the excretory clearance of the tracer, it was assumed that only negligible amounts of activity reached the small bowel. This was considered a reasonable assumption because of the short half-life of ^{18}F (109.8 minutes) and the imaging data supporting the elimination of the tracer almost solely by urinary excretion. Urinary excretion was measured directly from urine samples and was assumed to represent the total biological loss of ^{18}F from the body. Then, the total body retention was determined as 100% minus the urinary-excreted activity. This total body retention curve was used to determine the total body residence time in the same manner as for individual source organs.

OLINDA/EXM software was used to calculate the estimated absorbed doses for the individual source organs and for the whole body using the previously described residence time data. Since the phantom is hermaphroditic, it generates radiation dose estimates for testes, breasts, ovaries and uterus.

5.7 Evaluation of the performance of dynamic features in the distinction of different tissue types (Study IV)

Time-activity curves (TACs) were generated for every voxel of the predefined VOIs. A total of seven dynamic features were developed for the purpose of voxel classification (Table 5). The features were based on tissue-specific characteristics in the glucose metabolism, as well as transport due to differences in the expression of GLUT proteins (see chapter 2.3.1). Those differences were expected to be discernible in the analysis of dynamic uptake data from distinct tissue types. In addition, some features were constructed with information based on the visual inspection of TACs. The detailed information of dynamic features is described in the master's thesis of Mueez U. Din (Din 2014). SUV and all dynamic features were calculated for each of the voxels from the predefined VOIs. These predefined VOIs provided the best available ground-truth for labelling voxels according to tissue type.

Two classification algorithms, GMM and K-means, were utilized to evaluate performance of the dynamic features and SUV in discriminating different tissue types. The classification and performance evaluation were carried out with the programming software Matlab (Version: R2006b). There were four tissue types in the evaluation: primary tumor, inflammation, metastatic lymph node and healthy tissue surrounding the primary tumor. Of these tissue types, four binary classification experiments were performed discriminating 1) tumor vs. inflammatory tissue, 2) tumor vs. healthy tissue, 3) tumor vs. metastatic lymph node and 4) inflammatory tissue vs. metastatic lymph node.

Table 5 List of dynamic features utilized in the analyses of [^{18}F]FDG uptake in study IV (Table adopted from Publication IV).

Dyna- mic fea- ture	Description	Equation
D1	Retention index	Retention index = $(A_{\text{late}} - A_{\text{early}}) / A_{\text{early}}$
D2	Early slope	Early slope = $[\text{mean}(A_{15}, A_{16} \dots A_{20}) - \text{mean}(A_1, A_2 \dots A_{10})] / [\text{mean}(T_{15}, T_{16} \dots T_{20}) - \text{mean}(T_1, T_2 \dots T_{10})]$
D3	Area under the TAC ₂₀₋₂₁	Area under the TAC ₂₀₋₂₁ = $[(T_{21} - T_{20}) \times (A_{21} - A_{20}) / 2] + (T_{21} - T_{20}) \times A_{20}$
D4	Sum fluctuation 1-22	Sum fluctuation ₁₋₂₂ = $ A_2 - A_1 + A_3 - A_2 + A_4 - A_3 \dots + A_{22} - A_{21} $
D5	Variance of local change	Variance of local change = $\text{Var}[(A_2 - A_1), (A_3 - A_2) \dots (A_{22} - A_{21})]$
D6	Temporal variance	Temporal variance = $\text{Var}[A_1, A_2, A_3 \dots A_{22}]$
D7	Sum of three slopes	Sum of three slopes = Slope 1 + Slope 2 + Slope 3 where, Slope 1 = $[\text{mean}(A_{15}, A_{16} \dots A_{20}) - \text{max}(A_1, A_2 \dots A_5)] / [\text{mean}(T_{15}, T_{16} \dots T_{20}) - \text{max}(T_A)]$ Slope 2 = $(A_{21} - A_{20}) / (T_{21} - T_{20})$ Slope 3 = $(A_{22} - A_{21}) / (T_{22} - T_{21})$

“A” refers to the activity concentration and “T” to the time of the PET frame. The corresponding PET frame is presented with the number in the subscript. The subscript “early” refers to the first ten PET frames and the subscript “late” refers to the 21st PET frame

In each binary classification, a mixture of unlabeled data from two different tissue types was input to a classification algorithm, which was set up to divide the data into two classes based on the evaluated dynamic feature or SUV. The algorithm produced a label for the voxel according to whether the voxel belonged to the positive class (e.g., primary tumor) or negative class (e.g., healthy tissue). These labels were compared to the ground-truth labels in order to determine the specificity and sensitivity of the dynamic features and SUV. For the GMM algorithm, receiver operating characteristics (ROC) analysis was performed to present the performance of the algorithm with a combined measure of sensitivity and specificity. For the K-means, the specificity and sensitivity values were presented separately. As a final point, sensitivity and specificity of the dynamic features were compared with those of the static parameter SUV.

5.8 Statistical analysis (Study I-IV)

In study I, the arithmetic mean of the absorbed radiation doses of individual organs were calculated for two institutions (TURKU and PENN). In addition, a weighted arithmetic mean of the results was calculated using the number of subjects at the institutions as weighting factors. The variability of the individual parameters is presented with a standard deviation (SD) and coefficient of variation (COV). A two-tailed T-test was used to define whether there were any statistically significant changes in blood chemistry values (liver and renal function tests).

In study II, the number of experimental tumors was moderately low, and therefore the variables are reported as medians and interquartiles, unless otherwise stated. Pearson correlation coefficients were used to correlate PET tracer uptake parameters with the percentage of tumor growth rate per day, as well as in the correlation of the tumor volume and the uptake of [¹⁸F]EF5.

In Study III, a two-tailed paired T-test was used for comparison of inpatient differences in injected doses, injected doses per weight and acquisition starting times between the first and second [¹⁸F]EF5 PET/CT scans. Intraclass correlation coefficients (ICC) were calculated for normally distributed tumor level parameters. For HV and FHV, which were not normally distributed, a non-parametric Spearman rank correlation test was used. Pearson correlation coefficients were calculated for repeated voxel-level uptake parameters. Agreement between the repeated scans was assessed by constructing a Bland-Altman plot for both the tumor-level and voxel-level parameters. In addition, upper and lower limits of agreement (LoA) and coefficient of repeatability (CoR) were calculated.

In Study IV, a Wilcoxon rank sum test was used to investigate the statistical significance of differences between the performance of dynamic features and SUV. The non-parametric test was chosen because of the low number of subjects.

In all studies, P-values of less than 0.05 were considered statistically significant (two-tailed). For the test of normality, the Shapiro-Wilk test was used in cases of observations less than 50, and visual assessment was used in cases of observations more than 150 (voxel-level parameters in study III). The statistical analyses were generated using SAS software, version 9.3 or 9.4 for Windows (SAS institute, Cary, NC, USA).

6 RESULTS

6.1 Biodistribution and radiation dosimetry of [^{18}F]EF5 (Study I)

The radiation absorbed dose estimates calculated by OLINDA/EXM male phantom are presented in Table 6. The dose estimates were based on an assumed voiding interval of 4.8 hours. The critical organ was the urinary bladder (with the highest average dose of 0.12 ± 0.034 mSv/MBq, range 0.069–0.20 mSv/MBq), followed by the gall bladder, liver, kidney, brain, lungs and heart wall. The mean organ radiation dose was not higher than 0.026 mSv/MBq in any of the organs except urinary bladder and gall bladder (Table 6). The highest individual organ radiation dose (excluding the bladder wall) in all of the patients was 0.051 mSv/MBq. For the whole study population, the EDE was estimated to be 0.021 ± 0.003 , and the ED 0.018 ± 0.002 mSv/MBq. The comparison of the mean radiation dose values between the two study sites is also presented in Table 6. The only larger variations (1.5x) were observed among the radiation doses of urinary bladder and gall bladder. The apparent drug half-lives for TURKU and PENN patients were approximately 7.5 and 10.5 hours, respectively. These half-lives were determined using the activity in the heart as a surrogate for the blood activity, since by HPLC it was known that blood contained almost entirely non-metabolized drug.

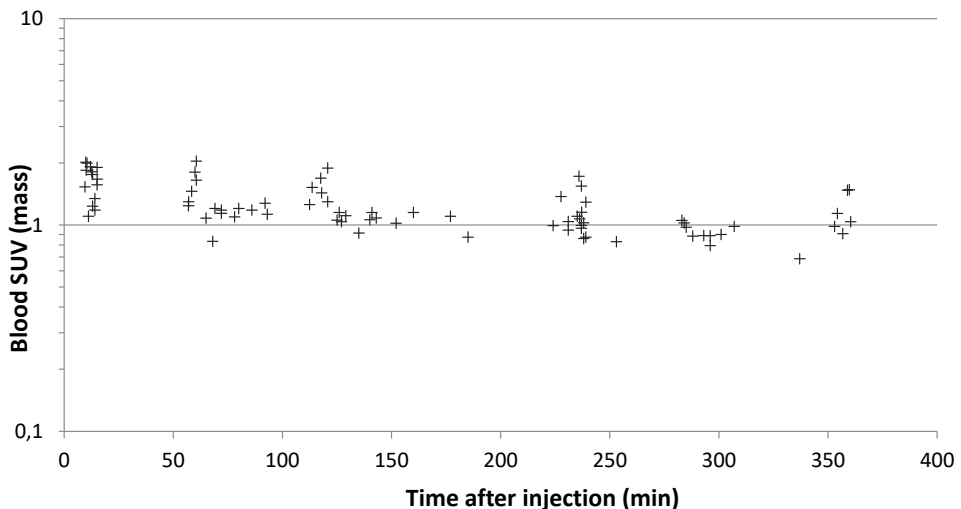


Figure 6 Blood SUV values calculated from gamma counts after the administration of [^{18}F]EF5 (Figure adopted from Publication I).

The mean urinary excretion of [^{18}F]EF5 was 25% (range 12.4–50%) of injected activity over 320 minutes (range 233–364) post-injection. In Figure 6, the blood

SUV data of individual subjects reflects the rapid equilibration of [^{18}F]EF5 over the whole body. The first mean blood SUV (at times < 15 minutes) was 1.63 ± 0.31 , and the overall mean of blood SUV values was 1.24 ± 0.33 .

Table 6 [^{18}F]EF5 mean radiation-absorbed dose estimates for the adult male phantom using assumption of 4.8-hour bladder voiding interval. (Table modified from Publication I).

Target organ	TURKU mean (mSv/MBq)	PENN mean (mSv/MBq)	Ratio TURKU: PENN	Weighted mean (mSv/MBq)	COV
Urinary bladder wall	1.5E-01	1.0E-01	1.50	1.2E-01	28%
Gall bladder wall	3.3E-02	2.2E-02	1.50	2.6E-02	36%
Liver	2.2E-02	2.5E-02	0.88	2.4E-02	20%
Kidneys	2.4E-02	2.3E-02	1.03	2.3E-02	17%
Uterus	2.0E-02	1.8E-02	1.11	1.9E-02	8%
Osteogenic cells	1.6E-02	1.7E-02	0.99	1.7E-02	3%
Ovaries	1.6E-02	1.5E-02	1.03	1.5E-02	3%
Lower large intestine wall	1.5E-02	1.5E-02	1.04	1.5E-02	3%
Small intestine	1.4E-02	1.4E-02	0.99	1.4E-02	2%
Heart wall	1.3E-02	1.6E-02	0.86	1.5E-02	14%
Upper large intestine wall	1.3E-02	1.4E-02	0.98	1.3E-02	2%
Pancreas	1.3E-02	1.4E-02	0.95	1.3E-02	4%
Adrenals	1.3E-02	1.3E-02	0.95	1.3E-02	4%
Testes	1.2E-02	1.2E-02	1.02	1.2E-02	2%
Stomach wall	1.2E-02	1.2E-02	0.95	1.2E-02	4%
Red marrow	1.2E-02	1.1E-02	1.07	1.1E-02	4%
Spleen	1.1E-02	1.2E-02	0.95	1.2E-02	4%
Muscle	1.1E-02	1.1E-02	0.96	1.1E-02	2%
Thymus	1.1E-02	1.0E-02	0.94	1.1E-02	5%
Thyroid	1.0E-02	1.1E-02	0.95	1.0E-02	5%
Brain	8.9E-03	7.8E-03	1.13	8.2E-03	16%
Breasts	8.3E-03	8.8E-03	0.94	8.6E-03	5%
Skin	8.1E-03	8.4E-03	0.96	8.3E-03	4%
Lungs	8.0E-03	8.7E-03	0.91	8.3E-03	8%
Total body	1.1E-02	1.2E-02	0.98	1.1E-02	2%
Effective dose equivalent	2.3E-02	2.0E-02	1.17	2.1E-02	12%
Effective dose	1.9E-02	1.7E-02	1.12	1.8E-02	10%

The data of individual sites and the pooled data are presented separately.

6.2 Clinical safety of [^{18}F]EF5 (Study I)

The administration of [^{18}F]EF5 was well tolerated in all study subjects. No clinically significant adverse events were noticed during the study. The monitoring of vital signs (i.e., heart rate, systolic and diastolic blood pressure, respiratory rate and temperature) and ECG did not reveal any significant changes between the results before and after the study drug injection. The results of the biochemical tests

(serum creatinine, BUN, AST, ALT or total bilirubin) were not affected by the administration of [^{18}F]EF5.

6.3 Uptake of PET tracers in experimental tumors and tumor growth rate (Study II)

Table 7 presents the growth rates and volumes of experimental tumors and uptake values of [^{18}F]EF5 and [^{18}F]FDG in individual scans. The median whole tumor uptake was higher (1.75% ID/g) for [^{18}F]FDG than for [^{18}F]EF5 (first and second scans: 1.40% ID/g and 1.50% ID/g, respectively). The intratumor [^{18}F]EF5 uptake varied considerably between the first and second scans, as the uptake in the tumors could either increase or decrease during the tumor growth (Table 7). An example of PET/CT images is presented in Figure 7.

The percentage of tumor growth rate per day and [^{18}F]FDG uptake showed a trend toward a relationship ($r = 0.348$, $p = 0.32$), as did [^{18}F]EF5 uptake in the first scan ($r = 0.398$, $p = 0.25$) although these relationships were not statistically significant. Instead, the uptake of [^{18}F]EF5 in the latter scan showed a stronger correlation with the tumor growth rate ($r = 0.766$), and this correlation was statistically significant ($p = 0.01$) (Figure 8). In addition, the corresponding relationships between the tumor growth rate and the HC 10% uptakes in tumors in these three scans were studied separately (Figure 9). The strongest, although non-significant, correlation was seen between the HC 10% uptake of the second [^{18}F]EF5 scan and tumor growth rate per day ($r = 0.503$, $p = 0.14$).

There was no relationship in the latter scan between the [^{18}F]EF5 uptake and the tumor volume ($r = -0.217$, $p = 0.55$). However, the tumor volume seemed to be in relation to the [^{18}F]EF5 uptake in the first scan, when the tumors were smaller ($r = 0.510$, $p = 0.13$), although this correlation was not statistically significant.

Table 7 $[^{18}\text{F}]$ FDG and $[^{18}\text{F}]$ EF5 uptake values, tumor volumes, and tumor growth rates (Table adopted from Publication II).

Tumor no.	Cell line	$[^{18}\text{F}]$ FDG uptake (%ID/g)	$[^{18}\text{F}]$ FDG uptake (HC 10%)	First $[^{18}\text{F}]$ EF5 uptake (%ID/g)	First $[^{18}\text{F}]$ EF5 uptake (HC 10%)	Second $[^{18}\text{F}]$ EF5 uptake (%ID/g)	Second $[^{18}\text{F}]$ EF5 uptake (HC 10%)	First and second $[^{18}\text{F}]$ EF5 scans time interval (days)	First $[^{18}\text{F}]$ EF5 tumor volume (mm^3)	Second $[^{18}\text{F}]$ EF5 tumor volume (mm^3)	Tumor growth rate (%/day)
1	8	1.59	2.15	0.54	0.90	0.99	1.60	26	29	183	8.20
2	8	1.31	2.21	1.41	3.45	0.68	1.03	26	91	685	8.69
3	8	1.51	2.31	1.39	2.86	0.95	1.15	26	45	275	7.38
4	34	1.80	2.99	2.35	3.15	2.42	2.89	5	325	367	14.08
5	34	3.06	4.44	1.96	2.56	2.75	3.64	7	330	408	11.92
6	74A	2.23	3.71	1.30	1.80	1.75	2.56	36	223	660	6.64
7	74A	2.76	3.89	0.88	1.30	2.67	3.34	14	53	105	12.08
8	70	1.06	2.89	1.50	3.18	1.37	2.62	15	340	569	6.11
9	70	1.70	5.13	1.39	2.17	1.03	2.15	35	93	274	5.29
10	70	4.58	10.89	2.16	3.28	1.62	3.39	35	30	168	9.17
Median		1.75	3.35	1.40	2.71	1.50	2.59	26	92	321	8.45
(Q1-Q3)		(1.51 to 2.76)	(2.31 to 4.44)	(1.30 to 1.96)	(1.80 to 3.18)	(0.99 to 2.42)	(1.60 to 3.34)	(14 to 35)	(45 to 325)	(183 to 569)	(6.64 to 11.92)

6.4 Direct oxygen measurements of experimental tumors (Study II)

Tumors 4 and 5 in study II were measured with the Licox system to determine the tissue oxygen tension ($p_{ti}O_2$). Both of these tumors were hypoxic, and $p_{ti}O_2$ values were 3.6 and 0.9 mmHg, respectively. An example of the $p_{ti}O_2$ measurement curve is presented in Figure 7.

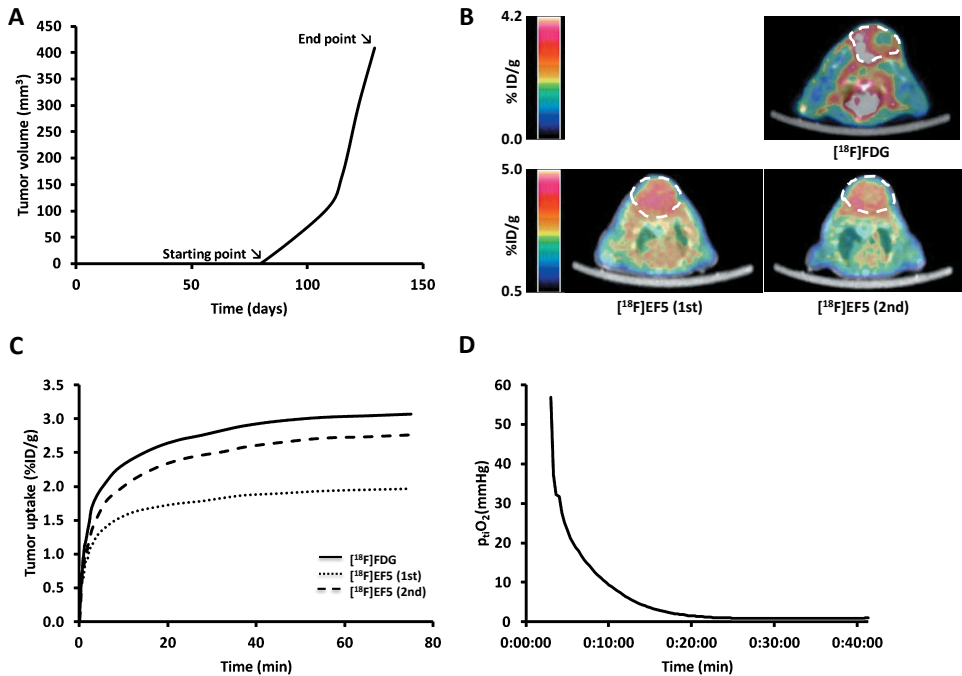


Figure 7 Growth curve, PET data and $p_{ti}O_2$ measurements from tumor no. 5 in Study II. (A) Growth curve of the tumor with the starting point and end point of the exponential growth period. (B) Axial PET/CT images of the tumor. (C) Time-activity curves of the tracer uptake into the tumor in the [18F]FDG scan and in the first and second [18F]EF5 scans. (D) Measurements of the partial pressure of oxygen in the tumor (Figure adopted from Publication II).

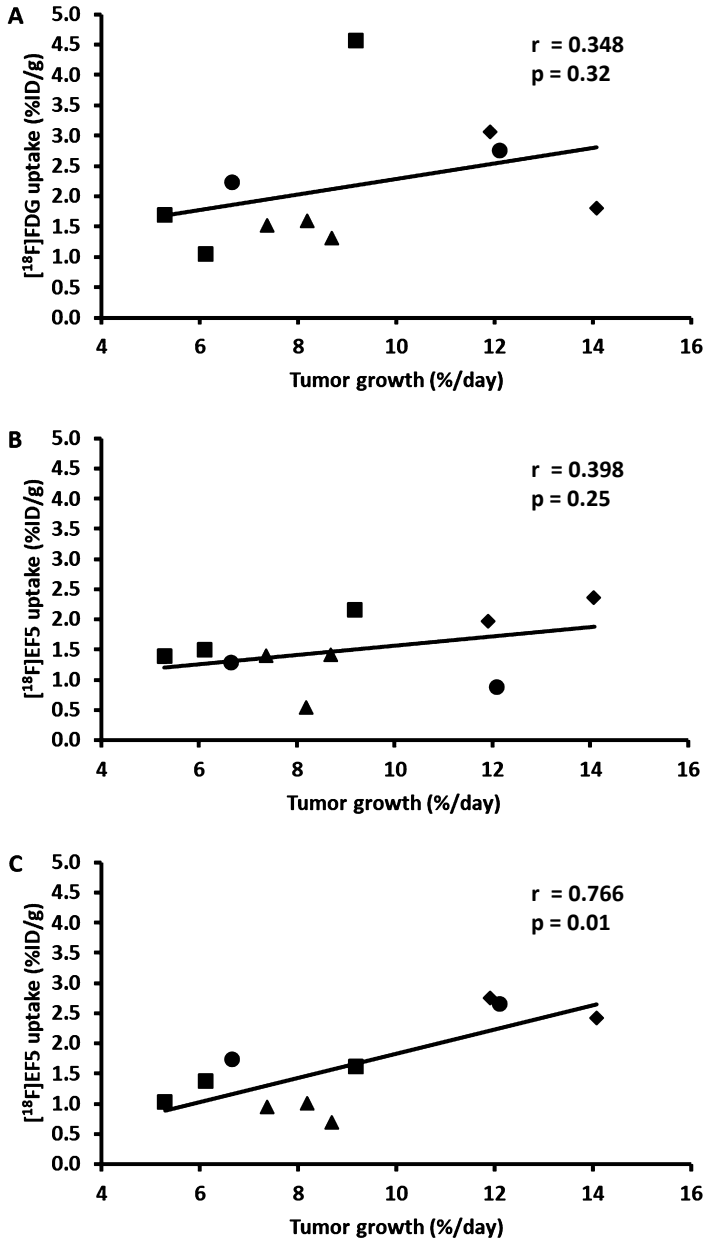


Figure 8 Whole tumor uptake values compared to the tumor growth rate. The black line indicates the linear relationship between tumor growth rate and the tracer uptake in the ^{18}F FDG-scans (A) and in the first (B) and second (C) ^{18}F EF5 scans. UT-SCC8 (filled triangle), UT-SCC34 (filled diamond), UT-SCC74A (filled circle), and UT-SCC70 (filled square) (Figure adopted from Publication II).

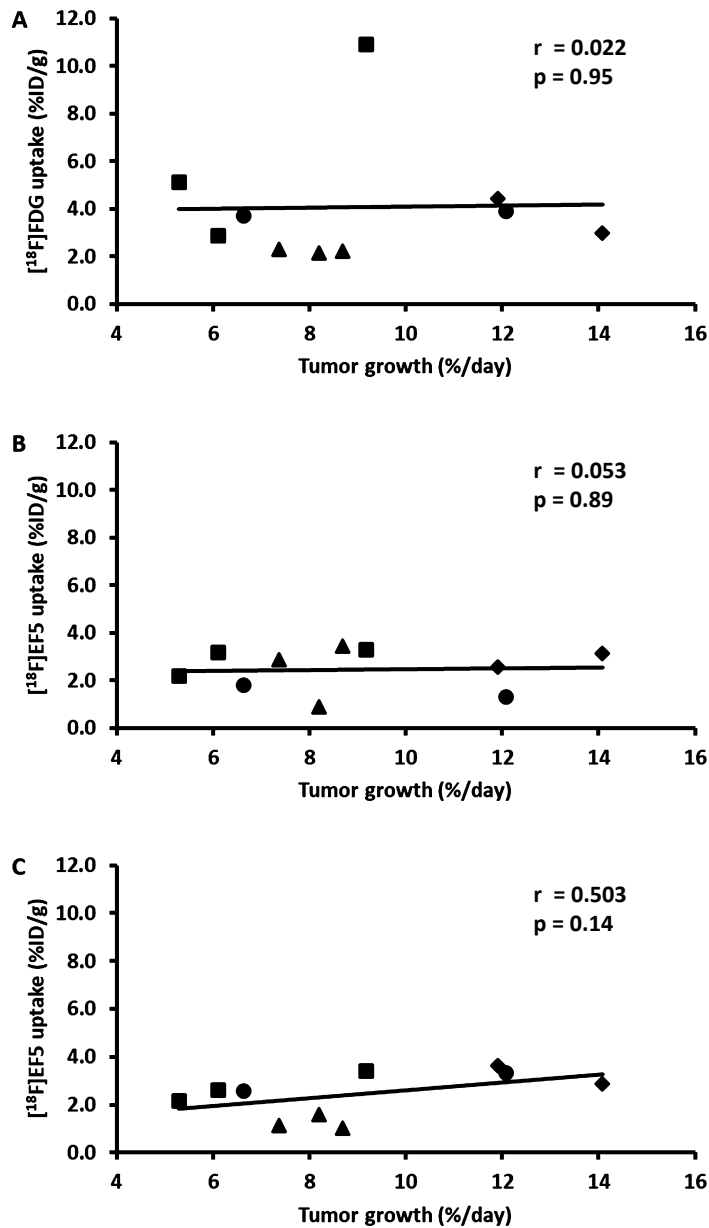


Figure 9 HC 10% uptake values compared to the tumor growth rate. The black line indicates the linear relationship between tumor growth rate and the tracer uptake in the $[^{18}\text{F}]\text{FDG}$ -scans (A) and in the first (B) and second (C) $[^{18}\text{F}]\text{EF5}$ scans. UT-SCC8 (filled triangle), UT-SCC34 (filled diamond), UT-SCC74A (filled circle), and UT-SCC70 (filled square) (Figure adopted from Publication II).

6.5 Repeatability of intratumor uptake in paired [^{18}F]EF5 PET/CT scans (Study III)

Patients with locally advanced pharyngeal cancer participated in study III. The average (\pm SD) tumor volume in the CT image was $41.4 \pm 26.9 \text{ cm}^3$ (range 8.9 – 94 cm^3), and the corresponding MATV in [^{18}F]FDG PET image was $39.0 \pm 26.7 \text{ cm}^3$ (range 7.2 – 100 cm^3). The mean (\pm SD) whole tumor uptake (SUVmean) of [^{18}F]EF5 among all patients was at the same level in the first scan (1.49 ± 0.16) and in the second scan (1.54 ± 0.21). Correspondingly, the SUVmax values in the first and second scans were 2.12 ± 0.34 and 2.09 ± 0.35 , respectively (Table 8). There was high correlation and high agreement between these parameters within individual patients. The ICCs for SUVmean and SUVmax were 0.81 ($p < 0.001$) and 0.85 ($p < 0.001$), respectively. The Bland-Altman plots of these parameters are presented in Figure 10. The mean (\pm SD) difference and relative CoR for SUVmean were 0.05 ± 0.11 and 15%, and the corresponding parameters for SUVmax were -0.02 ± 0.20 and 17%, respectively. Examples of paired [^{18}F]EF5 PET/CT images are presented in Figure 11.

Table 8 Tumor-level and muscle uptake parameters in the repeated [^{18}F]EF5 PET/CT scans (Table adopted from Publication III).

Patient nr	SUV _{mean}		SUV _{max}		TMR		FHV%		HV (cm ³)		SUV _{muscle}	
	Scan 1	Scan2	Scan 1	Scan2	Scan 1	Scan 2	Scan 1	Scan 2	Scan 1	Scan 2	Scan 1	Scan 2
1	1.61	1.75	1.99	2.19	1.43	1.49	21.2	34.5	1.5	2.5	1.12	1.18
2	1.26	1.24	1.57	1.52	1.30	1.28	3.8	1.2	1.3	0.4	0.97	0.97
3	1.59	1.58	2.08	2.06	1.29	1.28	6.8	3.5	3.4	1.8	1.23	1.24
4	1.27	1.22	1.83	1.75	1.17	1.18	4.9	4.3	1.0	0.9	1.09	1.03
5	1.55	1.49	2.33	1.95	1.34	1.27	19.1	6.7	4.0	1.4	1.15	1.18
6	1.65	1.68	2.46	2.59	1.52	1.55	40.5	45.2	40.6	45.3	1.08	1.09
7	1.40	1.64	2.67	2.43	1.46	1.48	34.2	40.3	18.3	21.6	0.96	1.10
8	1.71	1.89	2.40	2.53	1.45	1.64	32.6	63.7	16.4	32.0	1.18	1.15
9	1.38	1.48	1.85	2.05	1.43	1.47	27.8	32.4	10.4	12.1	0.96	1.01
10	1.52	1.43	2.02	1.87	1.21	1.17	1.5	0.3	0.3	0.0	1.25	1.22
Mean	1.49	1.54	2.12	2.09	1.36	1.38	19.3	23.2	9.7	11.8	1.10	1.12
SD	0.16	0.21	0.34	0.35	0.12	0.16	14.3	22.8	12.7	16.0	0.11	0.09

TMR tumor-to-muscle uptake ratio, FHV fractional hypoxic volume, HV hypoxic volume

The radioactivity measurements of background tissues, which were performed for reference, provided highly stable results. The activity in venous blood samples measured as SUV was observed to have a high correlation and agreement between the paired scans, since the ICC was 0.94 ($p < 0.001$) and relative CoR was 10%. Similarly, the SUV_{muscle} values were highly repeatable, as the ICC was 0.84 ($p < 0.001$) and the mean (\pm SD) difference was 0.15 ± 0.06 with the upper and lower LoA of 0.26 and 0.04, respectively, and the relative CoR was 10%.

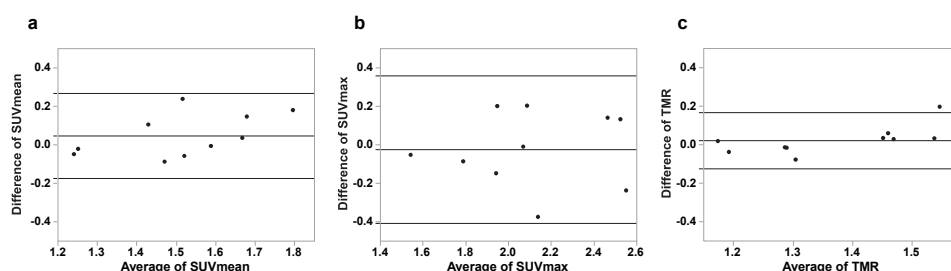


Figure 10 Bland-Altman plots of SUV_{mean} (a), SUV_{max} (b) and TMR (c) of repeated [¹⁸F]EF5 PET/CT scans. From top to bottom, the three solid line represent the upper LoA, mean difference and the lower LoA, respectively (Figure adopted from Publication III).

The highest repeatability for tumor level uptake parameters was observed within TMR. The ICC for TMR was 0.87 ($p < 0.0001$), and the mean difference was 0.02 ± 0.07 , with an upper and lower LoA of 0.17 and -0.12, respectively (Figure 10). The relative Cor for TMR was 10%. Both HV and FHV seemed to have a high correlation between the paired scans. The Spearman correlation coefficients for these parameters were $r = 0.93$ ($p < 0.0001$) and $r = 0.94$ ($p < 0.0001$), respectively.

The voxelwise scatterplots of TMR of repeated scans for individual patients are presented in Figure 12. The mean of the Pearson correlation coefficients of individual patients was 0.65 (range 0.48–0.87). The agreement parameters of voxel-by-voxel analysis between paired scans are presented in Table 9. The mean calculated from mean differences of voxel-level TMR of individual patients was 0.02 ± 0.07 . For the pooled dataset, the mean difference of voxelwise TMR was 0.03 ± 0.20 (Figure 13), and the absolute CoR and relative CoR were 0.39 and 28%, respectively.

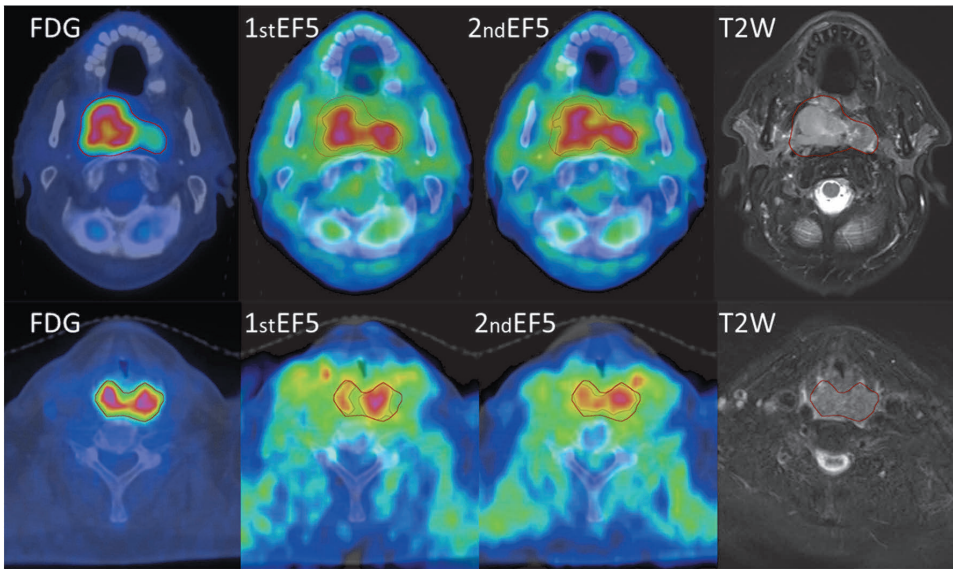


Figure 11 PET/CT and MR images of patients presenting with nasopharyngeal cancer (No. 6; upper row) and hypopharyngeal cancer (No. 7; lower row). From left to right, corresponding axial slices from diagnostic $[^{18}\text{F}]\text{FDG}$, the first and the second $[^{18}\text{F}]\text{EF5}$ PET/CT; and fat-suppressed T2-weighted MR images are shown. The red line denotes the metabolically active tumor volume delineation using SUV 5.0 as a threshold in the $[^{18}\text{F}]\text{FDG}$ PET image. The black line indicates hypoxic subvolume delineation using a tumor-to-muscle uptake ratio of 1.5 as a threshold in the $[^{18}\text{F}]\text{EF5}$ PET image. The inpatient voxel-by-voxel analysis showed a high correlation and agreement between the paired $[^{18}\text{F}]\text{EF5}$ PET/CT images for patient No. 6, while those for patient No. 7 were among the lowest of 10 patients (Figure adopted from Publication III).

There were no statistically significant differences between injected doses, injected doses per weight and scanning start times of individual patients within repeated $[^{18}\text{F}]\text{EF5}$ PET/CT scans (for all comparisons $p > 0.36$).

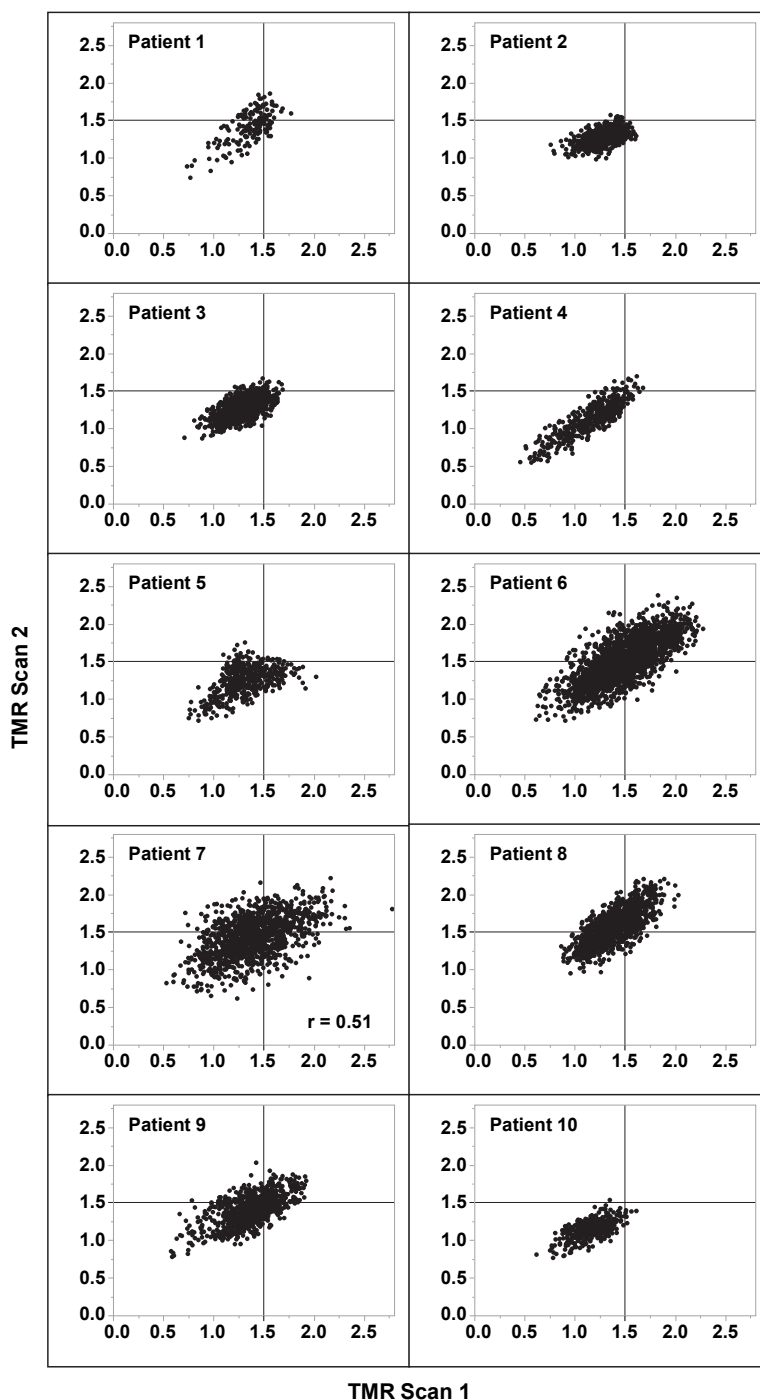


Figure 12 Scatterplots of voxelwise tumor-to-muscle uptake ratios (TMR). The X-axis represents the first $[^{18}\text{F}]\text{EF5}$ PET/CT scan and the Y-axis represents the second. Solid lines indicate the cutoff level for hypoxia (TMR 1.5) (Figure adopted from Publication III).

Table 9 Results of voxel-level agreement analysis between tumor-to-muscle uptake ratios of repeated [^{18}F]EF5 PET/CT scans (Table adopted from Publication III).

Patient no.	Number of voxels	Mean \pm SD difference (95 % CI)	Upper LoA	Lower LoA
1	165	0.05 \pm 0.16 (0.02 — 0.07)	0.36	-0.26
2	757	0.00 \pm 0.12 (-0.01 — 0.01)	0.23	-0.23
3	1159	-0.02 \pm 0.13 (-0.02 — -0.01)	0.23	-0.26
4	470	-0.03 \pm 0.12 (-0.04 — -0.02)	0.21	-0.27
5	476	-0.07 \pm 0.21 (-0.09 — -0.05)	0.34	-0.48
6	2306	0.02 \pm 0.20 (0.01 — 0.02)	0.40	-0.37
7	1233	0.03 \pm 0.28 (0.02 — 0.05)	0.59	-0.52
8	1155	0.18 \pm 0.16 (0.17 — 0.19)	0.48	-0.13
9	860	0.03 \pm 0.18 (0.02 — 0.04)	0.39	-0.33
10	394	-0.02 \pm 0.12 (-0.03 — 0.00)	0.22	-0.26
Pooled dataset	8975	0.03 \pm 0.20 (0.02 — 0.03)	0.41	-0.36

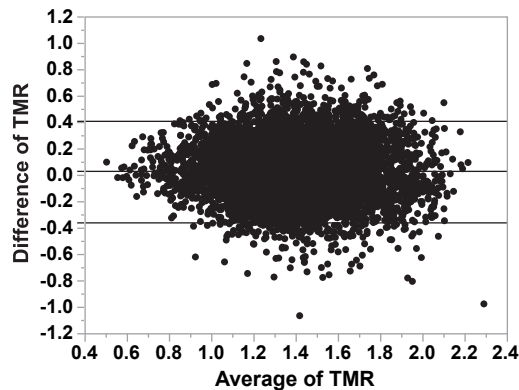


Figure 13 A Bland-Altman plot of voxelwise tumor-to-muscle uptake ratios (TMRs) from the pooled data of all patients. From top to bottom, the three solid lines represent the upper limit of agreement (LoA), the mean difference, and the lower LoA, respectively (Figure adopted from Publication III).

6.6 Analysis of dynamic [^{18}F]FDG images (Study IV)

An example of PET/CT images of Study IV is presented in Figure 14. The patients (nos. 1–3) with tonsillar carcinoma had lower [^{18}F]FDG uptake in their primary

tumors compared to the two patients (nos. 4–5) with non-tonsillar carcinoma. Moreover, the tracer uptake was higher in the inflammatory regions compared to that in the primary tumor among tonsillar carcinoma patients. In Figure 15 and Figure 16, a different shape of TACs of primary tumors among tonsillar carcinoma patients can be recognized compared to those of non-tonsillar carcinoma patients. When comparing the uptake values of all VOIs, it was observed that median SUV of the metastatic lymph nodes was lower than that of the inflammatory regions in the whole study population. The mean SUVs from all VOIs are presented in Table 10.

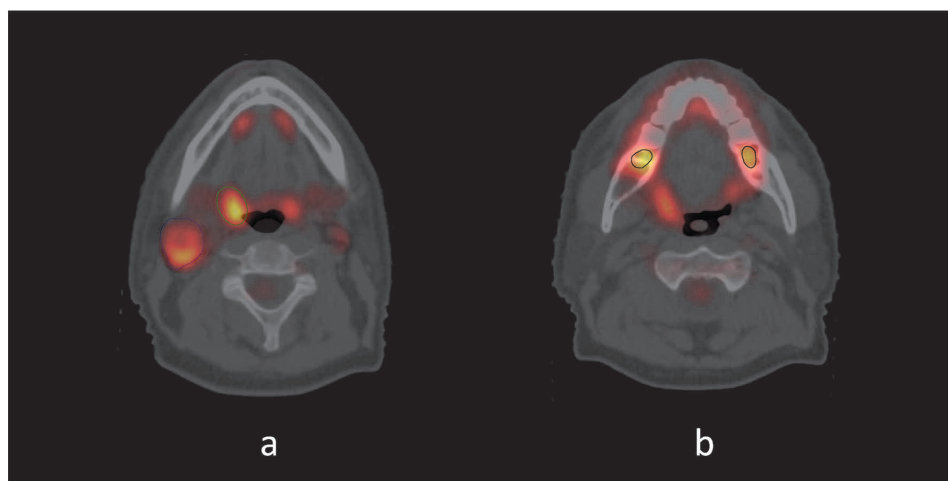


Figure 14 [^{18}F]FDG PET/CT images of patient no. 3 in Study IV. The primary tumor is located in the right palatine tonsil, and the metastatic lymph node is located on the right side of the neck (a). The dental inflammatory lesions on both sides of the mandible are visible (b) (Figure adopted from Publication IV).

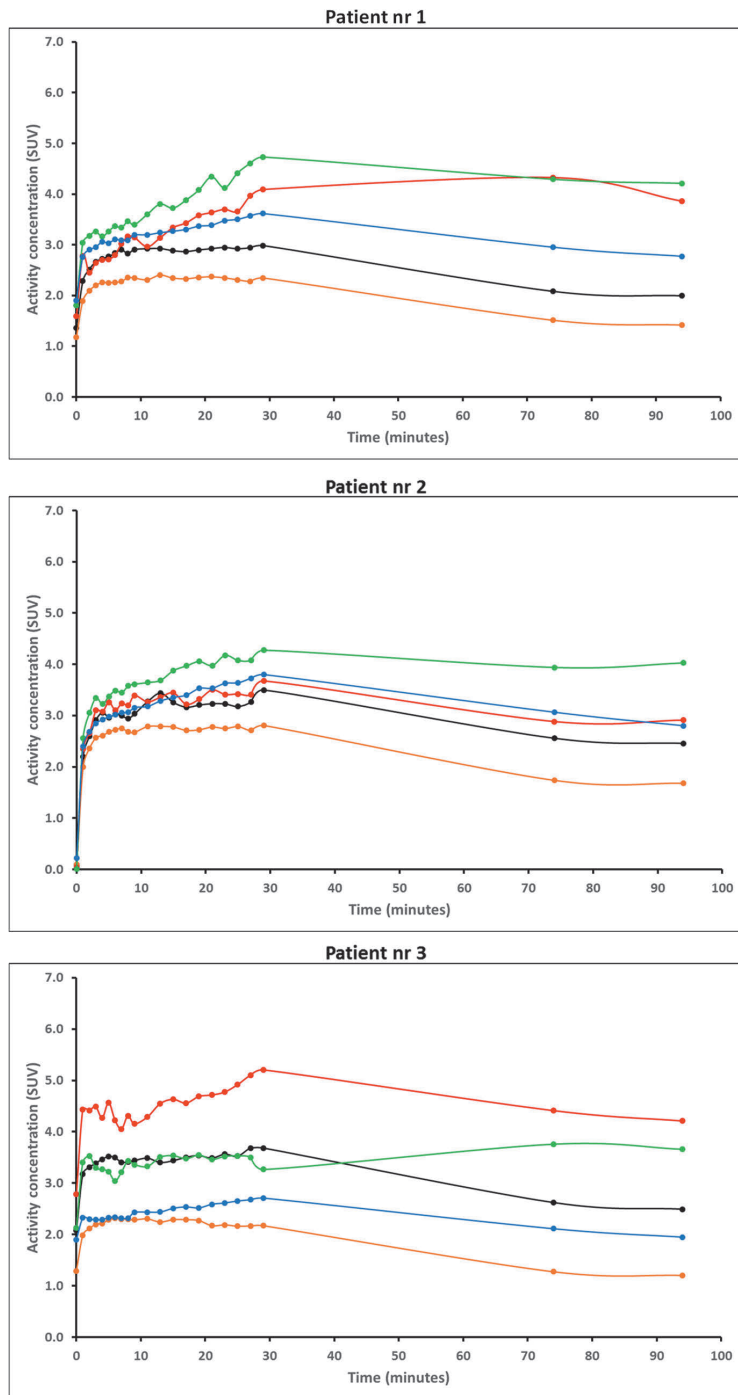


Figure 15 $[^{18}\text{F}]\text{FDG}$ time-activity curves of volumes of interests of patients 1–3 with HPV-positive tonsillar carcinoma. (black=primary tumor, orange=healthy tissue, blue=metastatic lymph node, red=inflammatory region left side, green=inflammatory region right side) (Figure adopted from Publication IV).

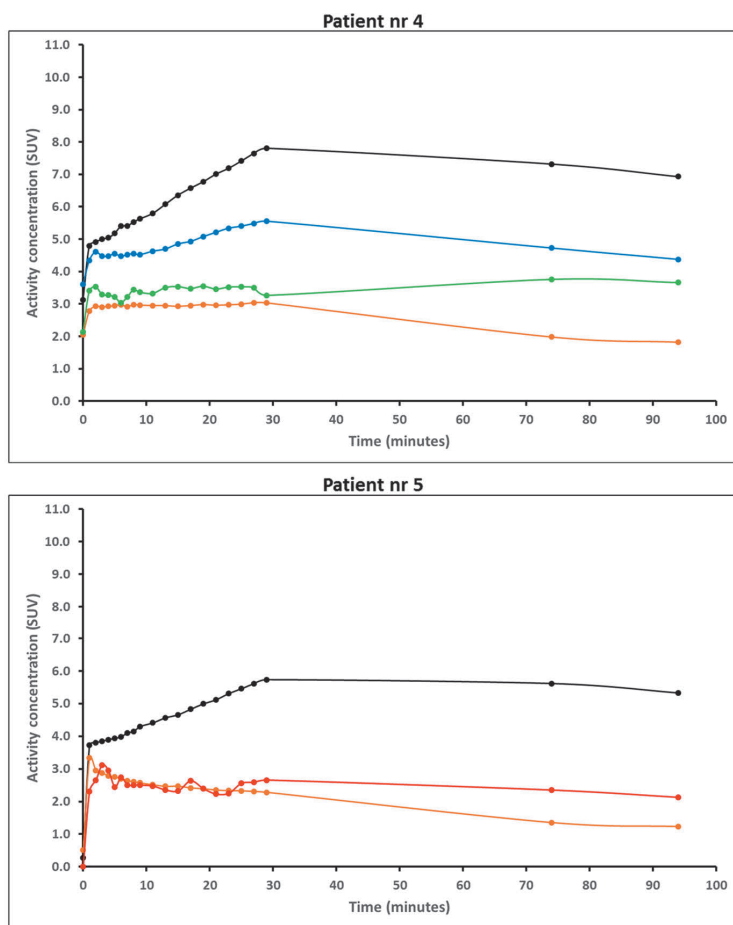


Figure 16 $[^{18}\text{F}]\text{FDG}$ time-activity curves of volumes of interests of patients with HPV-positive (No 4) and HPV-negative (No 5) non-tonsillar carcinoma. (black=primary tumor, orange=healthy tissue, blue=metastatic lymph node, red=inflammatory region left side, green=inflammatory region right side) (Figure adopted from Publication IV).

When discriminating the primary tumor from inflammation using the GMM algorithm, dynamic feature D3 showed a slightly better accuracy compared to SUV, although the difference was not statistically significant ($p = 0.82$). Among non-tonsillar carcinoma patients, D1 and D6 showed a better accuracy compared to SUV, but these differences were not significant ($p = 0.33$ for both two features). Using the K-means algorithm in the same tissue distinction procedure, D3 was not superior to the SUV in the whole patient population nor was D6 among the non-tonsillar carcinoma patients (Table 11).

Table 10 $[^{18}\text{F}]\text{FDG}$ mean standardized uptake values (SUV) of volumes of interest (Table adopted from publication IV).

Patient no.	Primary tumor	Metastatic lymph node	Inflammatory lesion left	Inflammatory lesion right	Healthy tissue
1	2.08	2.95	4.33	4.29	1.51
2	2.56	3.07	3.94	2.88	1.73
3	2.62	2.11	3.76	4.41	1.28
4	7.32	4.73	NA	3.82	1.98
5	5.61	NA	2.35	NA	1.36
Median	2.62	3.01	3.85	4.06	1.51

The dynamic features were also used in discriminating the voxels of the primary tumors from the healthy tissue surrounding the tumor. Nevertheless, none of the features showed a better discriminative ability compared to SUV. In addition, the same result was observed in the distinction between the metastatic lymph node and inflammation. On the other hand, when discriminating metastatic lymph node voxels from those of the primary tumor, D5 with K-means showed a slightly better sensitivity and specificity compared to the static parameter SUV (Table 11). All of the results from tissue distinction calculations are presented in Table 11.

Table 11 Performance of SUV and dynamic features in discrimination of voxel of different tissue types in dynamic [^{18}F]FDG PET images (Table adopted from Publication IV).

Volumes of interest in discrimination	Algorithm ¹ G=GMM K=K-MEANS	SUV	D1	D2	D3	D4	D5	D6	D7
Primary tumor and inflammation (all patients)	G	0.825	0.812	0.707	0.845	0.703	0.689	0.764	0.801
Primary tumor and inflammation (all patients)	K	0.723/0.896	0.645/0.877	0.667/0.631	0.691/0.929	0.592/0.713	0.556/0.726	0.600/0.405	0.629/0.704
Primary tumor and inflammation (tonsillar ca)	G	0.864	0.799	0.726	0.870	0.678	0.684	0.738	0.828
Primary tumor and inflammation (tonsillar ca)	K	0.811/0.861	0.685/0.836	0.741/0.507	0.765/0.905	0.606/0.651	0.595/0.690	0.629/0.373	0.688/0.606
Primary tumor and inflammation (non-tonsillar ca)	G	0.706	0.853	0.650	0.771	0.776	0.702	0.840	0.721
Primary tumor and inflammation (non-tonsillar ca)	K	0.458/1.000	0.522/1.000	0.447/1.000	0.468/1.000	0.550/0.900	0.437/0.833	0.512/0.500	0.451/1.000
Primary tumor and healthy tissue (all patients)	G	0.879	0.760	0.710	0.827	0.690	0.690	0.675	0.673
Primary tumor and healthy tissue (all patients)	K	0.624/0.932	0.641/0.725	0.519/0.428	0.580/0.778	0.525/0.669	0.462/0.835	0.358/0.763	0.523/0.711
Metastatic lymph node and primary tumor (all patients)	G	0.669	0.642	0.651	0.641	0.648	0.594	0.654	0.650
Metastatic lymph node and primary tumor (all patients)	K	0.291/0.716	0.294/0.610	0.475/0.613	0.302/0.707	0.560/0.713	0.329/0.842	0.131/0.867	0.230/0.605
Metastatic lymph node and inflammation (all patients)	G	0.783	0.623	0.681	0.763	0.704	0.727	0.678	0.568
Metastatic lymph node and inflammation (all patients)	K	0.791/0.630	0.598/0.519	0.498/0.565	0.765/0.639	0.638/0.542	0.397/0.756	0.469/0.604	0.669/0.461

¹The results of GMM classification are presented as area under the curve (AUC) from ROC analysis, where a value of 1.0 signifies the best possible discrimination. The results of K-means classification are presented as sensitivity/specificity, also in the range 0-1.0. Values in bold reveal where dynamic features perform better than SUV in classification

7 DISCUSSION

7.1 Biodistribution, dosimetry and clinical safety of [¹⁸F]EF5 (Study I)

The hypoxia tracer [¹⁸F]EF5 is more lipophilic than the other nitroimidazole compounds that have been used as hypoxia PET tracers (Fleming et al. 2015). It is well known that a lipophilic compound enters easily into background tissues and generally has a slower elimination rate in the body causing a decrease in the target-to-background contrast in PET images. On the other hand, lipophilicity is not only a drawback for a hypoxia PET tracer, since uniform biodistribution is a real advantage. This is especially true in cases of poorly perfused areas of tumor tissues, since the uptake of an ideal hypoxia PET tracer should not be limited by perfusion. A lipophilic tracer, such as [¹⁸F]EF5, is also feasible for brain imaging (see chapter 2.3.2.5). Furthermore, the high degree of biological stability is a clearly favorable characteristic of [¹⁸F]EF5, which compensates for the possible decrease in image contrast caused by lipophilicity.

Study I was conducted at two individual centers (TURKU and PENN) where the radiochemical synthesis of [¹⁸F]EF5 was performed according to the local procedures. In this study, oncologic patients with few or no signs of active cancer disease were enrolled. The major exclusion criteria were cardiac, renal, liver and hematologic dysfunction. These criteria prior to enrollment were based on the aim of obtaining data on pharmacokinetics of the tracer comparable to those of healthy subjects. At TURKU, a PET/CT scanner was used to provide anatomical reference with co-registered CT images. Consequently, more individual organs (pancreas, spleen and cortical bone) could be contoured and analyzed for the dosimetry at TURKU compared to PENN performing the similar protocol with a dedicated PET scanner.

The individual absorbed radiation doses were consistent between the groups of TURKU and PENN subjects. Only the COVs of absorbed doses of the urinary bladder wall and gall bladder exceeded 20%. The average COV for the whole pooled dataset was only 8%, and the corresponding COVs separately for TURKU and PENN datasets were 8% and 6%, respectively. Therefore we decided to use pooled data for absorbed radiation dose estimates of [¹⁸F]EF5.

The radiation dose calculations showed the EDE and ED for [¹⁸F]EF5 to be 0.021 ± 0.003 mSv/MBq and 0.018 ± 0.002 mSv/MBq, respectively. The highest mean absorbed radiation dose for an individual organ was that of the urinary bladder wall, 0.12 ± 0.034 mSv/MBq (mean \pm SD), with a range of 0.069–0.20 mSv/MBq.

This was an expected observation, since [^{18}F]EF5 is primarily eliminated in the urine. No individual subject had any other organ radiation dose exceeding 0.051 mSv/MBq, which is an important observation regarding the clinical use of [^{18}F]EF5. According to the time-activity data of individual organs and blood, the biodistribution of [^{18}F]EF5 seems to occur uniformly and rapidly within minutes of injection and remains relatively constant.

The highest variation between the data from the two independent study sites was observed in the two excretory organs (urinary bladder and gall bladder), in which the calculated doses in TURKU patients were 50% higher than those in PENN patients. After a thorough evaluation of all raw data, we concluded that this might be due to a faster tracer clearance rate in the TURKU patients, which is most likely caused by the lower drug concentration in patients of the TURKU group as a consequence of the high molar activity procedure for making labeled fluorine gas. The pharmacological half-lives of [^{18}F]EF5 for TURKU and PENN patients were estimated using data from the heart as a surrogate of blood activity; these values were 7.5 and 10.5 hours, respectively. Clearly, these values have to be considered as rough estimates, since activity data were obtained from a shorter period than the half-life time, and therefore the pharmacological half-lives were calculated using extrapolation. On the other hand, there was a 100-fold difference between corresponding drug concentrations of TURKU and PENN patients (~ 0.5 vs. 50 nM, respectively). Moreover, with non-labeled EF5, much higher drug concentrations (e.g. 50 μM) have been used, where a half-life of 11.7 hours has been observed (Koch et al. 2001). Thus, it might be tempting to conclude that the decrease in drug concentration causes a consistent trend of decrease in the biological half-life of [^{18}F]EF5. Nevertheless, a specific study focusing on the impact of concentration differences would be needed to obtain more evidence of this kind of trend in the biodistribution and elimination of the tracer.

Another study regarding the biodistribution and dosimetry of [^{18}F]EF5 was conducted prior to Study I at the University of Pennsylvania (Koch et al. 2010). This pilot study enrolled a smaller number of patients ($n=10$) compared to Study I ($n=16$) and utilized only a dedicated PET scanner, allowing for a smaller number of individual organs contoured for the dosimetry calculations. Furthermore, Study I was conducted in collaboration with two institutions with their own tracer productions and different PET scanners, which can be considered advantageous regarding the validity and reliability of radiation absorbed dose estimates. Nevertheless, the pilot study reported the ED for [^{18}F]EF5 to be 0.023 ± 0.005 mSv/MBq, which can be considered comparable to the results of Study I.

The radiation absorbed dose of [^{18}F]EF5 in imaging use can be considered to be at an acceptable level compared to several other fluorine-18 labeled PET tracers. The

EDE for [^{18}F]FDG has been reported to be 0.027 mSv/MBq (ICRP 1988). For [^{18}F]FMISO, the EDE has been estimated to be 0.013 mSv/MBq (Graham et al. 1997). The EDs for [^{18}F]FETNIM and [^{18}F]FAZA with a 4-hour voiding interval have been estimated to be 0.019 mSv/MBq and 0.014 mSv/MBq, respectively (Tolvanen et al. 2002, Savi et al. 2017), and for [^{18}F]HX4 with a 4.8-hour voiding interval to be 0.042 mSv/MBq (Doss et al. 2010). All of these dosimetry trials with nitroimidazole-based hypoxia tracers have reported the urinary bladder wall as the critical organ.

In study I, the safety of the administration of [^{18}F]EF5 was demonstrated by monitoring vital signs, ECG, biochemical tests and clinical adverse events during the study. Neither significant changes in these parameters nor any clinical adverse events were observed. Considering the extremely low drug concentration of radioactive EF5 used in the study, these results are in accordance with previous knowledge regarding the safety of non-labeled EF5, which has been used even in gram doses without any observed clinically significant toxicity (Koch et al. 2001).

7.2 Association between PET tracer uptake and experimental tumor growth (Study II)

Hypoxia is thought to be associated with rapidly growing tumors, since hypoxia promotes tumor invasiveness, angiogenesis and cell proliferation. Nevertheless, this association is far from simple, since tumor volume and hypoxia do not show a linear relationship. Clearly, tumor growth rate and tumor volume are separate parameters, but the association between tumor growth rate and hypoxia is poorly understood and can be studied only in an experimental setting. In a previous study, a correlation between the tumor growth rate of pancreatic cancer xenografts and hypoxia detected with IHC using anti-EF5 antibodies was reported (Chang et al. 2011). To our knowledge, there are no previously published studies evaluating the association between tumor growth rate and intratumoral hypoxia PET tracer uptake during the exponential growth period.

In study II, we performed two [^{18}F]EF5 PET/CT scans at different stages of the exponential tumor growth. This timing for imaging was designed in order to study the feasibility of [^{18}F]EF5 PET/CT imaging in the detection of the progression of tumor hypoxia in a preclinical setting. Practical issues (e.g., unpredictable tumor growth rates) limited the design of the study protocol; consequently, we could not obtain a constant time frame between the [^{18}F]EF5 scans. Instead, the [^{18}F]FDG scan and the latter [^{18}F]EF5 scan were performed on consecutive days. The Licox system was used in partial tissue oxygen pressure measurements for two tumors, which both were found to be hypoxic. The [^{18}F]EF5 uptake values of the latter scan

of these two tumors were at a higher level than the corresponding median [^{18}F]EF5 uptake value in the study population (Table 7).

The tumor growth rate and [^{18}F]FDG uptake in the late period of exponential tumor growth had a weak positive correlation ($r=0.348$). This correlation would have been expected to be somewhat stronger based on our previous experience in studies with comparable cell lines (Minn et al. 1995). The variation between the uptake values of [^{18}F]EF5 of the two scans was reasonably large, as expected. Several explanations for this observation may be presented. As the scans were performed at different stages of tumor growth, it is clearly understandable that both the perfusion and oxygen diffusion may be altered during the tumor growth. On the other hand, acute changes in hypoxia are evident, and their impact cannot be ruled out. Previous studies, both clinical and experimental, have been conducted to evaluate the repeatability of hypoxia PET tracer uptake over a shorter time period, as stated in chapter 2.3.2.6. So far, very little is known about changes in hypoxia tracer uptake in a malignant tumor over a larger time scale, and even less is known about the potential significance of these changes in the behavior of the tumor.

The tumor uptake in the first [^{18}F]EF5 scan had only a weak positive correlation ($r=0.398$) with the tumor growth rate. Instead, the correlation was clear ($r=0.766$) between the tumor growth rate and the uptake of [^{18}F]EF5 in the tumor in the latter scan performed during the late phase of exponential tumor growth. Also, the HC 10% was determined for all tracer uptake parameters. The HC 10% uptake of the second [^{18}F]EF5 scan was the only one pointing toward a relationship ($r=0.503$) with the tumor growth rate. Therefore, we concluded that uptakes of [^{18}F]FDG and [^{18}F]EF5 in the first scan are not dependent on the tumor growth rate.

An interesting question is why more rapidly growing tumors showed a higher [^{18}F]EF5 uptake at the late period of the exponential growth phase. Hypoxia itself might increase the tumor growth rate by promoting cell proliferation. On the other hand, rapid cell proliferation together with impaired angiogenesis may also lead to the development of hypoxia (Harris et al. 2002). A recent study reported an observed reduction in the growth rate of oral SCC xenografts after the tumors had been manipulated to become less hypoxic using transcutaneous carbon dioxide (Takeda et al. 2014). In that study, a decrease in expression was observed among HIF1- α , VEGF and two matrix metalloproteinases, MMP-2 and MMP-9, as well as several factors representing mitochondrial apoptosis. However, the factors affecting the growth of hypoxic tumors are still poorly understood. Therefore, further research is essential in order to be able to explain the observations of our study more thoroughly.

In our study, tumor volume and [^{18}F]EF5 uptake in the latter scan did not correlate with each other ($r= -0.217$). This is in accordance with previous reports, which

have found no correlation between tumor size and presence of hypoxia (Vaupel et al. 2007, Tochon-Danguy et al. 2002, Bentzen et al. 2002). On the other hand, we found a trend toward a relation between the tumor volume and [^{18}F]EF5 uptake in the first scan ($r=0.510$, $p=0.13$). Nevertheless, this weak association might be a consequence of blurred uptake values due to PVE in the smallest tumors. Altogether, when considering the results of Study II, the small and variable tumor volume in relation to scanner resolution has to be taken into account, especially when evaluating the findings of the first [^{18}F]EF5 scans. PVE may cause underestimation of the observed tracer uptake when the tumor is of a size less than three times the full width at half maximum of the reconstructed image resolution (Soret et al. 2007). Conversely, tumors were remarkably larger at the time of [^{18}F]FDG scans and the latter [^{18}F]EF5 scans, and therefore PVE was not considered to be a significant source of misleading conclusions among these observations.

The observed relationship between [^{18}F]EF5 uptake of the experimental tumor and tumor growth rate is interesting, although the number of observations in this study was relatively small. At the time of the latter [^{18}F]EF5 scan, the relationship was even stronger for hypoxic tracer than for the metabolic tracer ([^{18}F]FDG) which may be due to the timing of the latter scan when the hypoxic fraction is large. Nevertheless, a thorough evaluation of this association is needed using a larger study population to better recognize the background and significance of this observation.

7.3 Repeatability of hypoxia imaging using [^{18}F]EF5 PET/CT scans (Study III)

Test-retest reliability is a crucial characteristic to be assessed in the evaluation of oncologic PET imaging with a novel tracer. Considering the clinical feasibility of [^{18}F]EF5 PET/CT for guiding RT dose-escalation protocols, this is particularly important. On the other hand, cycling hypoxia may cause notable and sometimes rapid changes in tumor oxygenation (Dewhirst et al. 2008). Consequently, the repeatability of hypoxia PET imaging has been considered as a combination of the reproducibility of technical measurements and true changes in the measured phenomenon.

In Study III, we decided to use MATV for primary tumor delineation to facilitate comparison to two previous clinical hypoxia PET repeatability studies (Nehmeh et al. 2008, Grkovski et al. 2016). We prefer this method compared to CT-based delineation, which generally leads to a larger primary tumor volume. CT-based analysis might be more challenging, since tissues in the periphery of the tumor with

low [^{18}F]FDG uptake would be expected to show less dynamic hypoxia tracer uptake than those in the core of the tumor. Thus, the CT-based tumor delineation in the repeatability study might lead to a conclusion of erroneously high repeatability of intratumor tracer uptake (Hoeben et al. 2013b, Chirla and Marcu 2016). In this study, the average uptake of [^{18}F]EF5 in primary tumors was at a level comparable to those reported in previous studies of patients with HNC (Komar et al. 2008, Komar et al. 2014). Additionally, the uptake of [^{18}F]EF5 in the posterior neck muscles and activity measurements in venous blood samples showed highly repeatable results in support of highly stable uptake in reference tissue and steady activity concentration in the blood pool.

HV was defined using a TMR of 1.5 as a threshold representing hypoxic tissue. This level was derived from a previous study in which a voxelwise analysis of perfusion and uptake of [^{18}F]EF5 had been performed (Komar et al. 2008). A meta-analysis quantifying the statistical properties of hypoxic tumor subvolumes in HNC patients (Chirla and Marcu 2016) reported slightly larger median FHV in studies using [^{18}F]FMISO and [^{18}F]FETNIM PET/CT with MATV-based GTV delineation compared to our study with a median FHV of 20.2%. Nevertheless, any threshold for hypoxia is an estimation affected by several factors in methodology and image acquisition, and therefore it is important to analyze the whole scale of uptake rates in a repeatability study.

In Study III, the tumor level uptake of [^{18}F]EF5 was observed to be highly repeatable in the paired scans. The intrapatient correlation and agreement of SUVmean, SUVmax and TMR were high and comparable to those reported in HNC and lung cancer using [^{18}F]FMISO (Okamoto et al. 2013, Grkovksi et al. 2016) and [^{18}F]HX4 (Zegers et al. 2015b), while a single study (Nehmeh et al. 2008) reported a lower linear correlation between the paired scans. In previous discussions, this controversy has been speculated to be due to an inconsistent uptake time within the repeated scans, use of 2D or 3D acquisition modes and variability in performance of image co-registration algorithms (Grkovksi et al. 2016). Given the poorly known factors affecting the dynamicity of tumor hypoxia, it is evident that technical aspects and consistency of the acquisition protocol are critical to obtain highly reliable results. It is also notable that the uptake time, even when consistent within and between the subjects, might have an effect on the repeatability of the tracer uptake. Owing to the findings in our previous validation study (Komar et al. 2008), we performed acquisitions only at 3 hours from injection in Study III.

The repeatability of spatial distribution of [^{18}F]EF5 uptake was also assessed in the voxel-by-voxel analysis between the paired scans. We observed a strong correlation ($r > 0.5$) in 9 out of 10 patients when using a threshold for strong correlation adopted from two of the previous studies (Nehmeh et al. 2008, Zegers et al. 2015b).

The agreement analysis showed a slightly higher relative mean difference and relative CoR in this study compared to the studies of Zegers et al. (Zegers et al. 2015b), and Grkovski et al. (Grkovski et al. 2016). However, the comparison of voxel-level results with the previous studies is more challenging than that of tumor-level results due to several heterogeneities in acquisition parameters and statistical evaluation. The voxel size used is crucial for repeatability assessment, but this parameter was not reported by Okamoto et al. (Okamoto et al. 2013) and Zegers et al. (Zegers et al. 2015b). The image resolution in our study (voxel size 3.65 x 3.65 x 3.27 mm) was higher than those in the two studies that reported their voxel size (Nehmeh et al. 2008, Grkovski et al. 2016). Furthermore, the statistical methods used in these studies differ substantially from each other. Following the principles of repeatability assessment, we calculated both correlation and agreement values for all uptake parameters (Vaz et al. 2013).

The interval between repeated scans is essential with respect to dynamic changes in tumor oxygenation. Based on existing knowledge on temporal variation in tumor hypoxia, it is evident that a longer interval is generally associated with lower repeatability of hypoxia imaging. However, we did not observe any consistent trend for lower repeatability of our intratumor tracer uptake measurements with a median interval of 7 days compared to studies with an average interval of 1–3 days (Nehmeh et al. 2008, Okamoto et al. 2013, Zegers et al. 2015b, Grkovski et al. 2016, Yue et al. 2012). Therefore, the differences in intervals between these trials seem to play only a minor role in the repeatability assessment.

When comparing the primary tumor sites in our study to those in the previous three studies, the highest proportion of patients with oropharyngeal cancer is reported in the study of Nehmeh et al. (Nehmeh et al. 2008), followed by the present study, Zegers et al. (Zegers et al. 2015b) and Okamoto et al. (Okamoto et al. 2013), respectively. However, a descriptive evaluation of results (correlation and agreement when available) in all of the above-mentioned studies does not uncover any clear trend of differences in repeatability attributed to tumor site. Clearly, the number of subjects with individual tumor sites is too small to assess statistical significance of differences in repeatability. Another important parameter to be considered is tumor size, which was not reported in the study of Okamoto et al. (Okamoto et al. 2013). However, the mean and the range of tumor volumes in our study was comparable to those in the studies of Nehmeh et al. (Nehmeh et al. 2008) and Zegers et al. (Zegers et al. 2015b).

A comparison between the repeatability of [¹⁸F]EF5 PET/CT imaging and that of [¹⁸F]FDG PET/CT imaging has to be made very cautiously. A recent meta-analysis involving [¹⁸F]FDG PET/CT paid special attention to the statistical analysis of results derived from original studies regarding the repeatability of [¹⁸F]FDG uptake

in several types of cancer (Lodge 2017). In this meta-analysis, asymmetric borders were defined for significant changes in repeated [^{18}F]FDG uptake values (SUVmean, SUVmax) equal to relative CoRs determined in our study for corresponding values for [^{18}F]EF5 uptake. In general, intratumor [^{18}F]FDG uptake varies at a remarkably larger scale than corresponding [^{18}F]EF5 uptake. On the other hand, the repeatability of [^{18}F]FDG seem to be dependent on the level of uptake, since a low level of absolute uptake is associated with lower repeatability (de Langen et al. 2012). In Study III, with a reasonably narrow scale of intratumor [^{18}F]EF5 uptake rates, this kind of trend was not observed (Figure 12). Nevertheless, the test-retest variability of tumor level [^{18}F]EF5 uptake was observed to be lower than that reported for [^{18}F]FDG uptake (de Langen et al. 2012, Lodge 2017).

Some limitations in our study can be identified. Similar to the previous studies, the number of subjects was small. We found the workflow of this study to be particularly challenging in practice, and we definitely understand the complexity of conducting a large enrollment and multiple sequential imaging procedures in this kind of study protocol. Also, all of the study subjects were men. In addition, we can identify technical limitations in the repeatability assessment, such as the possibility of inaccuracies in the patient setup and co-registration of images, although optimal methods for immobilization and RT mask and neck support were used (Park and Park 2016). However, these challenges in image acquisition and processing are analogous to those in clinical practice.

This study indicates that the repeatability of [^{18}F]EF5 PET/CT in HNC is favorable for guiding RT dose escalation and adaptation procedures. The correlation and agreement among all tumor-level parameters were high between the paired [^{18}F]EF5 scans, and voxelwise comparison of uptakes showed predominantly good correlation and agreement. Consequently, the results are comparable to those reported in studies using [^{18}F]FMISO and [^{18}F]HX4 PET/CT.

7.4 Performance of dynamic features of [^{18}F]FDG uptake in the distinction of different tissue types (Study IV)

Along with the increasing use of [^{18}F]FDG PET/CT imaging in the management of HNC, it has become more evident that advanced procedures for data acquisition and analysis may improve the specificity of [^{18}F]FDG uptake in the detection of malignant tissue. The reliable detection of different tissue types would be crucial both in the staging procedure of the neck lymph nodes and in the distinction between the primary tumor, peritumoral inflammation and surrounding healthy tissue. In an attempt to reach this goal, a natural direction is the evaluation of the temporal dimension in PET imaging. DTPI (see chapter 2.3.1.4) is one of the most

straightforward of the protocols that have been evaluated, especially for staging purposes, but the currently available evidence does not support the clinical use of this approach (Shen et al. 2014, Carlson et al. 2013). A recent review article called for more quantitative approaches in the applications for [^{18}F]FDG PET/CT imaging in HNC (Manca 2016). In fact, very few studies have been performed in this field. Furthermore, robust imaging methods for tumor delineation are urgently needed, especially in the management of HPV-positive oropharyngeal cancer, given the possible consideration of de-intensification protocols. These facts were the main reasons for the implementation of Study IV.

After the dynamic [^{18}F]FDG PET/CT scans of the five patients with oropharyngeal carcinoma were performed, we constructed seven model-derived dynamic features (D1–D7) to be evaluated in the distinction of different tissue types. Some of these features were developed with the knowledge of glucose metabolism and GLUT protein expressions in different tissue types. Another basis for construction of some of the features was the visual inspection of voxel-derived TACs while paying attention to possible characteristics of different tissues.

The visual inspection of TACs provided the first interesting observation in Study IV. The shape of the primary tumor TACs in HPV-positive tonsillar carcinoma patients (nos. 1–3) resembled those of inflammatory tissues. Conversely, the non-tonsillar carcinoma patients (nos. 4–5) had steep rising TAC in primary tumor VOIs, which has been a frequently observed finding in several previous dynamic [^{18}F]FDG PET studies in different types of cancers (Sakamoto et al. 1997, Gupta et al. 1998, Janssen et al. 2009). To our knowledge, there are no previous reports of atypical dynamic accumulation of [^{18}F]FDG in tonsillar cancer compared to other malignancies, let alone explanations for this observation. Clearly, the small number of patients in this study limits any further considerations, but this observation does indicate the need for future investigation of similar patients. On the other hand, the lower level of [^{18}F]FDG uptake in HPV-positive tumors in comparison to HPV-negative tumors is in line with several previous reports (Schouten et al. 2015, Rasmussen et al. 2015), although this association is not consistent in the current literature (Huang et al. 2015).

D1 (retention index) was observed to be feasible for the distinction between tumor and healthy tissue in this study population. The idea of D1 resembles that in DTPI protocols, although in our study the first 10 time frames (0–10 min post injection) were used for the first time point compared to a much later time period (45–60 minutes post injection) used for the same purpose in several previous studies (Schillaci 2012, Abgral et al. 2013). Considering the entire VOIs of tumor and healthy tissue, there was no overlap of D1 values. On the other hand, the specificity

of D1 in the distinction of tumor and healthy tissue was lower in voxel-wise analyses using clustering algorithms. The probable explanation for this observation is the fact that manual contouring of the tumor volume is usually performed by over-segmenting the GTV in order to avoid a geographic miss in the RT plan.

D3 (area under the TAC between the 20th and 21st PET frames or 30–70 min) showed a slightly better accuracy compared to SUV in the discrimination of the primary tumor and inflammation. D6 (temporal variance) represents the total change in the tracer concentration over the entire acquisition time, and this feature reflects how quickly the signal becomes stable. When comparing again the primary tumor and inflammation, the features D1 and D6 also showed slightly higher specificity and sensitivity compared to those of SUV among non-tonsillar carcinoma patients. D1, D3 and D6 can be considered indicators of differences in the glucose metabolism and transport between different tissue types, but the biological background behind these results is so far poorly understood.

D5 (variance of local change) is a unique feature, since it is independent of the absolute tracer uptake rate. Instead, D5 is analogous to the ratio of rate constants K_1 and k_2 of the original Sokoloff equation describing the in-flux and out-flux of [¹⁸F]FDG through the cell membranes in dynamic PET studies (Minn et al. 1995b). In the patient population of Study IV, we observed slightly superior accuracy of D5 compared to SUV in the discrimination of primary tumor and metastatic lymph node. Nevertheless, we did not find a reasonable explanation for this result based on the theoretical background of the feature D5.

The two classification algorithms GMM and K-means provided different results with some dynamic features when determining specificity and sensitivity in the distinction of tissue types. As already presented in the Master thesis of Mueez U. Din, the higher performance obtained with K-means might be explained by the fact that K-means can better classify into separate groups data that do not show normal distribution (Din 2014). On the other hand, the GMM algorithm was also better than K-means in some calculations, which indicates that neither of the algorithms is superior in every situation. The better performance of GMM might be explained by the fact that GMM utilizes the expectation maximization algorithm, which estimates the maximum likelihood of the data point belonging to either of the classes (Din 2014).

The performance of dynamic features could be further analyzed by combining several features for the distinction of different tissue types. When combining more than one of the seven features, there are up to 120 different combinations available. Intuitively, the theoretical background of glucose transport and metabolism in different tissue types might be beneficial to take into account when choosing some of the possible combinations of these features for further evaluation. Nevertheless,

we estimated that this would have been beneficial only with a larger study population.

Several methods have been proposed for the task of tumor delineation as well as distinction of inflammatory and malignant uptakes in [^{18}F]FDG PET images (Shepherd et al. 2012). In a review article by Zaidi and El Naqa (2010), these methods have been divided into four groups: thresholding methods, variational approaches, stochastic modelling-based techniques and learning methods. The biological target volume (BTV) derived from the histopathological specimen of the tumor has been considered as a gold standard for the reference of these methods. One of the few studies using BTV reference compared different segmentation methods from all of the previously mentioned four groups among seven laryngeal cancer patients (Zaidi et al. 2012). A variant of fuzzy clustering-based segmentation, the spatial wavelet-based algorithm was observed to be the most accurate method compared to BTV. However, a recent study utilizing a GMM-based automatic segmentation tool with pure static threshold-based signal intensity assessment reported promising results in GTV delineation compared to BTV (Ligtenberg et al. 2017). At present, it can only be speculated, whether the accuracy of this method could be further improved using some kind of dynamic image acquisition protocol.

We did not conduct a routine blood glucose level monitoring in Study IV, which could be considered a weakness of the study. The patients were instructed to fast for four hours before the imaging session. A retrospective review of the medical records of our patients did not reveal any suspicion of abnormal glucose metabolism during the cancer treatment and follow-up period, let alone a history of diagnosed diabetes. The imaging protocol of Study IV was considerably uncomfortable for the patients in practice, because the patients had to be under a head and neck immobilization mask for a prolonged period of time. Our patients had a good performance status (WHO 0–1), and we recognize that for most of the standard patients our protocol would have been too difficult, if not unbearable. For the design of future dynamic studies, we therefore recommend taking into account the duration of the scan and patient comfort as essential factors for practical reasons.

The voxel-wise evaluation of a very high number of TACs provided an interesting platform for observation of differences in dynamic features of [^{18}F]FDG uptake in different tissue types. It is important to highlight that study IV was a pilot study with only a small number of study subjects, and therefore the findings need to be considered preliminary. Nevertheless, future research activities with a focus on the modeling of tracer uptake may benefit from our results.

7.5 Future perspectives

In recent years, the unique feasibility of hybrid PET imaging in HNC has been demonstrated in both the clinical setting and translational cancer research. On the other hand, the evolving challenges in the diagnosis and management of HNC will keep researchers busy developing and evaluating novel approaches in PET imaging.

Considerable efforts in hypoxia PET imaging by several groups with several tracers continue and hopefully will lead to a clinical application. For the past few years, the evaluation of the hypoxia tracer [^{18}F]EF5 has been in focus of our research group in Turku PET Centre and Turku University Hospital. The favorable imaging characteristics of [^{18}F]EF5 encourage us to continue further evaluation of this tracer, while the other most important hypoxia PET tracers, [^{18}F]FMISO, [^{18}F]FAZA and [^{18}F]HX4, complete the current view of advancements in clinical use of hypoxia PET imaging. The comparison of the uptake characteristics between these tracers will be essential for the planning of future hypoxia-related research activities, and perhaps novel hypoxia PET tracers will be introduced, although it may be challenging to prove their superiority over the existing ones.

Recently, it has been stated that the residual hypoxic subvolume in a tumor after a few fractions of RT is considered to be more applicable in the targeting of dose-escalation compared to the pretreatment hypoxic subvolume (Löck et al. 2017, Bollineni et al. 2014). In general, this approach could be implemented in clinical practice as a part of adaptive RT. Thus, a logical continuation for the clinical evaluation of [^{18}F]EF5 PET/CT imaging would be a study designed to investigate the stability and prognostic significance of the residual hypoxia of HNC tumors during RT. This kind of evaluation would be essential considering the results of the corresponding previous study using [^{18}F]FMISO PET/CT (Zschaecck et al. 2015), in which remarkable variability in the spatial distribution of the tracer was observed, as well as a reasonably low geographic overlap between stable hypoxic volumes and location of recurrences. The initial experience of the stability of [^{18}F]EF5 uptake is promising, and the uptake of a lipophilic tracer is assumed to be less dependent on perfusion. However, detailed knowledge of spatial variations in [^{18}F]EF5 tumor uptake during the course of RT is needed prior to the clinical implementation of adaptive or non-adaptive DPBN. Clearly, the role of [^{18}F]EF5 PET imaging should be thoroughly defined in the near future, since the era of the first interventional hypoxia PET-guided dose-escalation studies has already begun (Welz et al. 2017, Vera et al. 2017).

In addition to RT planning, hypoxia PET imaging is thought to be feasible for the selection of patients for other hypoxia-targeted treatment interventions. However,

there will probably not be only one optimal hypoxia PET tracer that could be used in all clinical scenarios (Carlin and Humm 2012). Consequently, it will be important to perform studies, in which the ability of hypoxia PET imaging with a particular tracer would be used to select patients for a specific hypoxia-related treatment intervention (Fleming et al. 2015). Until now, [^{18}F]EF5 PET imaging has been evaluated only in one preclinical study for this approach (Chitneni et al. 2013).

Tumor hypoxia is undeniably a central part of the biology of HNC. The evidence of the significance of hypoxia for radioresistance and for the development of more aggressive tumor phenotype leading also to a lower survival rate is solid and exceedingly homogenous (Vaupel and Mayer 2007b, Stadler et al. 1999, Nordmark et al. 2005). Nonetheless, the nature and diversity of tumor hypoxia remain challenging to understand. In particular, the results of attempts to overcome hypoxia in oncologic treatment have been modest (Baumann et al. 2016). This has been explained by the lack of feasible methods with potential for selection of patients with significant tumor hypoxia in clinical trials (Walsh et al. 2014). However, it is evident that hypoxia is not equally important in all patients even when present to the same extent. As an example, in HPV-positive oropharyngeal cancer, hypoxia does not seem to play as crucial role in treatment resistance compared to an HPV-negative tumor. Consequently, the concept of a “hypoxic driver phenotype” has been proposed, making it possible to specify the characteristics that are typical for those tumors in which hypoxia is a primary biological driver of tumor behavior (Dhani et al 2015).

Recent advances in genomics and bioinformatics have been considered to be the next revolution in personalized medicine. These advancements can also be expected to open several new doors for the study of tumor hypoxia (Curtis et al. 2016, Tawk et al. 2016). The digitalization of healthcare is another megatrend in clinical medicine that is expected to be revolutionary. One example of this is the utilization of big data, which provides the possibility to govern a huge amount of structured medical records combining biologic and epidemiologic information. This makes it possible to perform large-scale analyses and achieve complementary knowledge and experience in addition to those derived from randomized controlled trials (McNutt et al. 2016). Targeting tumor hypoxia in cancer treatment is a representative example of a procedure that would be expected to benefit greatly from big data, since etiologic, genomic and host-tumor interactions are thought to play an important role in the behavior of hypoxic tumors (Dhani et al. 2015). In the era of genomics, the role of PET imaging in the detection of tumor hypoxia needs to be clarified in the upcoming clinical trials involving the selection of patients for novel hypoxia-targeted therapies. For the present, PET imaging seems to remain a predominant method in this field due to its obvious benefits, such as easy repeatability

and the feasibility of whole tumor and whole body imaging (Hammond et al. 2014, Fleming et al. 2015, Peeters et al. 2015b).

The use of [^{18}F]FDG PET/CT has been established in the management of HNC, although there are still challenges to overcome, especially in the RT application. Dynamic [^{18}F]FDG PET may offer novel potential for target delineation, while more than a few attempts to use static imaging data have led only to modest results in studies using BTV as reference (Manca et al. 2016). On the other hand, several other approaches might be advantageous, such as the use of modern learning algorithms that might also show favorable performance in static images in the absence of true quantitative tracer uptake data. In recent years, the rapid development of automatic segmentation tools for [^{18}F]FDG PET images has led to several novel applications (Berthon et al. 2017), but very few of these have been evaluated with BTV reference. An ideal and consistent protocol for tumor segmentation would be beneficial not only for RT dose planning but also for several additional applications in the field of radiomics (Beichel et al. 2017).

This thesis has focused especially on PET/CT imaging of HNC in patients enrolled for RT. Meanwhile, the advent of PET/MR imaging has been proposed as particularly attractive in HNC. Indeed, MRI offers a number of benefits, such as several functional techniques and better motion correction compared to CT (Queiroz and Huellner 2015). The challenges in attenuation correction currently remain a subject of intense research in the utilization of PET/MRI, especially in the head and neck and brain regions. These problems in measurements of MRI-based attenuation maps render precise quantitation of PET tracer uptake less reliable than was initially expected. Hopefully, an appropriate solution for translating MRI acquisition to PET attenuation without loss of true quantitative PET data will be available in the near future (Mehranian et al. 2016).

In summary, there is an immense potential of PET imaging in the research and management of HNC for both curative and palliative approaches. Virtually an unlimited number of functional processes in HNC are potentially feasible for imaging. On the other hand, the limitations are mainly governed by the low spatial resolution, a fact that belongs to the nature of PET imaging. Overall, the current trends of clinical medicine and translational cancer research are highly promising for active utilization of hybrid PET imaging technology in HNC in the future.

8 CONCLUSIONS

This work focused on selected fields of methodology of PET/CT imaging in HNC. The evaluation of a novel hypoxia tracer [^{18}F]EF5 was the major effort. Moreover, advanced analyzing methods for dynamic [^{18}F]FDG images were assessed.

The specific conclusions of this work are:

1 Hypoxia PET tracer [^{18}F]EF5 is safe for human use, and its biodistribution and dosimetric profile in the human body are clinically acceptable. No unacceptable single organ radiation exposures or clinically significant adverse events were observed in our study.

2 The [^{18}F]EF5 uptake in the late phase of the exponential growth period was observed to be in association with the tumor growth rate in mice bearing HNC xenografts. However, the biological background of this observation remains obscure, since hypoxia may drive tumor progression but rapid cell proliferation may be the reason for the development of tumor hypoxia.

3 The intratumor uptake of [^{18}F]EF5 shows high repeatability between the paired scans performed for HNC patients within a median time interval of seven days. This observation encourages to continue the further evaluation of [^{18}F]EF5 PET/CT as a tool for hypoxia-related treatment interventions.

4 Some dynamic features of tracer uptake in the [^{18}F]FDG PET/CT image might provide additional information for the discrimination of tumor, inflammatory and healthy tissues in oropharyngeal cancer patients. Although the conducted small pilot study did not indicate any statistically significant improvement in the performance of dynamic features over SUV, we encourage future researchers to further evaluate the idea of advanced quantitative analysis and acquisition of dynamic data in [^{18}F]FDG PET/CT imaging of HNC patients.

ACKNOWLEDGEMENTS

This work was carried out at the Turku PET Centre and at the Department of Otorhinolaryngology – Head and Neck Surgery and the Department of Oncology and Radiotherapy, Turku University Hospital, Finland. In addition, Study I was performed in collaboration with the Perelman School of Medicine at the University of Pennsylvania, USA. The three clinical trials and the preclinical trial were conducted between December 2008 and September 2016. Prior to these four studies, I performed my very first scientific study and wrote an original article which is not included in the thesis (Silvonemi A, Pulkkinen J, Grénman R. *Acta Otolaryngol* 2010;130:1300-1305) in order to get an unofficial permission to start doctoral studies at the Department of Otorhinolaryngology – Head and Neck Surgery.

I would like to express my sincere gratitude to the following persons:

Professor Juhani Knuuti, Director of Turku PET Centre, and Professor Jussi Jero, Head of the Department of Otorhinolaryngology – Head and Neck Surgery, for providing excellent facilities to conduct research studies at Turku University Hospital.

Professor Heikki Minn, Head of the Department of Oncology and Radiotherapy, for principal supervision of this thesis. Heikki, it has been a great privilege and pleasure for me to be your student and work with you. I have always appreciated your brilliance and large scale expertise in oncological research. Furthermore, you have been an ideal supervisor in every way being also encouraging when some of the projects seemed very complicated for me.

Adjunct Professor, PhD Tove J. Grönroos for all these years supervising me in the world of PET research. Tove, your effort in teaching preclinical research methods was very important for me. It is impressive that you have always arranged time for my projects and for my numerous questions. I am very happy since you have kept your positive attitude the whole way through this prolonged project.

Professor and Chairman (Emeritus) Reidar Grénman for excellent supervision and boosting during these years. I'm very grateful to you for your educational efforts supporting my academic and professional endeavors.

Professor, head and neck surgeon, Antti Mäkitie, Head of the former National Graduate School of Clinical Investigation (years 2012-2015), for inspiring me greatly to do research in the field of otorhinolaryngology and head and neck oncology.

The reviewers of the thesis, Professor Esther G.C. Troost and Professor Eirik Malinen for their valuable comments and remarks improving the thesis manuscript.

Medical physicist, Ph.Lic. Sami Suilamo for hard work and flexibility during this project. Sami, your expertise in radiotherapy and medical imaging has been invaluable in several steps of this work. It was a real stroke of luck for me to have you as my principal collaborator!

M.Sc. Jonna Sinkkonen (Silén) for super collaboration. Jonna, your enormous contribution in cell culturing as well as expertise in preclinical experiments were invaluable.

PhD Tony Shepherd for the design and implementation of mathematical parts in Study IV. Tony, your creative thinking and expertise formed the basis for Study IV. I would like to express my sincere gratitude to you. Then, I would also like to thank M.Sc. Mueez U. Din for great collaboration in mathematical analyses.

Professor Olof Solin, Adjunct Professor Sarita Forsback and PhD Olli Eskola and other radiochemists in Turku PET Centre for invaluable contributions in the production of [^{18}F]EF5 as well as additional intellectual support in several steps of this work.

Professor Cameron J. Koch and Professor Sydney Evans and their research group at the University of Pennsylvania, for the development of EF5 and the pioneering work with the compound as well as for great collaboration. Furthermore, I would like to thank Adjunct Associate Professor Lilie L. Lin for wonderful teamwork when conducting Study I.

All co-authors of the four studies for great collaboration and flexibility. Especially, I would like to thank biostatistician, M.Sc. Eliisa Löytyniemi for the contribution in applying statistical methods in Studies II and III.

MD, PhD Gaber Komar for excellent remarks and advice for the studies with the radiotracer [^{18}F]EF5.

Thesis follow-up committee members, Professor Klaus Elenius and Adjunct Professor Sirkku Jyrkkiö for valuable support during the running of my doctoral studies.

The staff of Turku PET Centre and Medicity Research Laboratory as well as the staff of the Department of Oncology and Radiotherapy and the Department of Otorhinolaryngology – Head and Neck Surgery for super collaboration and flexibility and skillful work.

All my colleagues and workmates in Turku University Hospital, Salo Regional Hospital and Hospital Neo as well as in other workplaces for pleasant working days and friendship.

And then, all my friends both inside and outside the academic world in several affiliations, including but not limited to e.g. the former Cursus Medicaster and TSK. Thank you for being in my life. I'm still thinking clearly and coming back!

My parents Kristiina and Pekka Silvonemi for love and support and my sister Tarja and her husband Saku Joutsamo for invaluable non-scientific discussions. My parents as well as my parents-in-law Seija and Henrik Bergman for important support in our everyday life when taking care of our children and providing transport services for them.

Finally, my special thanks and apologizes are addressed to my family. My dear children, Oskari, Anni and Emma – every day you are reminding me what is really important in my life. I feel very sorry about having been too concentrated on research activities. Eventually, a new life will begin for us. My dear wife Maria, your love and support as well as endless patience have been important for me during these years, not forgetting your straight contribution to this project relating to “the synergistic benefit” in several scientific and practical issues derived from your own simultaneous doctoral thesis project.

This study was financially supported by the National Graduate School of Clinical Investigation, The Hospital District of Southwest Finland, the Varian Medical Systems, Cancer Foundation Finland sr, the Finnish Medical Foundation, the Foundation of Finnish Otorhinolaryngological Society, Orion Research Foundation sr, the Foundation for the Finnish Cancer Institute, Turku University Foundation, Finnish Cultural Foundation, Swedish Cultural Foundation in Finland and Southwestern Finnish Cancer Foundation. Their financial support is greatly acknowledged.

Turku, March 2018

Antti Silvonemi

REFERENCES

- Abgral R, Le Roux PY, Rousset J, Querellou S, Valette G, Nowak E, Turzo A, Tissot V, Marianowski R, Salaün PY. (2013) Prognostic value of dual-time-point ^{18}F -FDG PET-CT imaging in patients with head and neck squamous cell carcinoma. *Nucl Med Commun* 34:551-556
- Abgral R, Querellou S, Potard G, Le Roux PY, Le Duc-Pennec A, Marianovski R, Pradier O, Bizais Y, Kraeber-Bodéré F, Salaun PY. (2009) Does ^{18}F -FDG PET/CT improve the detection of posttreatment recurrence of head and neck squamous cell carcinoma in patients negative for disease on clinical follow-up? *J Nucl Med* 50:24-29
- Adelstein DJ, Li Y, Adams GL, Wagner H Jr, Kish JA, Ensley JF, Schuller DE, Forastiere AA. (2003) An intergroup phase III comparison of standard radiation therapy and two schedules of concurrent chemoradiotherapy in patients with unresectable squamous cell head and neck cancer. *J Clin Oncol* 21:92-98
- Alavi A, Reivich M. (2002). Guest editorial: the conception of FDG-PET imaging. *Semin Nucl Med* 32:2-5
- Ang KK, Harris J, Wheeler R, Weber R, Rosenthal DI, Nguyen-Tân PF, Westra WH, Chung CH, Jordan RC, Lu C, Kim H, Axelrod R, Silverman CC, Redmond KP, Gillison ML. (2010) Human papillomavirus and survival of patients with oropharyngeal cancer. *N Engl J Med* 363:24-35
- Argiris A, Karamouzis MV, Raben D, Ferris RL. (2008) Head and neck cancer. *Lancet* 371:1695-1709
- Aristophanous M, Penney BC, Martel MK, Pelizzari CA. (2007) A Gaussian mixture model for definition of lung tumor volumes in positron emission tomography. *Med Phys* 34:4223-4235
- Arteel GE, Thurman RG, Raleigh JA. (1998) Reductive metabolism of the hypoxia marker pimonidazole is regulated by oxygen tension independent of the pyridine nucleotide redox state. *Eur J Biochem* 253:743-750
- Baatenburg de Jong RJ, Hermans J, Molenaar J, Briaire JJ, le Cessie SS. (2001) Prediction of survival in patients with head and neck cancer. *Head Neck* 23:718-724
- Balogova S, Périé S, Kerrou K, Grahek D, Montravers F, Angelard B, Susini B, El Chater P, St Guily JL, Talbot JN. (2008) Prospective comparison of FDG and FET PET/CT in patients with head and neck squamous cell carcinoma. *Mol Imaging Biol* 10:364-373
- Barger RL Jr, Nandalur KR. (2012) Diagnostic performance of dual-time ^{18}F -FDG PET in the diagnosis of pulmonary nodules: a meta-analysis. *Acad Radiol* 19:153-158
- Bar-Shalom R, Valdivia AY, Blaurock MD. (2000) PET imaging in oncology. *Semin Nucl Med* 30:150-185
- Barthel H, Wilson H, Collingridge DR, Brown G, Osman S, Luthra SK, Brady F, Workman P, Price PM, Aboagye EO. (2004) In vivo evaluation of [^{18}F]fluoroetanidazole as a new marker for imaging tumour hypoxia with positron emission tomography. *Br J Cancer* 90:2232-2242
- Basu S, Kwee TC, Surti S, Akin EA, Yoo D, Alavi A. (2011) Fundamentals of PET and PET/CT imaging. *Ann N Y Acad Sci* 1228:1-18
- Baumann R, Depping R, Delaperriere M, Dunst J. (2016) Targeting hypoxia to overcome radiation resistance in head & neck cancers: real challenge or clinical fairytale? *Expert Rev Anticancer Ther* 16:751-758
- Bayer C, Shi K, Astner ST, Maftai CA, Vaupel P. (2011) Acute versus chronic hypoxia: why a simplified classification is simply not enough. *Int J Radiat Oncol Biol Phys* 80:965-968
- Beasley NJ, Leek R, Alam M, Turley H, Cox GJ, Gatter K, Millard P, Fuggie S, Harris AL. (2002) Hypoxia-inducible factors HIF-1 α and HIF-2 α in head and neck cancer: relationship to tumor biology and treatment outcome in surgically resected patients. *Cancer Res* 62:2493-2497
- Beasley NJ, Wykoff C, Watson PH, Leek R, Turley H, Gatter K, Pastorek J, Cox GJ, Ratcliffe P, Harris AL. (2001) Carbonic anhydrase IX, an endogenous hypoxia marker, expression in head and neck squamous cell carcinoma and its relationship to hypoxia, necrosis, and microvessel density. *Cancer Res* 61:5262-5267

- Becker M, Zaidi H. (2014) Imaging in head and neck squamous cell carcinoma: the potential role of PET/MRI. *Br J Radiol* 87:20130677
- Beichel RR, Smith BJ, Bauer C, Ulrich EJ, Ahmadvand P, Budzevich MM, Gillies RJ, Goldgof D, Grkovski M, Hamarneh G, Huang Q, Kinahan PE, Laymon CM, Mountz JM, Muzi JP, Muzi M, Nehmeh S, Oborski MJ, Tan Y, Zhao B, Sunderland JJ, Buatti JM. (2017) Multi-site quality and variability analysis of 3D FDG PET segmentations based on phantom and clinical image data. *Med Phys* 44:479-496
- Bentzen L, Keiding S, Horsman MR, Grönroos T, Hansen SB, Overgaard J. (2002) Assessment of hypoxia in experimental mice tumours by [¹⁸F]fluoromisonidazole PET and pO₂ electrode measurements: influence of tumour volume and carbogen breathing. *Acta Oncol* 41:304-312
- Bentzen L, Keiding S, Nordmark M, Falborg L, Hansen SB, Keller J, Nielsen OS, Overgaard J. (2003) Tumour oxygenation assessed by ¹⁸F-fluoromisonidazole PET and polarographic needle electrodes in human soft tissue tumours. *Radiother Oncol* 67:339-344
- Bentzen SM, Gregoire V. (2011) Molecular imaging-based dose painting: a novel paradigm for radiation therapy prescription. *Semin Radiat Oncol* 21:101-110
- Bergman J, Solin O. (1997) Fluorine-18-labeled fluorine gas for synthesis of tracer molecules. *Nucl Med Biol* 24:677-683
- Bernier J, Domenge C, Ozsahin M, Matuszewska K, Lefèbvre JL, Greiner RH, Giralt J, Maingon P, Rolland F, Bolla M, Cognetti F, Bourhis J, Kirkpatrick A, van Glabbeke M; European Organization for Research and Treatment of Cancer Trial 22931. (2004) Postoperative irradiation with or without concomitant chemotherapy for locally advanced head and neck cancer. *N Engl J Med* 350:1945-1952
- Berthon B, Evans M, Marshall C, Palaniappan N, Cole N, Jayaprakasam V, Rackley T, Spezi E. (2017) Head and neck target delineation using a novel PET automatic segmentation algorithm. *Radiother Oncol* 122:242-247
- Bertout JA, Patel SA, Simon MC. (2008) The impact of O₂ availability on human cancer. *Nat Rev Cancer* 8:967-975
- Berwouts D, Olteanu LA, Duprez F, Vercauteren T, De Gersem W, De Neve W, Van de Wiele C, Madani I. (2013) Three-phase adaptive dose-painting-by-numbers for head-and-neck cancer: initial results of the phase I clinical trial. *Radiother Oncol* 107:310-316
- Beswick DM, Gooding WE, Johnson JT, Branstetter BF 4th. (2012) Temporal patterns of head and neck squamous cell carcinoma recurrence with positron-emission tomography/computed tomography monitoring. *Laryngoscope* 122:1512-1517
- Bhatia A, Burtneiss B. (2015) Human papillomavirus-associated oropharyngeal cancer: defining risk groups and clinical trials. *J Clin Oncol* 33:3243-3250
- Bird D, Scarsbrook AF, Sykes J, Ramasamy S, Subesinghe M, Carey B, Wilson DJ, Roberts N, McDermott G, Karakaya E, Bayman E, Sen M, Speight R, Prestwich RJ. (2015) Multimodality imaging with CT, MR and FDG-PET for radiotherapy target volume delineation in oropharyngeal squamous cell carcinoma. *BMC Cancer* 2015 15:844
- Blot WJ, McLaughlin JK, Winn DM, Austin DF, Greenberg RS, Preston-Martin S, Bernstein L, Schoenberg JB, Stemhagen A, Fraumeni JF Jr. (1988) Smoking and drinking in relation to oral and pharyngeal cancer. *Cancer Res* 48:3282-3287
- Boellaard R. (2009) Standards for PET image acquisition and quantitative data analysis. *J Nucl Med* 50:11S-20S
- Bollineni VR, Kerner GS, Pruijm J, Steenbakkens RJ, Wiegman EM, Koole MJ, de Groot EH, Willemsen AT, Luurtsema G, Widder J, Groen HJ, Langendijk JA. (2013) PET imaging of tumor hypoxia using ¹⁸F-fluoroazomycin arabinoside in stage III-IV non-small cell lung cancer patients. *J Nucl Med* 54:1175-1180
- Bollineni VR, Koole MJ, Pruijm J, Brouwer CL, Wiegman EM, Groen HJ, Vlasman R, Halmos GB, Oosting SF, Langendijk JA, Widder J, Steenbakkens RJ. (2014) Dynamics of tumor hypoxia assessed by ¹⁸F-FAZA PET/CT in head and neck and lung cancer patients during chemoradiation: possible implications for radiotherapy treatment planning strategies. *Radiother Oncol* 113:198-203
- Bollineni VR, Kramer GM, Jansma EP, Liu Y, Oyen WJ. (2016) A systematic review on [¹⁸F]FLT-PET uptake as a measure of treatment response in cancer patients. *Eur J Cancer* 55:81-97

- Bonner JA, Harari PM, Giral J, Azarnia N, Shin DM, Cohen RB, Jones CU, Sur R, Raben D, Jassem J, Ove R, Kies MS, Baselga J, Yousoufian H, Amellal N, Rowinsky EK, Ang KK. (2006) Radiotherapy plus cetuximab for squamous-cell carcinoma of the head and neck. *N Engl J Med* 354:567-578
- Boomsma MJ, Bijl HP, Langendijk JA. (2011) Radiation-induced hypothyroidism in head and neck cancer patients: a systematic review. *Radiother Oncol* 99:1-5
- Branstetter BF, Blodgett TM, Zimmer LA, Snyderman CH, Johnson JT, Raman S, Meltzer CC. (2005) Head and neck malignancy: is PET/CT more accurate than PET or CT alone? *Radiology* 235:580-586
- Brizel DM, Scully SP, Harrelson JM, Layfield LJ, Bean JM, Prosnitz LR, Dewhirst MW. (1996) Tumor oxygenation predicts for the likelihood of distant metastases in human soft tissue sarcoma. *Cancer Res* 56:941-943
- Brizel DM, Sibley GS, Prosnitz LR, Scher RL, Dewhirst MW. (1997) Tumor hypoxia adversely affects the prognosis of carcinoma of the head and neck. *Int J Radiat Oncol Biol Phys* 38:285-289
- Brouwer CL, Steenbakkers RJ, Langendijk JA, Sijtsma NM. (2015) Identifying patients who may benefit from adaptive radiotherapy: Does the literature on anatomic and dosimetric changes in head and neck organs at risk during radiotherapy provide information to help? *Radiother Oncol* 115:285-294
- Browman GP, Wong G, Hodson I, Sathya J, Russell R, McAlpine L, Skingley P, Levine MN. (1993) Influence of cigarette smoking on the efficacy of radiation therapy in head and neck cancer. *N Engl J Med* 328:159-163
- Brown JM, Wilson WR. (2004) Exploiting tumour hypoxia in cancer treatment. *Nat Rev Cancer* 4:437-447
- Bruine de Bruin L, Bollineni VR, Wachters JE, Schuurin E, van Hemel BM, van der Wal JE, Slagter-Menkema L, de Bock GH, Steenbakkers RJ, Langendijk JA, Pruim J, van der Laan BF, Halmos GB. (2015) Assessment of hypoxic subvolumes in laryngeal cancer with ¹⁸F-fluoroazomycinaraboside (¹⁸F-FAZA)-PET/CT scanning and immunohistochemistry. *Radiother Oncol* 117:106-112
- Bui NL, Ong SH, Foong KW. (2015) Automatic segmentation of the nasal cavity and paranasal sinuses from cone-beam CT images. *Int J Comput Assist Radiol Surg* 10:1269-1277
- Busk M, Mortensen LS, Nordmark M, Overgaard J, Jakobsen S, Hansen KV, Theil J, Kallehauge JF, D'Andrea FP, Steiniche T, Horsman MR. (2013) PET hypoxia imaging with FAZA: reproducibility at baseline and during fractionated radiotherapy in tumour-bearing mice. *Eur J Nucl Med Mol Imaging* 40:186-197
- Cacicedo J, Navarro A, Del Hoyo O, Gomez-Iturriaga A, Alongi F, Medina JA, Elicin O, Skanjeti A, Giammarile F, Bilbao P, Casquero F, de Bari B, Dal Pra A. (2016) Role of fluorine-18 fluorodeoxyglucose PET/CT in head and neck oncology: the point of view of the radiation oncologist. *Br J Radiol* 89:20160217
- Calvo MB, Figueroa A, Pulido EG, Campelo RG, Aparicio LA. (2010) Potential role of sugar transporters in cancer and their relationship with anticancer therapy. *Int J Endocrinol* doi: 10.1155/2010/205357
- Carlin S, Humm JL. (2012) Pet of hypoxia: current and future perspectives. *J Nucl Med* 53:1171-1174
- Carlin S, Zhang H, Reese M, Ramos NN, Chen Q, Ricketts SA. (2014) A comparison of the imaging characteristics and microregional distribution of 4 hypoxia PET tracers. *J Nucl Med* 55:515-521
- Carlson ER, Schaefferkoetter J, Townsend D, McCoy JM, Campbell PD Jr, Long M. (2013) The use of multiple time point dynamic positron emission tomography/computed tomography in patients with oral/head and neck cancer does not predictably identify metastatic lymph nodes. *J Oral Maxillofac Surg* 71:162-177
- Carmeliet P, Jain RK. (2000) Angiogenesis in cancer and other diseases. *Nature* 407:249-257
- Carreau A, El Hafny-Rahbi B, Matejuk A, Grillon C, Kieda C. (2011) Why is the partial oxygen pressure of human tissues a crucial parameter? Small molecules and hypoxia. *J Cell Mol Med* 15:1239-1253
- Castadot P, Geets X, Lee JA, Grégoire V. (2011) Adaptive functional image-guided IMRT in pharyngo-laryngeal squamous cell carcinoma: is the gain in dose distribution worth the effort? *Radiother Oncol* 101:343-350
- Chang JH, Wada M, Anderson NJ, Lim Joon D, Lee ST, Gong SJ, Gunawardana DH, Sachinidis J, O'Keefe G, Gan HK, Khoo V, Scott AM. (2013) Hypoxia-targeted radiotherapy dose painting for head and neck cancer using ¹⁸F-FMISO PET: a biological modeling study. *Acta Oncol* 52:1723-1729

- Chang Q, Jurisica I, Do T, Hedley DW. (2011) Hypoxia predicts aggressive growth and spontaneous metastasis formation from orthotopically grown primary xenografts of human pancreatic cancer. *Cancer Res* 71:3110-3120
- Chapman JD. (1979) Hypoxic sensitizers – implications for radiation therapy. *N Engl J Med* 301:1429-1432
- Chaturvedi AK, Anderson WF, Lortet-Tieulent J, Curado MP, Ferlay J, Franceschi S, Rosenberg PS, Bray F, Gillison ML. (2013) Worldwide trends in incidence rates for oral cavity and oropharyngeal cancers. *J Clin Oncol* 31:4550-4559
- Cheal SM, Punzalan B, Doran MG, Evans MJ, Osborne JR, Lewis JS, Zanzonico P, Larson SM. (2014) Pairwise comparison of ^{89}Zr - and ^{124}I -labeled cG250 based on positron emission tomography imaging and nonlinear immunokinetic modeling: in vivo carbonic anhydrase IX receptor binding and internalization in mouse xenografts of clear-cell renal carcinoma. *Eur J Nucl Med Mol Imaging* 41:985-994
- Chen AM, Chen LM, Vaughan A, Sreeraman R, Farwell DG, Luu Q, Lau DH, Stuart K, Purdy JA, Vijayakumar S. (2011) Tobacco smoking during radiation therapy for head-and-neck cancer is associated with unfavorable outcome. *Int J Radiat Oncol Biol Phys* 79:414-419
- Chen L, Zhang Z, Kolb HC, Walsh JC, Zhang J, Guan Y. (2012) ^{18}F -HX4 hypoxia imaging with PET/CT in head and neck cancer: a comparison with ^{18}F -FMISO. *Nucl Med Commun* 33:1096-1102
- Chirla R, Marcu LG. (2016) PET-based quantification of statistical properties of hypoxic tumor subvolumes in head and neck cancer. *Phys Med* 32:23-35
- Chitneni SK, Bida GT, Dewhirst MW, Zalutsky MR. (2012) A simplified synthesis of the hypoxia imaging agent 2-(2-nitro-1H-imidazol-1-yl)-N-(2,2,3,3,3-[(^{18}F)]pentafluoropropyl)-acetamide([^{18}F]JEF5). *Nucl Med Biol* 39:1012-1018
- Chitneni SK, Bida GT, Yuan H, Palmer GM, Hay MP, Melcher T, Wilson WR, Zalutsky MR, Dewhirst MW. (2013) ^{18}F -EF5 PET imaging as an early response biomarker for the hypoxia-activated prodrug SN30000 combined with radiation treatment in a non-small cell lung cancer xenograft model. *J Nucl Med* 2013 54:1339-1346
- Chua ML, Wee JT, Hui EP, Chan AT. (2016) Nasopharyngeal carcinoma. *Lancet* 387:1012-1024
- Coskun HH, Medina JE, Robbins KT, Silver CE, Strojan P, Teymoortash A, Pellitteri PK, Rodrigo JP, Stoeckli SJ, Shaha AR, Suárez C, Hartl DM, de Bree R, Takes RP, Hamoir M, Pitman KT, Rinaldo A, Ferlito A. (2015) Current philosophy in the surgical management of neck metastases for head and neck squamous cell carcinoma. *Head Neck* 37:915-926
- Credé A, Locher M, Bredell M. (2012) Tongue cancer in young patients: case report of a 26-year-old patient. *Head Neck Oncol* 4:20
- Curtis KK, Wong WW, Ross HJ. (2016) Past approaches and future directions for targeting tumor hypoxia in squamous cell carcinomas of the head and neck. *Crit Rev Oncol Hematol* 103:86-98
- Daisne JF, Duprez T, Weynand B, Lonneux M, Hamoir M, Reyckler H, Grégoire V. (2004) Tumor volume in pharyngolaryngeal squamous cell carcinoma: comparison at CT, MR imaging and FDG PET and validation with surgical specimen. *Radiology* 233:93-100
- Daisne J-F, Sibomana M, Bol A, Doumont T, Lonneux M, Grégoire V. (2003) Tri-dimensional automatic segmentation of PET volumes based on measured source-to-back-ground ratios: influence of reconstruction algorithms. *Radiother Oncol* 69:247-250
- de Bree R, Takes RP, Castelijns JA, Medina JE, Stoeckli SJ, Mancuso AA, Hunt JL, Rodrigo JP, Triantafyllou A, Teymoortash A, Civantos FJ, Rinaldo A, Pitman KT, Hamoir M, Robbins KT, Silver CE, Hoekstra OS, Ferlito A. (2015) Advances in diagnostic modalities to detect occult lymph node metastases in head and neck squamous cell carcinoma. *Head Neck* 37:1829-1839
- de Langen AJ, Vincent A, Velasquez LM, van Tinteren H, Boellaard R, Shankar LK, Boers M, Smit EF, Stroobants S, Weber WA, Hoekstra OS. (2012) Repeatability of ^{18}F -FDG uptake measurements in tumors: a metaanalysis. *J Nucl Med* 53:701-708
- Dehdashti F, Grigsby PW, Lewis JS, Laforest R, Siegel BA, Welch MJ. (2008) Assessing tumor hypoxia in cervical cancer by PET with ^{60}Cu -labeled diacetyl-bis(N^4 -methylthiosemicarbazone). *J Nucl Med* 49:201-205

- Dehdashti F, Grigsby PW, Mintun MA, Lewis JS, Siegel BA, Welch MJ. (2003) Assessing tumor hypoxia in cervical cancer by positron emission tomography with ^{60}Cu -ATSM: relationship to therapeutic response – a preliminary report. *Int J Radiat Oncol Biol Phys* 55:1233-1238
- Dehdashti F, Mintun MA, Lewis JS, Bradley J, Govindan R, Laforest R, Welch MJ, Siegel BA. (2003b) In vivo assessment of tumor hypoxia in lung cancer with ^{60}Cu -ATSM. *Eur J Nucl Med Mol Imaging* 30:844-850
- Delouya G, Iqidbashian L, Houle A, Bélair M, Boucher L, Cohade C, Beaulieu S, Filion EJ, Coulombe G, Hinse M, Martel C, Després P, Nguyen-Tan PF. (2011) ^{18}F -FDG-PET imaging in radiotherapy tumor volume delineation in treatment of head and neck cancer. *Radiother Oncol* 101:362-368
- Dewhirst MW, Cao Y, Moeller B. (2008) Cycling hypoxia and free radicals regulate angiogenesis and radiotherapy response. *Nat Rev Cancer* 8:425-437
- Dewhirst MW. (2009) Relationships between cycling hypoxia, HIF-1, angiogenesis and oxidative stress. *Radiat Res* 172:653-665
- Dhani N, Fyles A, Hedley D, Milosevic M. (2015) The clinical significance of hypoxia in human cancers. *Semin Nucl Med* 45:110-121
- Differding S, Hanin FX, Grégoire V. (2015) PET imaging biomarkers in head and neck cancer. *Eur J Nucl Med Mol Imaging* 42:613-622
- Din M (2014) Differentiation of metabolically distinct areas within head and neck region using dynamic ^{18}F -FDG positron emission tomography imaging. Master Thesis, University of Turku, available on-line <http://urn.fi/URN:NBN:fi-fe201401281303>
- Dolbier WR Jr, Li AR, Koch CJ, Shiue CY, Kachur AV. (2001) ^{18}F -EF5, a marker for PET detection of hypoxia: synthesis of precursor and a new fluorination procedure. *Appl Radiat Isot* 54:73-80
- Doss M, Zhang JJ, Bélanger MJ, Stubbs JB, Hostetler ED, Alpaugh K, Kolb HC, Yu JQ. (2010) Biodistribution and radiation dosimetry of the hypoxia marker ^{18}F -HX4 in monkeys and humans determined from whole-body PET/CT. *Nucl Med Commun* 31:1016-1024
- Duan C. (2016) Hypoxia-inducible factor 3 biology: complexities and emerging themes. *Am J Physiol Cell Physiol* 310:C260-C269
- Dubois L, Landuyt W, Cloetens L, Bol A, Bormans G, Haustermans K, Labar D, Nuyts J, Grégoire V, Mortelmans L. (2009) ^{18}F]EF3 is not superior to ^{18}F]FMISO for PET-based hypoxia evaluation as measured in a rat rhabdomyosarcoma tumour model. *Eur J Nucl Med Mol Imaging* 36:209-218
- Dubois L, Landuyt W, Haustermans K, Dupont P, Bormans G, Vermaelen P, Flamen P, Verbeken E, Mortelmans L. (2004) Evaluation of hypoxia in an experimental rat tumour model by ^{18}F]fluoromisonidazole PET and immunohistochemistry. *Br J Cancer* 91:1947-1954
- Dunet V, Rossier C, Buck A, Stupp R, Prior JO. (2012) Performance of ^{18}F -fluoro-ethyl-tyrosine (^{18}F -FET) PET for the differential diagnosis of primary brain tumor: a systematic review and Metaanalysis. *J Nucl Med* 53:207-214
- Duprez F, De Neve W, De Gerssem W, Coghe M, Madani I. (2011) Adaptive dose painting by numbers for head-and-neck cancer. *Int J Radiat Oncol Biol Phys* 80:1045-1055
- Eales KL, Hollinshead KER, Tennant DA. (2016) Hypoxia and metabolic adaptation of cancer cells. *Oncogenesis* 5:e190
- Erler JT, Bennewith KL, Nicolau M, Dornhöfer N, Kong C, Le QT, Chi JT, Jeffrey SS, Giaccia AJ. (2006) Lysyl oxidase is essential for hypoxia-induced metastasis. *Nature* 440:1222-1226
- Eschmann SM, Paulsen F, Bedeshem C, Machulla HJ, Hehr T, Bamberg M, Bares R. (2007) Hypoxia-imaging with ^{18}F -misonidazole and PET: changes of kinetics during radiotherapy of head-and-neck cancer. *Radiother Oncol* 83:406-410
- Eschmann SM, Paulsen F, Reimold M, Dittmann H, Welz S, Reischl G, Machulla HJ, Bares R. (2005) Prognostic impact of hypoxia imaging with ^{18}F -misonidazole PET in non-small cell lung cancer and head and neck cancer before radiotherapy. *J Nucl Med* 46:253-260
- Eskola O, Grönroos TJ, Forsback S, Tuomela J, Komar G, Bergman J, Härkönen P, Haaparanta M, Minn H, Solin O. (2012) Tracer level electrophilic synthesis and pharmacokinetics of the hypoxia tracer ^{18}F]EF5. *Mol Imaging Biol* 14:205-212

- Evangelista L, Cervino AR, Chondrogiannis S, Marzola MC, Maffione AM, Colletti PM, Muzzio PC, Rubello D. (2014) Comparison between anatomical cross-sectional imaging and ^{18}F -FDG PET/CT in the staging, restaging, treatment response, and long-term surveillance, of squamous cell head and neck cancer: a systematic literature overview. *Nucl Med Commun* 35:123-134
- Evans SM, Du KL, Chalian AA, Mick R, Zhang PJ, Hahn SM, Quon H, Lustig R, Weinstein GS, Koch CJ. (2007) Patterns and levels of hypoxia in head and neck squamous cell carcinomas and their relationship to patient outcome. *Int J Radiat Oncol Biol Phys* 69:1024-1031
- Evans SM, Fraker D, Hahn SM, Gleason K, Jenkins WT, Jenkins K, Hwang WT, Zhang P, Mick R, Koch CJ. (2006) EF5 binding and clinical outcome in human soft tissue sarcomas. *Int J Radiat Oncol Biol Phys* 64:922-927
- Ferlay J, Soerjomataram I, Dikshit R, Eser S, Mathers C, Rebelo M, Parkin DM, Forman D, Bray F. (2015) Cancer incidence and mortality worldwide: sources, methods and major patterns in GLOBOCAN 2012. *Int J Cancer* 136:E359-386
- Fillies T, Werkmeister R, van Diest PJ, Brandt B, Joos U, Buerger H. (2005) HIF-1 α overexpression indicates a good prognosis in early stage squamous cell carcinomas of the oral floor. *BMC Cancer* 5:84
- Fleming IN, Manavaki R, Blower PJ, West C, Williams KJ, Harris AL, Domarkas J, Lord S, Baldry C, Gilbert FJ. (2015) Imaging tumour hypoxia with positron emission tomography. *Br J Cancer* 112:238-250
- Fujibayashi Y, Taniuchi H, Yonekura Y, Ohtani H, Konishi J, Yokoyama A. (1997) Copper-62-ATSM: a new hypoxia imaging agent with high membrane permeability and low redox potential. *J Nucl Med* 38:1155-1160
- Gagel B, Piroth M, Pinkawa M, Reinartz P, Zimny M, Kaiser HJ, Stanzel S, Asadpour B, Demirel C, Hamacher K, Coenen HH, Scholbach T, Maneschi P, DiMartino E, Eble MJ. (2007) pO polarography, contrast enhanced color duplex sonography (CDS), [^{18}F] fluoromisonidazole and [^{18}F] fluorodeoxyglucose positron emission tomography: validated methods for the evaluation of therapy-relevant tumor oxygenation or only bricks in the puzzle of tumor hypoxia? *BMC Cancer* 7:113
- Gagel B, Reinartz P, Dimartino E, Zimny M, Pinkawa M, Maneschi P, Stanzel S, Hamacher K, Coenen HH, Westhofen M, Büll U, Eble MJ. (2004) pO₂ Polarography versus positron emission tomography ([^{18}F] fluoromisonidazole, [^{18}F]-2-fluoro-2'-deoxyglucose). An appraisal of radiotherapeutically relevant hypoxia. *Strahlenther Onkol* 180:616-622
- Gao S, Li S, Yang X, Tang Q. (2014) ^{18}F FDG PET-CT for distant metastases in patients with recurrent head and neck cancer after definitive treatment. A meta-analysis. *Oral Oncol* 50:163-167
- Gatenby RA, Gillies RJ. (2004) Why do cancers have high aerobic glycolysis? *Nat Rev Cancer* 4:891-899
- Geets X, Lee JA, Bol A, Lonneux M, Grégoire V. (2007) A gradient-based method for segmenting FDG-PET images: methodology and validation. *Eur J Nucl Med Mol Imaging* 34:1427-1438
- Gong L, Zhang W, Zhou J, Lu J, Xiong H, Shi X, Chen J. (2013) Prognostic value of HIFs expression in head and neck cancer: a systematic review. *PLoS One* 8(9):e75094,doi:10.1371/journal.pone.0075094
- Gourin CG, Podolsky RH. (2006) Racial disparities in patients with head and neck squamous cell carcinoma. *Laryngoscope* 116:1093-1106
- Graeber TG, Osmanian C, Jacks T, Housman DE, Koch CJ, Lowe SW, Giaccia AJ. (1996) Hypoxia-mediated selection of cells with diminished apoptotic potential in solid tumours. *Nature* 379:88-91
- Graham MM, Peterson LM, Link JM, Evans ML, Rasey JS, Koh WJ, Caldwell JH, Krohn KA. (1997) Fluorine-18-fluoromisonidazole radiation dosimetry in imaging studies. *J Nucl Med* 38:1631-1636
- Green B, Bisase B, Godden D, Mitchell DA, Brennan PA. (2016) Current surgical management of metastases in the neck from mucosal squamous cell carcinoma of the head and neck. *Br J Oral Maxillofac Surg* 54:135-140
- Grégoire V, Langendijk JA, Nuyts S. (2015) Advances in radiotherapy for head and neck cancer. *J Clin Oncol* 33:3277-3284
- Grkovski M, Schwartz J, Rimner A, Schöder H, Carlin SD, Zanzonico PB, Humm JL, Nehmeh SA. (2016) Reproducibility of ^{18}F -fluoromisonidazole intratumour distribution in non-small cell lung cancer. *EJNMMI Research* 6:79

- Grönroos T, Bentzen L, Marjamäki P, Murata R, Horsman MR, Keiding S, Eskola O, Haaparanta M, Minn H, Solin O. (2004) Comparison of the biodistribution of two hypoxia markers [^{18}F]FETNIM and [^{18}F]FMISO in an experimental mammary carcinoma. *Eur J Nucl Med Mol Imaging* 31:513-520
- Grönroos T, Eskola O, Lehtiö K, Minn H, Marjamäki P, Bergman J, Haaparanta M, Forsback S, Solin O. (2001) Pharmacokinetics of [^{18}F]FETNIM: a potential marker for PET. *J Nucl Med* 42:1397-1404
- Grosu AL, Souvatzoglou M, Röper B, Dobritz M, Wiedenmann N, Jacob V, Wester HJ, Reischl G, Machulla HJ, Schwaiger M, Molls M, Piert M. (2007) Hypoxia imaging with FAZA-PET and theoretical considerations with regard to dose painting for individualization of radiotherapy in patients with head and neck cancer. *Int J Radiat Oncol Biol Phys* 69:541-551
- Gupta N, Gill H, Graeber G, Bishop H, Hurst J, Stephens T. (1998) Dynamic positron emission tomography with F-18 fluorodeoxyglucose imaging in differentiation of benign from malignant lung/mediastinal lesions. *Chest* 114:1105-1111
- Gupta T, Master Z, Kannan S, Agarwal JP, Ghosh-Laskar S, Rangarajan V, Murthy V, Budrukkar A. (2011) Diagnostic performance of post-treatment FDG PET or FDG PET/CT imaging in head and neck cancer: a systemic review and meta-analysis. *Eur J Nucl Med Mol Imaging* 38: 2083-2095
- Haerle SK, Fischer DR, Schmid DT, Ahmad N, Huber GF, Buck A. (2011) ^{18}F -FET PET/CT in advanced head and neck squamous cell carcinoma: an intra-individual comparison with ^{18}F -FDG PET/CT. *Mol Imaging Biol* 13:1036-1042
- Haerle SK, Schmid DT, Ahmad N, Hany TF, Stoeckli SJ. (2011b) The value of ^{18}F -FDG PET/CT for the detection of distant metastases in high risk patients with head and neck squamous cell carcinoma. *Oral Oncol* 47:653-659
- Haffty BG, Hurley R, Peters LJ. (1999) Radiation therapy with hyperbaric oxygen at 4 atmospheres pressure in the management of squamous cell carcinoma of the head and neck: results of a randomized clinical trial. *Cancer J Sci Am* 5:341-347
- Hammond EM, Asselin MC, Forster D, O'Connor JP, Senra JM, Williams KJ. (2014) The meaning, measurement and modification of hypoxia in the laboratory and the clinic. *Clin Oncol* 26:277-288
- Harris AL. (2002) Hypoxia—a key regulatory factor in tumor growth. *Nat Rev Cancer* 2:38-47
- Hawkins PG, Kadam AS, Jackson WC, Eisbruch A. (2018) Organ-sparing in radiotherapy for head-and-neck cancer: improving quality of life. *Semin Radiat Oncol* 28:46-52
- Höckel M, Schlenger K, Aral B, Mitze M, Schäffer U, Vaupel P. (1996) Association between tumor hypoxia and malignant progression in advanced cancer of the uterine cervix. *Cancer Res* 56:4509-4515
- Hoeben BA, Bussink J, Troost EG, Oyen WJ, Kaanders JH. (2013b) Molecular PET imaging for biology-guided adaptive radiotherapy of head and neck cancer. *Acta Oncol* 52:1257-1271
- Hoeben BA, Kaanders JH, Franssen GM, Troost EG, Rijken PF, Oosterwijk E, van Dongen GA, Oyen WJ, Boerman OC, Bussink J. (2010) PET of hypoxia with ^{89}Zr -labeled cG250-F(ab')₂ in head and neck tumors. *J Nucl Med* 51:1076-1083
- Hoeben BA, Troost EG, Span PN, van Herpen CM, Bussink J, Oyen WJ, Kaanders JH. (2013) ^{18}F -FLT PET during radiotherapy or chemoradiotherapy in head and neck squamous cell carcinoma is an early predictor of outcome. *J Nucl Med* 54:532-540
- Hoff CM. (2012) Importance of hemoglobin concentration and its modification for the outcome of head and neck cancer patients treated with radiotherapy. *Acta Oncol* 51:419-432
- Hofheinz F, Apostolova I, Oehme L, Kotzerke J, van den Hoff J. (2017) Test-retest variability in lesion SUV and lesion SUR in ^{18}F -FDG PET: an analysis of data from two prospective multicenter trials. *J Nucl Med* 58:1770-1775
- Höglund J, Shirvan A, Antoni G, Gustavsson SÅ, Långström B, Ringheim A, Sörensen J, Ben-Ami M, Ziv I. (2011) ^{18}F -ML-10, a PET tracer for apoptosis: a first human study. *J Nucl Med* 52:720-725

- Hong A, Zhang M, Veillard AS, Jahanbani J, Lee CS, Jones D, Harnett G, Clark J, Elliot M, Milross C, Rose B. (2013) The prognostic significance of hypoxia inducing factor 1- α in oropharyngeal cancer in relation to human papillomavirus status. *Oral Oncol* 49:354-359
- Horiuchi M, Yasuda S, Shohtsu A, Ide M. (1998) Four cases of Warthin's tumor of the parotid gland detected with PET. *Ann Nucl Med* 12:47-50
- Horsman MR, Mortensen LS, Petersen JB, Busk M, Overgaard J. (2012) Imaging hypoxia to improve radiotherapy outcome. *Nat Rev Clin Oncol* 9:674-687
- Horsman MR. (1998) Measurement of tumor oxygenation. *Int J Radiat Oncol Biol Phys* 42:701-704
- Huang YT, Ravi Kumar AS, Bhuta S. (2015) 18F-FDG PET/CT as a semiquantitative imaging marker in HPV-p16-positive oropharyngeal squamous cell cancers. *Nucl Med Commun* 36:16-20
- ICRP Publication 53. Radiation dose to patients from radiopharmaceuticals. *Ann ICRP* 1988;18:1
- International Commission on Radiological Protection. Recommendations of the International Commission on Radiological Protection. ICRP Publication No. 26. *Ann ICRP* 1976; 1(3)
- International Commission on Radiological Protection. Recommendations of the International Commission on Radiological Protection. ICRP Publication No. 60. *Ann ICRP* 1991;21(1-3).
- Isles MG, McConkey C, Mehanna HM. (2008) A systematic review and meta-analysis of the role of positron emission tomography in the follow up of head and neck squamous cell carcinoma following radiotherapy or chemoradiotherapy. *Clin Otolaryngol* 33:210-222
- Janssen HL, Haustermans KM, Balm AJ, Begg AC. (2005) Hypoxia in head and neck cancer: how much, how important? *Head Neck* 27:622-638
- Janssen MH, Aerts HJ, Öllers MC, Bosmans G, Lee JA, Buijsen J, Ruyscher DD, Lambin P, Lammering G, Dekker AL. (2009) Tumor delineation based on time-activity curve differences assessed with dynamic fluorodeoxyglucose positron emission tomography-computed tomography in rectal cancer patients. *Int J Radiat Oncol Biol Phys* 73:456-465
- Janssens GO, Rademakers SE, Terhaard CH, Doornaert PA, Bijl HP, van den Ende P, Chin A, Marres HA, de Bree R, van der Kogel AJ, Hoogsteen IJ, Bussink J, Span PN, Kaanders JH. (2012) Accelerated radiotherapy with carbogen and nicotinamide for laryngeal cancer: results of a phase III randomized trial. *J Clin Oncol* 30:1777-1783
- Johnson JT, Branstetter BF 4th. (2014) PET/CT in head and neck oncology: State-of-the-art 2013. *Laryngoscope* 124:913-915
- Josse O, Labar D, Georges B, Grégoire V, Marchand-Brynaert J. (2001) Synthesis of [18F]-labeled EF3 [2-(2-nitroimidazol-1-yl)-N-(3,3,3-trifluoropropyl)-acetamide], a marker for PET detection of hypoxia. *Bioorg Med Chem* 9:665-675
- Kaalep A, Sera T, Oyen W, Krause BJ, Chiti A, Liu Y, Boellaard R. (2018) EANM/EARL FDG-PET/CT accreditation – summary results from the first 200 accredited imaging systems. *Eur J Nucl Med Mol Imaging* 45:412-422
- Kaanders JH, Wijffels KI, Marres HA, Ljungkvist AS, Pop LA, van den Hoogen FJ, de Wilde PC, Bussink J, Raleigh JA, van der Kogel AJ. (2002) Pimonidazole binding and tumor vascularity predict for treatment outcome in head and neck cancer. *Cancer Res* 62:7066-7074
- Karakatsanis NA, Lodge MA, Tahari AK, Zhou Y, Wahl RL, Rahmim A. (2013) Dynamic whole-body PET parametric imaging: I. Concept, acquisition protocol optimization and clinical application. *Phys Med Biol* 58:7391-7418
- Kelada OJ, Carlson DJ. (2014) Molecular imaging of tumor hypoxia with positron emission tomography. *Radiat Res* 181:335-349
- Kelloff GJ, Hoffman JM, Johnson B, Scher HI, Siegel BA, Cheng EY, Cheson BD, O'Shaughnessy J, Guyton KZ, Mankoff DA, Shankar L, Larson SM, Sigman CC, Schilsky RL, Sullivan DC. (2005) Progress and promise of FDG-PET imaging for cancer patient management and oncologic drug development. *Clin Cancer Res* 11:2785-2808

- Kenborg L, Jørgensen AD, Budtz-Jørgensen E, Knudsen LE, Hansen J. (2010) Occupational exposure to the sun and risk of skin and lip cancer among male wage earners in Denmark: a population-based case-control study. *Cancer Causes Control* 21:1347-1355
- Kennedy KA, Rockwell S, Sartorelli AC. (1980) Preferential activation of mitomycin C to cytotoxic metabolites by hypoxic tumor cells. *Cancer Res* 40:2356-2360
- Khan N, Oriuchi N, Ninomiya H, Higuchi T, Kamada H, Endo K. (2004) Positron emission tomographic imaging with ^{11}C -choline in differential diagnosis of head and neck tumors: comparison with ^{18}F -FDG PET. *Ann Nucl Med* 18:409-417
- Klaassen R, Bennink RJ, van Tienhoven G, Bijlsma MF, Besselink MG, van Berge Hegnegouwen MI, Wilmink JW, Nederveen AJ, Windhorst AD, Hulshof MC, van Laarhoven HW. (2015) Feasibility and repeatability of PET with the hypoxia tracer [^{18}F]HX4 in oesophageal and pancreatic cancer. *Radiother Oncol* 116:94-99
- Koch CJ, Evans SM. (2015) Optimizing hypoxia detection and treatment strategies. *Semin Nucl Med* 45:163-176
- Koch CJ, Hahn SM, Rockwell K Jr, Covey JM, McKenna WG, Evans SM. (2001) Pharmacokinetics of EF5 [2-(2-nitro-1H-imidazol-1-yl)-N-(2,2,3,3,3-pentafluoropropyl)acetamide] in human patients: implications for hypoxia measurements in vivo by 2-nitroimidazoles. *Cancer Chemother Pharmacol* 48:177-187
- Koch CJ, Scheuermann JS, Divgi C, Judy KD, Kachur AV, Freifelder R, Reddin JS, Karp J, Stubbs JB, Hahn SM, Driesbaugh J, Smith D, Prendergast S, Evans SM. (2010) Biodistribution and dosimetry of ^{18}F -EF5 in cancer patients with preliminary comparison of ^{18}F -EF5 uptake versus EF5 binding in human glioblastoma. *Eur J Nucl Med Mol Imaging* 37:2048-2059
- Koch CJ. (2002) Measurement of absolute oxygen levels in cells and tissues using oxygen sensors and 2-nitroimidazole EF5. *Methods Enzymol* 352:3-31
- Koh WJ, Bergman KS, Rasey JS, Peterson LM, Evans ML, Graham MM, Grierson JR, Lindsley KL, Lewellen TK, Krohn KA, Griffin TW. (1995) Evaluation of oxygenation status during fractionated radiotherapy in human nonsmall cell lung cancers using [^{18}F]fluoromisonidazole positron emission tomography. *Int J Radiat Oncol Biol Phys* 33:391-398
- Koh WJ, Rasey JS, Evans ML, Grierson JR, Lewellen TK, Graham MM, Krohn KA, Griffin TW. (1992) Imaging of hypoxia in human tumors with [^{18}F]fluoromisonidazole. *Int J Radiat Oncol Biol Phys* 22:199-212
- Kolb HC, Finn MG, Sharpless KB. (2001) Click Chemistry: diverse chemical function from a few good reactions. *Angew Chem Int Ed Engl* 40:2004-2021
- Komar G, Lehtiö K, Seppänen M, Eskola O, Levola H, Lindholm P, Sipilä H, Seppälä J, Grénman R, Solin O, Minn H. (2014) Prognostic value of tumour blood flow, [^{18}F]EF5 and [^{18}F]FDG PET/CT imaging in patients with head and neck cancer treated with radiochemotherapy. *Eur J Nucl Med Mol Imaging* 41:2042-2050
- Komar G, Seppänen M, Eskola O, Lindholm P, Grönroos TJ, Forsback S, Sipilä H, Evans SM, Solin O, Minn H. (2008) ^{18}F -EF5: a new PET tracer for imaging hypoxia in head and neck cancer. *J Nucl Med* 49:1944-1951
- Koritzinsky M. (2015) Metformin: a novel biological modifier of tumor response to radiation therapy. *Int J Radiat Oncol Biol Phys* 93:454-464
- Krabbe CA, Balink H, Roodenburg JL, Dol J, de Visscher JG. (2011) Performance of ^{18}F -FDG PET/contrast-enhanced CT in the staging of squamous cell carcinoma of the oral cavity and oropharynx. *Int J Oral Maxillofac Surg* 40:1263-1270
- Kwee TC, Kwee RM. (2009) Combined FDG-PET/CT for the detection of unknown primary tumors: systematic review and meta-analysis. *Eur Radiol* 19:731-744
- Kyzas PA, Evangelou E, Denaxa-Kyza D, Ioannidis JP. (2008) ^{18}F -fluorodeoxyglucose positron emission tomography to evaluate cervical node metastases in patients with head and neck squamous cell carcinoma: a meta-analysis. *J Natl Cancer Inst* 100:712-720

- Laforest R, Dehdashti F, Lewis JS, Schwarz SW. (2005) Dosimetry of $^{60/61/62/64}\text{Cu}$ -ATSM: a hypoxia imaging agent for PET. *Eur J Nucl Med Mol Imaging* 32:764-770
- LaGory EL, Giaccia AJ. (2016) The ever-expanding role of HIF in tumour and stromal biology. *Nat Cell Biol* 18:356-365
- Lambade PN, Lambade D, Goel M. (2013) Osteoradionecrosis of the mandible: a review. *Oral Maxillofac Surg* 17:243-249
- Lambin P, Ramaekers BL, van Mastrigt GA, van den Ende P, de Jong J, de Ruyscher DK, Pijls-Johannesma M. (2009) Erythropoietin as an adjuvant treatment with (chemo)radiation therapy for head and neck cancer. *Cochrane Database Syst Rev* 3:CD006158. doi: 10.1002/14651858.CD006158.pub2.
- Lammertsma AA. (2017) Forward to the past: The case for quantitative PET imaging. *J Nucl Med* 58:1019-1024
- Laughlin KM, Evans SM, Jenkins WT, Tracy M, Chan CY, Lord EM, Koch CJ. (1996) Biodistribution of the nitroimidazole EF5 (2-[2-nitro-1H-imidazol-1-yl]-N-(2,2,3,3,3-pentafluoropropyl)acetamide) in mice bearing subcutaneous EMT6 tumors. *J Pharmacol Exp Ther* 277:1049-1057
- Lawrentschuk N, Lee FT, Jones G, Rigopoulos A, Mountain A, O'Keefe G, Papenfuss AT, Bolton DM, Davis ID, Scott AM. (2011) Investigation of hypoxia and carbonic anhydrase IX expression in a renal cell carcinoma xenograft model with oxygen tension measurements and ^{124}I -cG250 PET/CT. *Urol Oncol* 29:411-420
- Leclerc M, Lartigau E, Lacornerie T, Daisne JF, Kramar A, Grégoire V. (2015) Primary tumor delineation based on ^{18}F FDG PET for locally advanced head and neck cancer treated by chemo-radiotherapy. *Radiother Oncol* 116:87-93
- Lee DJ, Cosmatos D, Marcial VA, Fu KK, Rotman M, Cooper JS, Ortiz HG, Beitler JJ, Abrams RA, Curran WJ, Coleman CN, Wasserman TH. (1995) Results of an RTOG phase III trial (RTOG 85-27) comparing radiotherapy plus etanidazole with radiotherapy alone for locally advanced head and neck carcinomas. *Int J Radiat Oncol Biol Phys* 32:567-576
- Lee N, Schoder H, Beattie B, Lanning R, Riaz N, McBride S, Katabi N, Li D, Yarusi B, Chan S, Mitrani L, Zhang Z, Pfister DG, Sherman E, Baxi S, Boyle J, Morris LG, Ganly I, Wong R, Humm J. (2016) Strategy of using intratreatment hypoxia imaging to selectively and safely guide radiation dose de-escalation concurrent with chemotherapy for locoregionally advanced human papillomavirus-related oropharyngeal carcinoma. *Int J Radiat Oncol Biol Phys* 96:9-17
- Lee WR, Berkey B, Marcial V, Fu KK, Cooper JS, Vikram B, Coia LR, Rotman M, Ortiz H. (1998) Anemia is associated with decreased survival and increased locoregional failure in patients with locally advanced head and neck carcinoma: a secondary analysis of RTOG 85-27. *Int J Radiat Oncol Biol Phys* 42:1069-1075
- Lehtiö K, Eskola O, Viljanen T, Oikonen V, Grönroos T, Sillanmäki L, Grénman R, Minn H. (2004) Imaging perfusion and hypoxia with PET to predict radiotherapy response in head-and-neck cancer. *Int J Radiat Oncol Biol Phys* 59:971-982
- Lehtiö K, Oikonen V, Grönroos T, Eskola O, Kalliokoski K, Bergman J, Solin O, Grénman R, Nuutila P, Minn H. (2001) Imaging of blood flow and hypoxia in head and neck cancer: initial evaluation with $[(15)\text{O}]\text{H}(2)\text{O}$ and $[(18)\text{F}]\text{fluoroerythronitroimidazole}$ PET. *J Nucl Med* 42:1643-1652
- Leusink FK, van Es RJ, de Bree R, Baatenburg de Jong RJ, van Hooff SR, Holstege FC, Slootweg PJ, Brakenhoff RH, Takes RP. (2012) Novel diagnostic modalities for assessment of the clinically node-negative neck in oral squamous-cell carcinoma. *Lancet Oncol* 13:e554-e561
- Lewis JS, McCarthy DW, McCarthy TJ, Fujibayashi Y, Welch MJ. (1999) Evaluation of ^{64}Cu -ATSM in vitro and in vivo in a hypoxic tumor model. *J Nucl Med* 40:177-183
- Li J, Zhang G, Wang X, Li XF. (2015) Is carbonic anhydrase IX a validated target for molecular imaging of cancer and hypoxia? *Future Oncol* 11:1531-1541
- Li L, Hu M, Zhu H, Zhao W, Yang G, Yu J. (2010) Comparison of ^{18}F -Fluoroerythronitroimidazole and ^{18}F -fluorodeoxyglucose positron emission tomography and prognostic value in locally advanced non-small-cell lung cancer. *Clin Lung Cancer* 11:335-340

- Ligtenberg H, Jager EA, Caldas-Magalhaes J, Schakel T, Pameijer FA, Kasperts N, Willems SM, Terhaar CH, Raaijmakers CP, Philippens ME. (2017) Modality-specific target definition for laryngeal and hypopharyngeal cancer on FDG-PET, CT and MRI. *Radiother Oncol* 123:63-70
- Lin S, Ma R, Zheng XY, Yu H, Liang X, Lin H, Cai XJ. (2014) Meta-analysis of immunohistochemical expression of hypoxia inducible factor-1 α as a prognostic role in gastric cancer. *World J Gastroenterol* 20:1107-1113
- Lindholm P, Leskinen-Kallio S, Grénman R, Lehtikoinen P, Nägren K, Teräs M, Ruotsalainen U, Joensuu H. (1995) Evaluation of response to radiotherapy in head and neck cancer by positron emission tomography and [^{11}C]methionine. *Int J Radiat Oncol Biol Phys* 32:787-794
- Lindholm P, Leskinen-Kallio S, Minn H, Bergman J, Haaparanta M, Lehtikoinen P, Nägren K, Ruotsalainen U, Teräs M, Joensuu H. (1993) Comparison of fluorine-18-fluorodeoxyglucose and carbon-11-methionine in head and neck cancer. *J Nucl Med* 34:1711-1716
- Ling CC, Humm J, Larson S, Amols H, Fuks Z, Leibel S, Koutcher JA. (2000) Towards multidimensional radiotherapy (MD-CRT): biological imaging and biological conformality. *Int J Radiat Oncol Biol Phys* 47:551-560
- Ljungkvist AS, Bussink J, Kaanders JH, van der Kogel AJ. (2007) Dynamics of tumor hypoxia measured with bioreductive hypoxic cell markers. *Radiat Res* 167:127-145
- Löck S, Perrin R, Seidlitz A, Bandurska-Luque A, Zschaek S, Zöphel K, Krause M, Steinbach J, Kotzerke J, Zips D, Troost EGC, Baumann M. (2017) Residual tumour hypoxia in head-and-neck cancer patients undergoing primary radiochemotherapy, final results of a prospective trial on repeat FMISO-PET imaging. *Radiother Oncol* 124:533-540
- Lodge MA. (2017) Repeatability of SUV in Oncologic ^{18}F -FDG PET. *J Nucl Med* 58:523-532
- Lord EM, Harwell L, Koch CJ. (1993) Detection of hypoxic cells by monoclonal antibody recognizing 2-nitroimidazole adducts. *Cancer Res* 53:5721-5726
- Ma Z, Tavares JM, Jorge RN. (2009) A review of the current segmentation algorithms for medical images. In Proceedings of the first international conference on computer imaging theory and applications, pages 135-140. doi: 10.5220/0001793501350140
- Madani I, Duprez F, Boterberg T, Van de Wiele C, Bonte K, Deron P, De Gerssem W, Coghe M, De Neve W. (2011) Maximum tolerated dose in a phase I trial on adaptive dose painting by numbers for head and neck cancer. *Radiother Oncol* 101:351-355
- Mahy P, De Bast M, Leveque PH, Gillart J, Labar D, Marchand J, Gregoire V. (2004) Preclinical validation of the hypoxia tracer 2-(2-nitroimidazol-1-yl)-N-(3,3,3-[(^{18}F]trifluoropropyl)acetamide,[(^{18}F)]EF3. *Eur J Nucl Med Mol Imaging* 31:1263-1272
- Mahy P, Geets X, Lonneux M, Levêque P, Christian N, De Bast M, Gillart J, Labar D, Lee J, Grégoire V. (2008) Determination of tumour hypoxia with [^{18}F]EF3 in patients with head and neck tumours: a phase I study to assess the tracer pharmacokinetics, biodistribution and metabolism. *Eur J Nucl Med Mol Imaging* 35:1282-1289
- Manca G, Vanzi E, Rubello D, Giammarile F, Grassetto G, Wong KK, Perkins AC, Colletti PM, Volterrani D. (2016) ^{18}F -FDG PET/CT quantification in head and neck squamous cell cancer: principles, technical issues and clinical applications. *Eur J Nucl Med Mol Imaging* 43:1360-1375
- Masoud GN, Li W. (2015) HIF-1 α pathway: role, regulation and intervention for cancer therapy. *Acta Pharm Sin B* 5:378-389
- McLaughlin JK, Gridley G, Block G, Winn DM, Preston-Martin S, Schoenberg JB, Greenberg RS, Stemhagen A, Austin DF, Ershow AG et al. (1988) Dietary factors in oral and pharyngeal cancer. *J Natl Cancer Inst* 80:1237-1243
- McNutt TR, Moore KL, Quon H. (2016) Needs and challenges for big data in radiation oncology. *Int J Radiat Oncol Biol Phys* 95:909-915
- Mehanna H, Wong WL, McConkey CC, Rahman JK, Robinson M, Hartley AG, Nutting C, Powell N, Al-Booz H, Robinson M, Junor E, Rizwanullah M, von Zeidler SV, Wiesmann H, Hulme C, Smith AF, Hall P, Dunn J, PET-Neck Management Group. (2016) PET-CT surveillance versus neck dissection in advanced head and neck cancer. *N Engl J Med* 374:1444-1454

- Mehranian A, Arabi H, Zaidi H. (2016) Vision 20/20: Magnetic resonance imaging-guided attenuation correction in PET/MRI: Challenges, solutions and opportunities. *Med Phys* 43:1130-1155
- Mellanen P, Minn H, Grénman R, Härkönen P. (1994) Expression of glucose transporters in head-and-neck tumors. *Int J Cancer* 56:622-629
- Mena E, Thippasandra S, Yanamadala A, Redy S, Pattanayak P, Subramaniam RM. (2017) Molecular imaging and precision medicine in head and neck cancer. *PET Clin* 12:7-25
- Mendenhall WM, Morris CG, Amdur RJ, Mendenhall NP, Siemann DW. (2005) Radiotherapy alone or combined with carbogen breathing for squamous cell carcinoma of the head and neck: a prospective, randomized trial. *Cancer* 104:332-337
- Minagawa Y, Shizukuishi K, Koike I, Horiuchi C, Watanuki K, Hata M, Omura M, Odagiri K, Tohnai I, Inoue T, Tateishi U. (2011) Assessment of tumor hypoxia by ⁶²Cu-ATSM PET/CT as a predictor of response in head and neck cancer: a pilot study. *Ann Nucl Med* 25:339-345
- Minn H, Clavo AC, Grénman R, Wahl RL. (1995) In vitro comparison of cell proliferation kinetics and uptake of tritiated fluorodeoxyglucose and L-methionine in squamous-cell carcinoma of the head and neck. *J Nucl Med* 36:252-258
- Minn H, Zasadny KR, Quint LE, Wahl RL. (1995b) Lung cancer: reproducibility of quantitative measurements for evaluating 2-[F-18]-fluoro-2-deoxy-D-glucose uptake at PET. *Radiology* 196:167-173
- Mistry IN, Thomas M, Calder EDD, Conway SJ, Hammond EM. (2017) Clinical advances of hypoxia-activated prodrugs in combination with radiation therapy. *Int J Radiat Oncol Biol Phys* 98:1183-1196
- Mochizuki T, Tsukamoto E, Kuge Y, Kanegae K, Zhao S, Hikosaka K, Hosokawa M, Kohanawa M, Tamaki N. (2001) FDG uptake and glucose transporter subtype expressions in experimental tumor and inflammation models. *J Nucl Med* 42:1551-1555
- Moreira J, Tobias A, O'Brien MP, Agulnik M. (2017) Targeted therapy in head and neck cancer: an update on current clinical developments in Epidermal growth factor receptor-targeted therapy and immunotherapies. *Drugs* 77:843-857
- Mortensen LS, Johansen J, Kallehauge J, Primdahl H, Busk M, Lassen P, Alsner J, Sørensen BS, Toustrup K, Jakobsen S, Petersen J, Petersen H, Theil J, Nordmark M, Overgaard J. (2012) FAZA PET/CT hypoxia imaging in patients with squamous cell carcinoma of the head and neck treated with radiotherapy: results from the DAHANCA 24 trial. *Radiother Oncol* 105:14-20
- Moule RN, Kayani I, Prior T, Lemon C, Goodchild K, Sanghera B, Wong WL, Saunders MI. (2011) Adaptive ¹⁸Fluoro-2-deoxyglucose positron emission tomography/computed tomography-based target volume delineation in radiotherapy planning of head and neck cancer. *Clin Oncol* 23:364-371
- Murakami R, Uozumi H, Hirai T, Nishimura R, Shiraishi S, Ota K, Murakami D, Tomiguchi S, Oya N, Katsuragawa S, Yamashita Y. (2007) Impact of FDG-PET/CT imaging on nodal staging for head-and-neck squamous cell carcinoma. *Int J Radiat Oncol Biol Phys* 68:377-382
- Nehmeh SA, Lee NY, Schröder H, Squire O, Zanzonico PB, Erdi YE, Greco C, Mageras G, Pham HS, Larson SM, Ling CC, Humm JL. (2008) Reproducibility of intratumor distribution of (18)F-fluoromisonidazole in head and neck cancer. *Int J Radiat Oncol Biol Phys* 70:235-242
- Ng SH, Yen TC, Chang JT, Chan SC, Ko SF, Wang HM, Lee LY, Kang CJ, Wong AM, Liao CT. (2006) Prospective study of [18F]fluorodeoxyglucose positron emission tomography and computed tomography and magnetic resonance imaging in oral cavity squamous cell carcinoma with palpably negative neck. *J Clin Oncol* 24:4371-4376
- Noij DP, de Jong MC, Mulders LG, Marcus JT, de Bree R, Lavini C, de Graaf P, Castelijns JA. (2015) Contrast-enhanced perfusion magnetic resonance imaging for head and neck squamous cell carcinoma: a systematic review. *Oral Oncol* 51:124-138
- Nordmark M, Alsner J, Keller J, Nielsen OS, Jensen OM, Horsman MR, Overgaard J. (2001) Hypoxia in human soft tissue sarcomas: adverse impact on survival and no association with p53 mutations. *Br J Cancer* 84:1070-1075

- Nordsmark M, Bentzen SM, Rudat V, Brizel D, Lartigau E, Stadler P, Becker A, Adam M, Molls M, Dunst J, Terris DJ, Overgaard J. (2005) Prognostic value of tumor oxygenation in 397 head and neck tumors after primary radiation therapy. An international multi-center study. *Radiother Oncol* 77:18-24
- Nordsmark M, Overgaard J. (2000) A confirmatory prognostic study on oxygenation status and loco-regional control in advanced head and neck squamous cell carcinoma treated by radiation therapy. *Radiother Oncol* 57:39-43
- Okamoto S, Shiga T, Yasuda K, Ito YM, Magota K, Kasai K, Kuge Y, Shirato H, Tamaki N. (2013) High reproducibility of tumor hypoxia evaluated by ^{18}F -fluoromisonidazole PET for head and neck cancer. *J Nucl Med* 54:201-207
- Okamoto S, Shiga T, Yasuda K, Watanabe S, Hirata K, Nishijima KI, Magota K, Kasai K, Onimaru R, Tuchiya K, Kuge Y, Shirato H, Tamaki N. (2016) The reoxygenation of hypoxia and the reduction of glucose metabolism in head and neck cancer by fractionated radiotherapy with intensity-modulated radiation therapy. *Eur J Nucl Med Mol Imaging* 43:2147-2154
- Olive PL, Banáth JP, Aquino-Parsons C. (2001) Measuring hypoxia in solid tumours – is there a gold standard? *Acta Oncol* 40:917-923
- Oliveira FP, Tavares JM. (2014) Medical image registration: a review. *Comput Methods Biomech Biomed Engin* 17:73-93
- Osborne DR, Acuff S. (2016) Whole-body dynamic imaging with continuous bed motion PET/CT. *Nucl Med Commun* 37:428-431
- Overgaard J, Hansen HS, Andersen AP, Hjelm-Hansen M, Jørgensen K, Sandberg E, Berthelsen A, Hammer R, Pedersen M. (1989) Misonidazole combined with split-course radiotherapy in the treatment of invasive carcinoma of larynx and pharynx: report from the DAHANCA 2 study. *Int J Radiat Oncol Biol Phys* 16:1065-1068
- Overgaard J, Hansen HS, Overgaard M, Bastholt L, Berthelsen A, Specht L, Lindeløv B, Jørgensen K. (1998) A randomized double-blind phase III study of nimorazole as a hypoxic radiosensitizer of primary radiotherapy in supraglottic larynx and pharynx carcinoma. Results of the Danish Head and Neck Cancer study (DAHANCA) Protocol 5-85. *Radiother Oncol* 46:135-146
- Overgaard J. (2011) Hypoxic modification of radiotherapy in squamous cell carcinoma of the head and neck – a systematic review and meta-analysis. *Radiother Oncol* 100:22-32
- Oxford centre for evidence based medicine levels of evidence (March 2009). <http://www.cebm.net/oxford-centre-evidence-based-medicine-levels-evidence-march-2009/>
- Paldino MJ, Wong TZ, Reardon DA, Friedman HS, Barboriak DP. (2011) Prognostic significance of parameters derived from co-registered ^{18}F -fluorodeoxyglucose PET and contrast-enhanced MRI in patients with high-grade glioma. *Br J Radiol* 84:327-334
- Panek R, Welsh L, Dunlop A, Wong KH, Riddell AM, Koh DM, Schmidt MA, Doran S, Mcquaid D, Hopkinson G, Richardson C, Nutting CM, Bhide SA, Harrington KJ, Robinson SP, Newbold KL, Leach MO. (2016) Repeatability and sensitivity of T2* measurements in patients with head and neck squamous cell carcinoma at 3T. *J Magn Reson Imaging* 44:72-80
- Park ET, Park SK. (2016) Setup uncertainties for inter-fractional head and neck cancer in radiotherapy. *Oncotarget* 7:46662-46667
- Patlak CS, Blasberg RG, Fenstermacher JD. (1983) Graphical evaluation of blood-to-brain transfer constants from multiple-time uptake data. *J Cereb Blood Flow Metab* 3:1-7
- Pauleit D, Zimmermann A, Stoffels G, Bauer D, Risse J, Flüß MO, Hamacher K, Coenen HH, Langen KJ. (2006) ^{18}F -FET PET compared with ^{18}F -FDG PET and CT in patients with head and neck cancer. *J Nucl Med* 47:256-261
- Peeters SG, Zegers CM, Lieuwes NG, van Elmpt W, Eriksson J, van Dongen GA, Dubois L, Lambin P. (2015) A comparative study of the hypoxia PET tracers ^{18}F]HX4, ^{18}F]FAZA and ^{18}F]FMISO in a preclinical tumor model. *Int J Radiat Oncol Biol Phys* 91:351-359
- Peeters SG, Zegers CM, Yaromina A, Van Elmpt W, Dubois L, Lambin P. (2015b) Current pre-clinical and clinical applications of hypoxia PET imaging using 2-nitroimidazoles. *Q J Nucl Med Mol Imaging* 59:39-57

- Pescador N, Villar D, Cifuentes D, Garcia-Rocha M, Ortiz-Barahona A, Vazquez S, Ordoñez A, Cuevas Y, Saez-Morales D, Garcia-Bermejo ML, Landazuri MO, Guinovart J, del Peso L. (2010) Hypoxia promotes glycogen accumulation through hypoxia inducible factor (HIF)-mediated induction of glycogen synthase 1. *PLoS One* 5(3):e9644
- Pfister DG, Ang KK, Brizel DM, Burtness BA, Busse PM, Caudell JJ, Cmelak AJ, Colevas AD, Dunphy F, Eisele DW, Gilbert J, Gillison ML, Haddad RI, Haughey BH, Hicks WL Jr, Hitchcock YJ, Kies MS, Lydiatt WM, Maghami E, Martins R, McCaffrey T, Mittal BB, Pinto HA, Ridge JA, Samant S, Schuller DE, Shah JP, Spencer S, Weber RS, Wolf GT, Worden F, Yom SS, McMillian NR, Hughes M; National Comprehensive Cancer Network. (2013) Head and neck cancers, version 2.2013. Featured updates to the NCCN guidelines. *J Natl Compr Canc Netw* 11:917-923
- Pham DL, Xu C, Prince JL. (2000) Current methods in medical image segmentation. *Annu Rev Biomed Eng* 2:315-337
- Phillips RM. (2016) Targeting the hypoxic fraction of tumours using hypoxia-activated prodrugs. *Cancer Chemother Pharmacol* 77:441-457
- Piert M, Machulla HJ, Picchio M, Reischl G, Ziegler S, Kumar P, Wester HJ, Beck R, McEwan AJ, Wiebe LI, Schwaiger M. (2005) Hypoxia-specific tumor imaging with 18F-fluoroazomycin arabinoside. *J Nucl Med* 46:106-113
- Potter M, Newport E, Morten KJ. (2016) The Warburg effect: 80 years on. *Biochem Soc Trans* 44:1499-1505
- Queiroz MA, Huellner MW. (2015) PET/MR in cancers of the head and neck. *Semin Nucl Med* 45:248-265
- Querellou S, Abgral R, Le Roux PY, Nowak E, Valette G, Potard G, Le Duc-Pennec A, Cavarec MB, Marianovski R, Salaün PY. (2012) Prognostic value of fluorine-18 fluorodeoxyglucose positron-emission tomography imaging in patients with head and neck squamous cell carcinoma. *Head Neck* 34:462-468
- Racker E. (1974) History of the Pasteur effect and its pathobiology. *Mol Cell Biochem* 5:17-23
- Rajendran JG, Krohn KA. (2015) F-18 fluoromisonidazole for imaging tumor hypoxia: imaging the microenvironment for personalized cancer therapy. *Semin Nucl Med* 45:151-162
- Rajendran JG, Schwartz DL, O'Sullivan J, Peterson LM, Ng P, Scharnhorst J, Grierson JR, Krohn KA. (2006) Tumor hypoxia imaging with [F-18] fluoromisonidazole positron emission tomography in head and neck cancer. *Clin Cancer Res* 12:5435-5441
- Rajendran JG, Wilson DC, Conrad EU, Peterson LM, Bruckner JD, Rasey JS, Chin LK, Hofstrand PD, Grierson JR, Eary JF, Krohn KA. (2003) [¹⁸F]FMISO and [¹⁸F]FDG PET imaging in soft tissue sarcomas: correlation of hypoxia, metabolism and VEGF expression. *Eur J Nucl Med Mol Imaging* 30:695-704
- Rasey JS, Grunbaum Z, Magee S, Nelson NJ, Olive PL, Durand RE, Krohn KA. (1987) Characterization of radiolabeled fluoromisonidazole as a probe for hypoxic cells. *Radiat Res* 111:292-304
- Rasey JS, Hofstrand PD, Chin LK, Tewson TJ. (1999) Characterization of [¹⁸F]fluoroetamidazole, a new radiopharmaceutical for detecting tumor hypoxia. *J Nucl Med* 40:1072-1079
- Rasey JS, Koh WJ, Evans ML, Peterson LM, Lewellen TK, Graham MM, Krohn KA. (1996) Quantifying regional hypoxia in human tumors with positron emission tomography of [¹⁸F]fluoromisonidazole: a pretherapy study of 37 patients. *Int J Radiat Oncol Biol Phys* 36:417-428
- Rasmussen GB, Vogelius IR, Rasmussen JH, Schumaker L, Ioffe O, Cullen K, Fischer BM, Therkildsen MH, Specht L, Bentzen SM. (2015) Immunohistochemical biomarkers and FDG uptake on PET/CT in head and neck squamous cell carcinoma. *Acta Oncol* 54:1408-1415
- Reischl G, Dorow DS, Cullinane C, Katsifis A, Roselt P, Binns D, Hicks RJ. (2007) Imaging of tumor hypoxia with [¹²⁴I]IAZA in comparison with [¹⁸F]FMISO and [¹⁸F]FAZA – first small animal PET results. *J Pharm Pharm Sci* 10:203-211
- Ren W, Mi D, Yang K, Cao N, Tian J, Li Z, Ma B. (2013) The expression of hypoxia-inducible factor-1 α and its clinical significance in lung cancer: a systematic review and meta-analysis. *Swiss Med Wkly* 143:w13855

- Renfro LA, An MW, Mandrekar SJ. (2017) Precision oncology: A new era of cancer clinical trials. *Cancer Lett* 387:121-126
- Ringash J. (2015) Survivorship and quality of life in head and neck cancer. *J Clin Oncol* 33:3322-3327
- Rischin D, Hicks RJ, Fisher R, Binns D, Corry J, Porceddu S, Peters LJ. (2006) Prognostic significance of [18F]-misonidazole positron emission tomography-detected tumor hypoxia in patients with advanced head and neck cancer randomly assigned to chemoradiation with or without tirapazamine: a substudy of Trans-Tasman Radiation Oncology Group Study 98.02. *J Clin Oncol* 24:2098-2104
- Rischin D, Peters L, Fisher R, Macann A, Denham J, Poulsen M, Jackson M, Kenny L, Penniment M, Corry J, Lamb D, McClure B. (2005) Tirapazamine, cisplatin, and radiation versus fluorouracil, cisplatin, and radiation in patients with locally advanced head and neck cancer: a randomized phase II trial of the Trans-Tasman Radiation Oncology Group (TROG 98.02). *J Clin Oncol* 23:79-87
- Rischin D, Peters LJ, O'Sullivan B, Giralt J, Fisher R, Yuen K, Trotti A, Bernier J, Bourhis J, Ringash J, Henke M, Kenny L. (2010) Tirapazamine, cisplatin, and radiation versus cisplatin and radiation for advanced squamous cell carcinoma of the head and neck (TROG 02.02, HeadSTART): a phase III trial of the Trans-Tasman Radiation Oncology Group. *J Clin Oncol* 28:2989-2995
- Robbins KT, Ferlito A, Shah JP, Hamoir M, Takes RP, Strojan P, Khafif A, Silver CE, Rinaldo A, Medina JE. (2013) The evolving role of selective neck dissection for head and neck squamous cell carcinoma. *Eur Arch Otorhinolaryngol* 270:1195-1202
- Rödström PO, Jontell M, Mattsson U, Holmberg E. (2004) Cancer and oral lichen planus in a Swedish population. *Oral Oncol* 40:131-138
- Rohde M, Nielsen AL, Johansen J, Sørensen JA, Nguyen N, Diaz A, Nielsen MK, Asmussen JT, Christiansen JM, Gerke O, Thomassen A, Alavi A, Høilund-Carlson PF, Godballe C. (2017) Head-to-head comparison of chest x-ray/head and neck MRI, chest CT/head and neck MRI, and 18F-FDG-PET/CT for detection of distant metastases and synchronous cancer in oral, pharyngeal and laryngeal cancer. *J Nucl Med* 58:1919-1924
- Rudat V, Vanselow B, Wollensack P, Bettscheider C, Osman-Ahmet S, Eble MJ, Dietz A. (2000) Repeatability and prognostic impact of the pretreatment pO₂ histography in patients with advanced head and neck cancer. *Radiother Oncol* 57:31-37
- Saga T, Inubushi M, Koizumi M, Yoshikawa K, Zhang MR, Obata T, Tanimoto K, Harada R, Uno T, Fujibayashi Y (2016) Prognostic value of PET/CT with ¹⁸F-fluoroazomycin arabinoside for patients with head and neck squamous cell carcinomas receiving chemoradiotherapy. *Ann Nucl Med* 30:217-224
- Sakamoto H, Nakai Y, Ohashi Y, Okamura T, Ochi H. (1997) Positron emission tomographic imaging of head and neck lesions. *Eur Arch Otorhinolaryngol* 254 Suppl1:S123-126
- Sato J, Kitagawa Y, Yamazaki Y, Hata H, Okamoto S, Shiga T, Shindoh M, Kuge Y, Tamaki N. (2013) ¹⁸F-fluoromisonidazole PET uptake is correlated with hypoxia-inducible factor-1 α expression in oral squamous cell carcinoma. *J Nucl Med* 54:1060-1065
- Savi A, Incerti E, Fallanca F, Bettinardi V, Rossetti F, Monterisi C, Compierchio A, Negri G, Zannini P, Gianolli L, Picchio M (2017). First evaluation of PET-based human biodistribution and dosimetry of ¹⁸F-FAZA, a tracer for imaging tumor hypoxia. *J Nucl Med* 58:1224-1229
- Schillaci O. (2012) Use of dual-point fluorodeoxyglucose imaging to enhance sensitivity and specificity. *Semin Nucl Med* 42:267-280
- Schinagl DA, Hoffman AL, Vogel WV, van Dalen JA, Verstappen SM, Oyen WJ, Kaanders JH. (2009) Can FDG-PET assist in radiotherapy target volume definition of metastatic lymph nodes in head-and-neck cancer? *Radiother Oncol* 91:95-100
- Schinagl DA, Vogel WV, Hoffmann AL, van Dalen JA, Oyen WJ, Kaanders JH. (2007) Comparison of five segmentation tools for 18F-fluoro-deoxy-glucose-positron emission tomography-based target volume definition in head and neck cancer. *Int J Radiat Oncol Biol Phys* 69:1282-1289

- Schouten CS, Hakim S, Boellaard R, Bloemena E, Doornaert PA, Witte BI, Braakhuis BJ, Brakenhoff RH, Leemans CR, Hoekstra OS, de Bree R. (2015) Interaction of quantitative ^{18}F -FDG-PET-CT imaging parameters and human papillomavirus status in oropharyngeal squamous cell carcinoma. *Head Neck* 38:529-535
- Schuetz M, Schmid MP, Pötter R, Kommata S, Georg D, Lukic D, Dudeczak R, Kletter K, Dimopoulos J, Karanikas G, Bachtary B. (2010) Evaluating repetitive ^{18}F -fluoroazomycin-arabinoside (^{18}F FAZA) PET in the setting of MRI guided adaptive radiotherapy in cervical cancer. *Acta Oncol* 49:941-947
- Semenza GL. (2007) Evaluation of HIF-1 inhibitors as anticancer agents. *Drug Discov Today* 12:853-859
- Servagi-Vernat S, Differding S, Hanin FX, Labar D, Bol A, Lee JA, Grégoire V. (2014) A prospective clinical study of ^{18}F -FAZA PET/CT hypoxia imaging in head and neck squamous cell carcinoma before and during radiation therapy. *Eur J Nucl Med Mol Imaging* 41:1544-1552
- Servagi-Vernat S, Differding S, Sterpin E, Hanin FX, Labar D, Bol A, Lee JA, Grégoire V. (2015) Hypoxia-guided adaptive radiation dose escalation in head and neck carcinoma: a planning study. *Acta Oncol* 54:1008-1016
- Severinghaus JW, Astrup PB. (1986) History of blood gas analysis. IV. Leland Clark's oxygen electrode. *J Clin Monit* 2:125-139
- Shen G, Deng H, Hu S, Jia Z. (2014) Potential performance of dual-time-point ^{18}F -FDG PET/CT compared with single-time-point imaging for differential diagnosis of metastatic lymph nodes: a meta-analysis. *Nucl Med Commun* 35:1003-1010
- Shepherd T, Teräs M, Beichel RR, Boellaard R, Bruynooghe M, Dicken V, Gooding MJ, Julian PJ, Lee JA, Lefèvre S, Mix M, Naranjo V, Wu X, Zaidi H, Zeng Z, Minn H. (2012) Comparative study with new accuracy metrics for target volume contouring in PET image guided radiation therapy. *IEEE Trans Med Imaging* 31:2006-2024
- Siddikuzzaman, Grace VM, Guruvayoorappan C. (2011) Lysyl oxidase: a potential target for cancer therapy. *Inflammopharmacology* 19:117-129
- Simpson DR, Lawson JD, Nath SK, Rose BS, Mundt AJ, Mell LK. (2010) A survey of image-guided radiation therapy use in the United States. *Cancer* 116:3953-3960
- Simpson IA, Dwyer D, Malide D, Moley KH, Travis A, Vannucci SJ. (2008) The facilitative glucose transporter GLUT3: 20 years of distinction. *Am J Physiol Endocrinol Metab* 295:E242-253
- Soret M, Bacharach SL, Buvat I. (2007) Partial-volume effect in PET tumor imaging. *J Nucl Med* 48:932-945
- Sorger D, Patt M, Kumar P, Wiebe LI, Barthel H, Seese A, Dannenberg C, Tannapfel A, Kluge R, Sabri O. (2003) [^{18}F]Fluoroazomycin-arabinoside (^{18}F FAZA) and [^{18}F]Fluoromisonidazole (^{18}F FMISO): a comparative study of their selective uptake in hypoxic cells and PET imaging in experimental rat tumors. *Nucl Med Biol* 30:317-326
- Souvatoglou M, Grosu AL, Röper B, Krause BJ, Beck R, Reischl G, Picchio M, Machulla HJ, Wester HJ, Piert M. (2007) Tumour hypoxia imaging with [^{18}F]FAZA PET in head and neck cancer patients: a pilot study. *Eur J Nucl Med Mol Imaging* 34:1566-1575
- Stabin MG, Sparks RB, Crowe E. (2005) OLINDA/EXM: the second-generation personal computer software for internal dose assessment in nuclear medicine. *J Nucl Med* 46:1023-1027
- Stadler P, Becker A, Feldmann HJ, Hänsgen G, Dunst J, Würschmidt F, Molls M. (1999) Influence of the hypoxic subvolume on the survival of patients with head and neck cancer. *Int J Radiat Oncol Biol Phys* 44:749-754
- Sun X, Niu G, Chan N, Shen B, Chen X. (2011) Tumor hypoxia imaging. *Mol Imaging Biol* 13:399-410
- Swartz JE, Pothen AJ, Stegeman I, Willems SM, Grolman W. (2015) Clinical implications of hypoxia biomarker expression in head and neck squamous cell carcinoma: a systematic review. *Cancer Med* 4:1101-1116
- Swiecicki PL, Malloy KM, Worden FP. (2016) Advanced oropharyngeal squamous cell carcinoma: Pathogenesis, treatment, and novel therapeutic approaches. *World J Clin Oncol* 7:15-26

- Takeda D, Hasegawa T, Ueha T, Imai Y, Sakakibara A, Minoda M, Kawamoto T, Minamikawa T, Shibuya Y, Akisue T, Sakai Y, Kurosaka M, Komori T. (2014) Transcutaneous carbon dioxide induces mitochondrial apoptosis and suppresses metastasis of oral squamous cell carcinoma in vivo. *PLoS One* 9(7):e100530. doi:10.1371/journal.pone.0100530
- Tawk B, Schwager C, Deffaa O, Dyckhoff G, Warta R, Linge A, Krause M, Weichert W, Baumann M, Herold-Mende C, Debus J, Abdollahi A. (2016) Comparative analysis of transcriptomics based hypoxia signatures in head- and neck squamous cell carcinoma. *Radiother Oncol* 118:350-358
- Tewson TJ (1997) Synthesis of [^{18}F]fluoroetamidazole: a potential new tracer for imaging hypoxia. *Nucl Med Biol* 24:755-760
- Thie JA. (2004) Understanding the standardized uptake value, its methods, and implications for usage. *J Nucl Med* 45:1431-1434
- Thomlinson RH, Gray LH. (1955) The histological structure of some human lung cancers and the possible implications for radiotherapy. *Br J Cancer* 9:539-549
- Thorwarth D, Eschmann SM, Holzner F, Paulsen F, Alber M (2006). Combined uptake of [^{18}F]FDG and [^{18}F]FMISO correlates with radiation therapy outcome in head-and-neck cancer patients. *Radiother Oncol* 80:151-156
- Tochon-Danguy HJ, Sachinidis JI, Chan F, Chan G, Hall C, Cher L, Stylli S, Hill J, Kaye A, Scott AM. (2002) Imaging and quantitation of the hypoxic cell fraction of viable tumor in an animal model of intracerebral high grade glioma using [^{18}F]fluoromisonidazole (FMISO). *Nucl Med Biol* 29:191-197
- Tolvanen T, Lehtiö K, Kulmala J, Oikonen V, Eskola O, Bergman J, Minn H. (2002) 18F-Fluoroerythronitroimidazole radiation dosimetry in cancer studies. *J Nucl Med* 43:1674-1680
- Toustrup K, Sørensen BS, Lassen P, Wiuf C, Alsner J, Overgaard J; Danish Head and Neck Cancer Group (DAHANCA). (2012) Gene expression classifier predicts for hypoxic modification of radiotherapy with nimorazole in squamous cell carcinomas of the head and neck. *Radiother Oncol* 102:122-129
- Toustrup K, Sørensen BS, Metwally MA, Tramm T, Mortensen LS, Overgaard J, Alsner J. (2016) Validation of a 15-gene hypoxia classifier in head and neck cancer for prospective use in clinical trials. *Acta Oncol* 55:1091-1098
- Tran LB, Bol A, Labar D, Jordan B, Magat J, Mignon L, Grégoire V, Gallez B. (2012) Hypoxia imaging with the nitroimidazole ^{18}F -FAZA PET tracer: a comparison with OxyLite, EPR Oximetry and ^{19}F -MRI relaxometry. *Radiother Oncol* 105:29-35
- Troost EG, Bussink J, Hoffmann AL, Boerman OC, Oyen WJ, Kaanders JH. (2010) ^{18}F -FLT PET/CT for early response monitoring and dose escalation in oropharyngeal tumors. *J Nucl Med* 51:866-874
- Troost EG, Laverman P, Kaanders JH, Philippens M, Lok J, Oyen WJ, van der Kogel AJ, Boerman OC, Bussink J. (2006) Imaging hypoxia after oxygenation-modification: comparing [^{18}F]FMISO autoradiography with pimonidazole immunohistochemistry in human xenograft tumors. *Radiother Oncol* 80:157-164
- Troost EG, Schinagl DA, Bussink J, Oyen WJ, Kaanders JH. (2010b) Clinical evidence on PET-CT for radiation therapy planning in head and neck tumours. *Radiother Oncol* 96:328-334
- Troost EG, Vogel WV, Merckx MA, Slootweg PJ, Marres HA, Peeters WJ, Bussink J, van der Kogel AJ, Oyen WJ, Kaanders JH. (2007) ^{18}F -FLT PET does not discriminate between reactive and metastatic lymph nodes in primary head and neck cancer patients. *J Nucl Med* 48:726-735
- Tsujikawa T, Asahi S, Oh M, Sato Y, Narita N, Makino A, Mori T, Kiyono Y, Tsuchida T, Kimura H, Fujieda S, Okazawa H. (2016) Assessment of the tumor redox status in head and neck cancer by ^{62}Cu -ATSM PET. *PLoS One* 11(5):e0155635
- Turkington TG. (2001) Introduction to PET instrumentation. *J Nucl Med Technol* 29:4-11
- Urtasun RC, Parliament MB, McEwan AJ, Mercer JR, Mannan RH, Wiebe LI, Morin C, Chapman JD. (1996) Measurement of hypoxia in human tumours by non-invasive spect imaging of iodoazomycin arabinoside. *Br J Cancer Suppl.* 27:S209-212

- Valtorta S, Belloli S, Sanvito F, Masiello V, Di Grigoli G, Monterisi C, Fazio F, Picchio M, Moresco RM. (2013) Comparison of ^{18}F -fluoroazomycin-arabinofuranoside and ^{64}Cu -diacetyl-bis(N4-methylthiosemicarbazone) in preclinical models of cancer. *J Nucl Med* 54:1106-1112
- van den Bogaert W, van der Schueren E, Horiot JC, Chaplain G, Devilha M, Raposo S, Leonor J, Schraub S, Chenal C, Barthelme E, et al. (1986) Early results of EORTC randomized clinical trial on multiple fractions per day (MFD) and misonidazole in advanced head and neck cancer. *Int J Radiat Oncol Biol Phys* 12:587-591
- van den Hoff J, Oehme L, Schramm G, Maus J, Lougovski A, Petr J, Beuthien-Baumann B, Hofheinz F. (2013) The PET-derived tumor-to-blood standard uptake ratio (SUR) is superior to tumor SUV as a surrogate parameter of the metabolic rate of FDG. *EJNMMI Res* 3:77
- van der Meij EH, Mast H, van der Waal I. (2007). The possible premalignant character of oral lichen planus and oral lichenoid lesions: A prospective five-year follow-up study of 192 patients. *Oral Oncol* 43:742-748
- van Dijk LK, Boerman OC, Kaanders JH, Bussink J. (2015) PET imaging in head and neck cancer patients to monitor treatment response: A future role for EGFR-targeted imaging. *Clin Cancer Res* 21:3602-3609
- van Loon J, Janssen MH, Öllers M, Aerts HJ, Dubois L, Hochstenbag M, Dingemans AM, Lalisang R, Brans B, Windhorst B, van Dongen GA, Kolb H, Zhang J, De Ruyscher D, Lambin P. (2010) PET imaging of hypoxia using [^{18}F]HX4: a phase I trial. *Eur J Nucl Med Mol Imaging* 37:1663-1668
- Vaupel P, Höckel M, Mayer A. (2007) Detection and characterization of tumor hypoxia using pO_2 histography. *Antioxid Redox Signal* 9:1221-1235
- Vaupel P, Kallinowski F, Okunieff P. (1989) Blood Flow, oxygen and nutrient supply, and metabolic microenvironment of human tumors: a review. *Cancer Res* 49:6449-6465
- Vaupel P, Mayer A, Höckel M. (2004) Tumor hypoxia and malignant progression. *Methods Enzymol* 381:335-354
- Vaupel P, Mayer A. (2007b) Hypoxia in cancer: significance and impact on clinical outcome. *Cancer Metastasis Rev* 26:225-239
- Vaupel P, Schlenger K, Knoop C, Höckel M. (1991) Oxygenation of human tumors: evaluation of tissue oxygen distribution in breast cancers by computerized O_2 tension measurements. *Cancer Res* 51:3316-3322
- Vaz S, Falkmer T, Passmore AE, Parsons R, Andreou P. (2013) The case for using the repeatability coefficient when calculating test-retest reliability. *PLoS ONE* 8(9):e73990
- Vera P, Thureau S, Chaumet-Riffaud P, Modzelewski R, Bohn P, Vermandel M, Hapdey S, Pallardy A, Mahé MA, Lacombe M, Boisselier P, Guillemard S, Olivier P, Beckendorf V, Salem N, Charrier N, Chajon E, Devillers A, Aide N, Danhier S, Denis F, Muratet JP, Martin E, Riedinger AB, Koleznikov-Gauthier H, Dansin E, Massabeau C, Courbon F, Farcy Jacquet MP, Kotzki PO, Houzard C, Mornex F, Vervueren L, Paumier A, Fernandez P, Salaun M, Dubray B. (2017) Phase II study of a radiotherapy total dose increase in hypoxic lesions identified by ^{18}F -misonidazole PET/CT in patients with non-small cell lung carcinoma (RTEP5 Study). *J Nucl Med* 58:1045-1053
- Vercellino L, Groheux D, Thoury A, Delord M, Schlageter MH, Delpech Y, Barré E, Baruch-Hennequin V, Tylski P, Homyrda L, Walker F, Barranger E, Hindicé E. (2012) Hypoxia imaging of uterine cervix carcinoma with (18)F-FETNIM PET/CT. *Clin Nucl Med* 37:1065-1068
- Vermorken JB, Mesia R, Rivera F, Remenar E, Kawecki A, Rottey S, Erfan J, Zabolotny D, Kienzer HR, Cupissol D, Peyrade F, Benasso M, Vynnychenko I, De Raucourt D, Bokemeyer C, Schueler A, Amellal N, Hitt R. (2008) Platinum-based chemotherapy plus cetuximab in head and neck cancer. *N Engl J Med* 359:1116-1127
- von Pawel J, von Roemeling R, Gatzemeier U, Boyer M, Elisson LO, Clark P, Talbot D, Rey A, Butler TW, Hirsh V, Olver I, Bergman B, Ayoub J, Richardson G, Dunlop D, Arcenas A, Vescio R, Viallet J, Treat J. (2000) Tirapazamine plus cisplatin versus cisplatin in advanced non-small-cell lung cancer: A report of the international CATAPULT I study group. Cisplatin and Tirapazamine in subjects with advanced previously untreated non-small-cell lung tumors. *J Clin Oncol* 18:1351-1359

- Walsh JC, Lebedev A, Aten E, Madsen K, Marciano L, Kolb HC. (2014) The clinical importance of assessing tumor hypoxia: relationship of tumor hypoxia to prognosis and therapeutic opportunities. *Antioxid Redox Signal* 21:1516-1554
- Wang D, Schultz CJ, Jursinic PA, Bialkowski M, Zhu XR, Brown WD, Rand SD, Michel MA, Campbell BH, Wong S, Li XA, Wilson JF. (2006) Initial experience of FDG-PET/CT guided IMRT of head-and-neck carcinoma. *Int J Radiat Oncol Biol Phys* 65:143-151
- Wang W, He YF, Sun QK, Wang Y, Han XH, Peng DF, Yao YW, Ji CS, Hu B. (2014) Hypoxia-inducible factor 1 α in breast cancer prognosis. *Clin Chim Acta* 428:32-37
- Wang YF, Liu RS, Chu PY, Chang FC, Tai SK, Tsai TL, Huang JL, Chang SY. (2009) Positron emission tomography in surveillance of head and neck squamous cell carcinoma after definitive chemotherapy. *Head Neck* 31:442-451
- Warburg O. (1930) *The metabolism of tumours*. London, UK: Constable and Company
- Wei Y, Zhao W, Huang Y, Yu Q, Zhu S, Wang S, Zhao S, Hu X, Yu J, Yuan S. (2016) A comparative study of noninvasive hypoxia imaging with 18F-fluoroerythronitroimidazole and 18F-fluoromisonidazole PET/CT in patients with lung cancer. *PLoS ONE* 11(6):e0157606. doi:10.1371/journal.pone.0157606
- Welsh L, Panek R, Riddell A, Wong K, Leach MO, Tavassoli M, Rahman D, Schmidt M, Hurley T, Grove L, Richards T, Koh DM, Nutting C, Harrington K, Newbold K, Bhide S. (2017) Blood transfusion during radical chemo-radiotherapy does not reduce tumour hypoxia in squamous cell cancer of the head and neck. *Br J Cancer* 116:28-35
- Welz S, Mönnich D, Pfannenbergl C, Nikolaou K, Reimold M, La Fougère C, Reischl G, Mauz PS, Paulsen F, Alber M, Belka C, Zips D, Thorwarth D. (2017) Prognostic value of dynamic hypoxia PET in head and neck cancer: Results from a planned interim analysis of a randomized phase II hypoxia-image guided dose escalation trial. *Radiother Oncol* 124:526-532
- Whisenant JG, Peterson TE, Fluckiger JU, Tantawy MN, Ayers GD, Yankeelov TE. (2013) Reproducibility of static and dynamic ¹⁸F-FDG, ¹⁸F-FLT, and ¹⁸F-FMISO MicroPET studies in a murine model of HER2+ breast cancer. *Mol Imaging Biol* 15:87-96
- Wiedenmann NE, Bucher S, Hentschel M, Mix M, Vach W, Bittner MI, Nestle U, Pfeiffer J, Weber WA, Grosu AL. (2015) Serial [18F]-fluoromisonidazole PET during radiochemotherapy for locally advanced head and neck cancer and its correlation with outcome. *Radiother Oncol* 117:113-117
- Wilson WR, Hay MP. (2011) Targeting hypoxia in cancer therapy. *Nat Rev Cancer* 11:393-410
- Wong RJ. (2008) Current status of FDG-PET for head and neck cancer. *J Surg Oncol* 97:649-652
- Wong WL, Sonoda LI, Gharpurhy A, Gollub F, Wellsted D, Goodchild K, Lemon C, Farrell R, Saunders M. (2012) 18F-fluorodeoxyglucose positron emission tomography/computed tomography in the assessment of occult primary head and neck cancers — an audit and review of published studies. *Clin Oncol* 24:190-195
- Xie P, Li M, Zhao H, Sun X, Fu Z, Yu J. (2011) ¹⁸F-FDG PET or PET-CT to evaluate prognosis for head and neck cancer: a meta-analysis. *J Cancer Res Clin Oncol* 137:1085-1093
- Yang DJ, Wallace S, Cherif A, Li C, Gretzer MB, Kim EE, Podoloff DA. (1995) Development of F-18-labeled fluoroerythronitroimidazole as a PET agent for imaging tumor hypoxia. *Radiology* 194:795-800
- Yuan H, Schroeder T, Bowsher JE, Hedlund LW, Wong T, Dewhirst MW. (2006) Intertumoral differences in hypoxia selectivity of the PET imaging agent ⁶⁴Cu(II)-diacetyl-bis(N⁴-methylthiosemicarbazone). *J Nucl Med* 47:989-998
- Yue J, Yang Y, Cabrera AR, Sun X, Zhao S, Xie P, Zheng J, Ma L, Fu Z, Yu J. (2012) Measuring tumor hypoxia with ¹⁸F-FETNIM PET in esophageal squamous cell carcinoma: a pilot clinical study. *Dis Esophagus* 25:54-61
- Zaidi H, Abdoli M, Fuentes CL, El Naqa IM. (2012) Comparative methods for PET image segmentation in pharyngolaryngeal squamous cell carcinoma. *Eur J Nucl Med Mol Imaging* 39:881-891

- Zaidi H, El Naqa I. (2010) PET-guided delineation of radiation therapy treatment volumes: a survey of image segmentation techniques. *Eur J Nucl Med Mol Imaging* 37:2165-2187
- Zegers CM, Hoebbers FJ, van Elmpt W, Bons JA, Öllers MC, Troost EG, Eekers D, Balmaekers L, Arts-Pechtold M, Mottaghy FM, Lambin P. (2016) Evaluation of tumour hypoxia during radiotherapy using [^{18}F]HX4 PET imaging and blood biomarkers in patients with head and neck cancer. *Eur J Nucl Med Mol Imaging* 43:2139-2146
- Zegers CM, van Elmpt W, Hoebbers FJ, Troost EG, Öllers MC, Mottaghy FM, Lambin P. (2015) Imaging of tumour hypoxia and metabolism in patients with head and neck squamous cell carcinoma. *Acta Oncol* 54:1378-1384
- Zegers CM, van Elmpt W, Szardenings K, Kolb H, Waxman A, Subramaniam RM, Moon DH, Brunetti JC, Srinivas SM, Lambin P, Chien D. (2015b) Repeatability of hypoxia PET imaging using [^{18}F]HX4 in lung and head and neck cancer patients: a prospective multicenter trial. *Eur J Nucl Med Mol Imaging* 42:1840-1849
- Zegers CM, van Elmpt W, Wierts R, Reymen B, Sharifi H, Öllers MC, Hoebbers F, Troost EG, Wanders R, van Baardwijk A, Brans B, Eriksson J, Windhorst B, Mottaghy FM, De Ruyscher D, Lambin P. (2013) Hypoxia imaging with [^{18}F]HX4 PET in NSCLC patients: defining optimal imaging parameters. *Radiother Oncol* 109:58-64
- Zhao J, Du F, Luo Y, Shen G, Zheng F, Xu B. (2015) The emerging role of hypoxia-inducible factor-2 involved in chemo/radioreistance in solid tumors. *Cancer Treat Rev* 41:623-633
- Zheng Y, Ni Y, Huang X, Wang Z, Han W. (2013) Overexpression of HIF-1 α indicates a poor prognosis in tongue carcinoma and may be associated with tumour metastasis. *Oncol Lett* 5:1285-1289
- Zhu L, Wang N. (2013) ^{18}F -fluorodeoxyglucose positron emission tomography-computed tomography as a diagnostic tool in patients with cervical nodal metastases of unknown primary site: a meta-analysis. *Surg Oncol* 22:190-194
- Ziemer LS, Evans SM, Kachur AV, Shuman AL, Cardi CA, Jenkins WT, Karp JS, Alavi A, Dolbier WR Jr, Koch CJ. (2003) Noninvasive imaging of tumor hypoxia in rats using the 2-nitroimidazole ^{18}F -EF5. *Eur J Nucl Med Mol Imaging* 30:259-266
- Zips D, Zöphel K, Abolmaali N, Perrin R, Abramjuk A, Haase R, Appold S, Steinbach J, Kotzerke J, Baumann M. (2012) Exploratory prospective trial of hypoxia-specific PET imaging during radiochemotherapy in patients with locally advanced head-and-neck cancer. *Radiother Oncol* 105:21-28
- Zschaecck S, Haase R, Abolmaali N, Perrin R, Stützer K, Appold S, Steinbach J, Kotzerke J, Zips D, Richter C, Gudziol V, Krause M, Zöphel K, Baumann M. (2015) Spatial distribution of FMISO in head and neck squamous cell carcinomas during radiochemotherapy and its correlation to pattern of failure. *Acta Oncol* 54:1355-1363

Annales Universitatis Turkuensis



Turun yliopisto
University of Turku

ISBN 978-951-29-7185-5 (PRINT)
ISBN 978-951-29-7186-2 (PDF)
ISSN 0355-9483 (Print) | ISSN 2343-3213 (Online)